2011

Development Of Energy Absorbing Laminated Fiberglass Composites Using Electrospun Glass Nanofibers

Evan Kimbro
North Carolina Agricultural and Technical State University

DEVELOPMENT OF ENERGY ABSORBING LAMINATED FIBERGLASS COMPOSITES USING ELECTROSPUN GLASS NANOFIBERS

by

Evan Kimbro

A dissertation submitted to the graduate faculty
in partial fulfillment of the requirements for the degree of
DOCTOR OF PHILOSOPHY

Department: Mechanical Engineering
Major Mechanical Engineering
Major Professor: Dr. Ajit Kelkar

North Carolina Agricultural & Technical State University
Greensboro, North Carolina
2011

ABSTRACT

Kimbro, Evan. DEVELOPMENT OF ENERGY ABSORBING LAMINATED FIBERGLASS COMPOSITES USING ELECTROSPUN GLASS NANOFIBERS. **(Major Advisor: Ajit Kelkar)**, North Carolina Agricultural and Technical State University

The ability to predict failure of composite laminates due to delaminations is critical because of its subsurface nature. Traditional strengthening methods such as stitching and Z-pinning, while improving interlaminar properties in woven composites, lead to a reduction of the in-plane properties. Electrospun non-woven sheets of nanofibrous mat applied at interfacial regions offer an option to traditional treatments. Applications where protrusion energy must be dissipated completely would benefit the most from the use of the electrospinning treatment. Examples are bullet proof vests and vehicle armor. Penetration of a projectile through a composite material may be avoided by creating more energy absorbent crack surfaces.

The objective of the present study was to increase the energy absorption capability of a composite laminate subjected to an impact of a projectile. The use of Tetra Ethyl Orthosilicate (TEOS) chemically engineered glass nanofibers manufactured with the electrospinning technique in woven glass fiber resin pre-impregnated composite laminates was investigated for their potential to improve the interlaminar properties. Electrospun glass fiber mats were produced using a computer controlled collector plate in conjunction with a high voltage power supply and a syringe injection pump. Electrospun glass nanofibers pre-impregnated woven mats were manufactured using a vacuum bag

method and cured in a computer controlled oven. The interlaminar properties of the nano engineered hybrid composites were obtained using low velocity impact tests and were compared with those without the presence of electrospun nanofiber layers. Impacted specimens were examined using C-scan analysis to determine impact damage dimensions. Compression-After-Impact (CAI) coupons were obtained from the impact tested specimen and were further tested for residual strength. Microscopic examinations were performed to study the progressive failure mechanism. A decrease of 27% residual compression strength was observed when electrospinning nanofibers were added to the lamina interfaces. The study indicated that the electrospun fiber embedded coupons had higher damage areas compared to those without electrospun fiber layers, indicating more impact energy absorption capability in the electrospun fiber-embedded coupons.

School of Graduate Studies
North Carolina Agricultural and Technical State University

This is to certify that the Doctoral Dissertation of

Evan Kimbro

has met the dissertation requirements of
North Carolina Agricultural and Technical State University

Greensboro, North Carolina
2011

Approved by:

Dr. Ajit Kelkar Major Professor	Dr. Jagannathan Sankar Committee Member
Dr. Mannur Sundaresan Committee Member	Dr. Ram Mohan Committee Member
Dr. Ronnie Bolick Committee Member	Dr. Samuel Owusu-Ofori Department Chairperson

Dr. Sanjiv Sarin
Interim Associate Vice Chancellor for Research and Graduate Dean

DEDICATION

I dedicate this work to my father Donald Spencer Kimbro and my mother Kathy Rodgers Kimbro for the kind upbringing I received. I also dedicate this to my wife, Christina Cabe Kimbro, for the endless support she has provided me during my educational years.

BIOGRAPHICAL SKETCH

Evan Kimbro was born on November 21, 1977 to Donald Spencer Kimbro and Kathy Rodgers Kimbro in Greensboro, North Carolina. He has two brothers, Allen who is older and Nathan who is younger. He received his high school diploma from Southern Guilford High School. He received his Bachelor of Science (BS) degree in physics from the University of North Carolina at Greensboro in 2002. He received his Master of Science in Mechanical Engineering (MSME) degree at North Carolina Agricultural and Technical State University in the spring of 2006.

He was raised in Greensboro, North Carolina. He came from a traditional family that preserved the value of education. He took a special interest during his early youth in automotive technology and aviation technology during his early youth. While attending high school, he committed himself to after-school activities such as a member of the school's soccer and baseball teams. He pursued his dream of receiving a private pilot's license at the age of 25.

Professionally, during his schooling he worked as an automotive technician from the age of 18 to this current date in order to support himself. He became an automotive service excellence (ASE) master technician at a youthful age of 22 years. This has been a valuable asset in his pursuit of his educational degrees.

ACKNOWLEDGMENTS

With a great deal of respect and gratitude I would like to express my dearest thanks to Dr. Ajit Kelkar for his tireless effort in my education. He guided me with great care and wisdom through my graduate school career to ensure the best training. His great knowledge has fulfilled my quest for deeper educational growth. Additionally, I would like to sincerely thank Dr. Ronnie Bolick for the vast amount of time he provided me in the laboratory work. His practical knowledge has been of great service.

I would also like to sincerely thank Dr. Jagannathan Sankar, Professor of Mechanical Engineering and Director of Engineering Research Center, Dr. Ram Mohan, Professor of Computation Science and Engineering and Dr. Mannur Sundaresan, Professor of Mechanical Engineering for their tremendous efforts in assisting me. They are the endearing core of the mechanical engineering experience.

I would like to acknowledge the support of the Center for Advanced Materials and Smart Structures, the Office of Naval Research, Dr. Ignacio, and Dr. Ray for the funding which allowed me to work on this project.

I would also like to thank my family, especially my wife Christina, for the enduring composure she provided during my graduate years.

TABLE OF CONTENTS

LIST OF FIGURES

LIST OF TABLES

NOMENCLATURE

D_{ij}	Bending Matrix (Composite Laminated Structures)
Q_{ij}	Stiffness Matrix (Composite Laminated Structures)
n	Number of plies
h	Current ply/thickness/height
k	Counter
CAI	Compression after impact
σ_{res}	Residual stress
P_{ult}	Ultimate load
a	Area/crack length
τ_i	Interlaminar stress/shear stress
P	Load
b	Width
G_{IC}	Critical energy release rate (mode I)
UFS	Ultrathin fibrous sheets
F	Force
E	Modulus/electric field
∇	Operator
q	Charge
ε_o	Permittivity of free space
r	Radial direction/radius

ρ	Density
π	Pi
SEM	Scanning electron microscope
m	Meter/mass
”	Inch
%	Percent
Pa	Pascal
TEOS	Tetraethylorthosilicate
ε	Strain
σ	Stress
γ	Shear strain
V	Volume
W	Weight
G	Shear modulus
Π	Potential Function
kV	KiloVolts
in	Inch
Hg	Mercury
p	Momentum
I	Impulse
g	Gravitational constant
lb_f	Pounds (force)

kip	1000 lb_f
hz	Hertz (cycle/sec)
ν	Poisson’s ratio/displacement
V	Volume fraction
W	Weight fraction
K	Stress concentration
u	Displacement
ω	Displacement
δ	Displacement
t	Time

CHAPTER 1

INTRODUCTION

The application of composite materials has exploded in the everyday real world. Energy absorbing composite materials are not prevalent in many real world applications that could benefit from such materials. Applications in things such as jet engine fan blades, body armor, tank armor, helicopter floor boards, and aviation wings are just a few examples which require energy absorbing composite materials. Energy absorption by composite materials is a complicated multi-phased event that needs attention and improvement. Combat military units could benefit greatly from such materials to save troop lives. This research work focus and intent are on techniques for improving the energy absorption capability of composite materials with specific applications which include body armor and helicopter floor boards. Other spin-off applications such as fan blades in jet engines may evolve from this work. Jet engine fan blades have traditionally been made of metallic materials such as single crystal titanium, which is expensive and difficult to manufacture. Improvements in energy absorbing composite materials would encourage extensive use in composite fan blades for jet engines. Metal blades experience creep, a phenomenon that causes elongation over extended periods of time under constant loading conditions [1]. Composite materials do not have problems with creep resistance. Another application of energy absorbing composite materials is in body armor. Body armor for military troop survival is crucial. By increasing energy absorption of composite materials, their effectiveness in body armor may be improved. Additionally,

composites are light weight and high strength which could potentially lower the load an infantry troop would have to carry.

Composites have a broad range of applications including bicycles, automobiles, airplanes and sporting equipment. Their low weight and density, as well and high specific strength, make them suitable for applications where strength and lightweight are desirable [2]. Airplanes are one such example. The behavior of laminated composites under tensile loading is well understood and a well researched area. Current specific applications of polymer matrix composites (PMC) are found in skins of aircraft, beams for bridges, helicopter blades, turbine applications, boat hulls, boat masts, doors, panels, rotors, and structural frames. Therefore, it is clear that during the use for these applications, damage due to foreign objects inadvertently impacting the composite plate may be inevitable. With increased engineering applications, a more in-depth understanding of the behavior of composites subjected to impact loading is desirable.

The engineering significance of most composite materials is their light weight, high specific tensile strength, fatigue resistance, and corrosion resistance. It is well known that their greatest vulnerabilities are compression strength and impact resistance. The inherent nature of impact induced failure of composites is complicated. There is a considerable difference between metallic and composite structures when subjected to low velocity impact loading. Metallic materials have multiple mechanisms for energy absorption. One such mechanism is dislocation movement. When dislocations move they allow the metal to change shape. A large amount of energy must be input to the metal in order for this to occur. Metallic materials' advantage lies within its ability to

absorb energy as it deforms plastically [1]. In general, except where absolutely necessary, the consideration of impact failure is almost always ignored during the design phase of a composite structure. For example, a steel column in a building frame generally would not be considered for impact failure. Also, the impact failure of the leading edge of airplane wing would not be considered as a failure mechanism for metallic wings. However, an impact upon a composite wing which, may not be visible, may reduce its compressive strength by 60% [3, 4].

Many investigations have been made on the impact resistance and the damage process of polymer matrix composites [3, 5-24]. Damage modes typically associated with low velocity impact consist of matrix cracking, delamination, ultimate rupture, or fiber breakage. The first stage of impact failure is matrix cracking. This occurs when the impactor strikes the leading edge of the composite panel. Matrix cracking does not degrade the composites' ability to carry a load. Resistance to cracking is solely dependent upon the polymer matrix used during the manufacturing of the composite. Resistance to cracking is a matrix dominated event. The second stage of progressive failure is delamination. This may induce shear stresses which cause cracks between the lamina and depends upon the loading mode. Mixed mode stresses may be induced depending upon the degree of bending present. The presence of mixed mode shear in the interlaminar region accelerated the formation of matrix cracks and is a catalyst for failure.

Efforts to improve delamination resistance include 3-dimensional weaves, application of vertical fibers (z-pins), and stitching the fabric before matrix impregnation. Interleave, or 3-D weaves, are tremendously expensive and complicated to manufacture

requiring specialized equipment and operators. They provide superior mechanical properties. Their improved mechanical properties do not currently outweigh the extra expense of manufacturing the weave. Z-pins are generally easy to install and provide an effective means to increase the interlaminar fracture toughness of a composite laminate. However, during the z-pinning process undesirable side effects may occur such as displacing the fibers around them to create pockets where resin can collect. These pockets can be catalysts for matrix cracks to form. Applying z-pins generally degrade the in-plane properties of the composite laminate [25]. Another way to improve the delamination resistance composite is stitching. Stitching is the easiest method to apply to the laminate, but it is also most detrimental to in-plane performance. During the stitching process, the needle that applies the stitch can shear tows in half thus lowering the tensile strength and hence reducing residual strength [26].

A promising process known as electrospinning has been developed for use in many applications. In an electrospinning process, small diameter nanofibers are manufactured to create a fibrous mat. Electrospinning uses an electric field created by a high voltage power supply to generate a fiber of varying diameters from solution gelatin (sol-gel) to a ground collector. There are various uses for the fiber mat. The process originally developed around 1934 by Formahals [27] has gained the attention of several areas including the bio-medical and mechanical engineering fields. Electrospinning has also been used in research involving biomedical tissue engineering and drug enhancements [28-39]. Electrospinning is a fast and low cost manufacturing technique that can be easily scaled up. One use of nanofibers is application between the layers of a

laminated composite panel. When interlaminar cracks form, as during the second stage of progressive failure during an impact event, the fibrous mat could mitigate damage by increasing mode I fracture toughness ($G_{IC,}$), otherwise known as the critical energy release rate.

Electrospinning offers research and manufacturing a low cost technique to fabricate nanofiber mats to improve interlaminar toughness of a composite material. The overall performance of the composite can be increased, while optimization of its use may not degrade the in-plane properties. The most recent research using the low cost simple setup nature of the electrospinning technique has concentrated on low molecular weight polymer and its use in the bio-medical field. Electrospinning research for the purpose of mechanical property improvement is still in its infancy. The present investigation addresses how electrospun glass nanofibers enhance energy absorbing composites. The following sections presents detailed literature review pertaining to composites subjected to low velocity impact loading and electrospinning techniques.

1.1 Impact Testing

Impact testing is a procedure that is used to evaluate materials in a dynamic loading. Correlation between impact energy and interlaminar shear stresses were of particular concern to engineers in the early stages of composite research. Drop tower testing of composite panels is a popular method used by researchers to characterize material systems. A schematic of a typical drop tower tester is shown in Figure 1.1. Drop towers use guided weights dropped onto specimens to test impact qualities. Early

testing of composite panels used drop towers or drop mechanisms to physically observe damage [40]. Early research on impact damage was conducted to simply characterize damage and establish baseline databases for various material systems. Once physical observations were made, analytical models [41] were developed to help predict and understand the nature of impact failures.

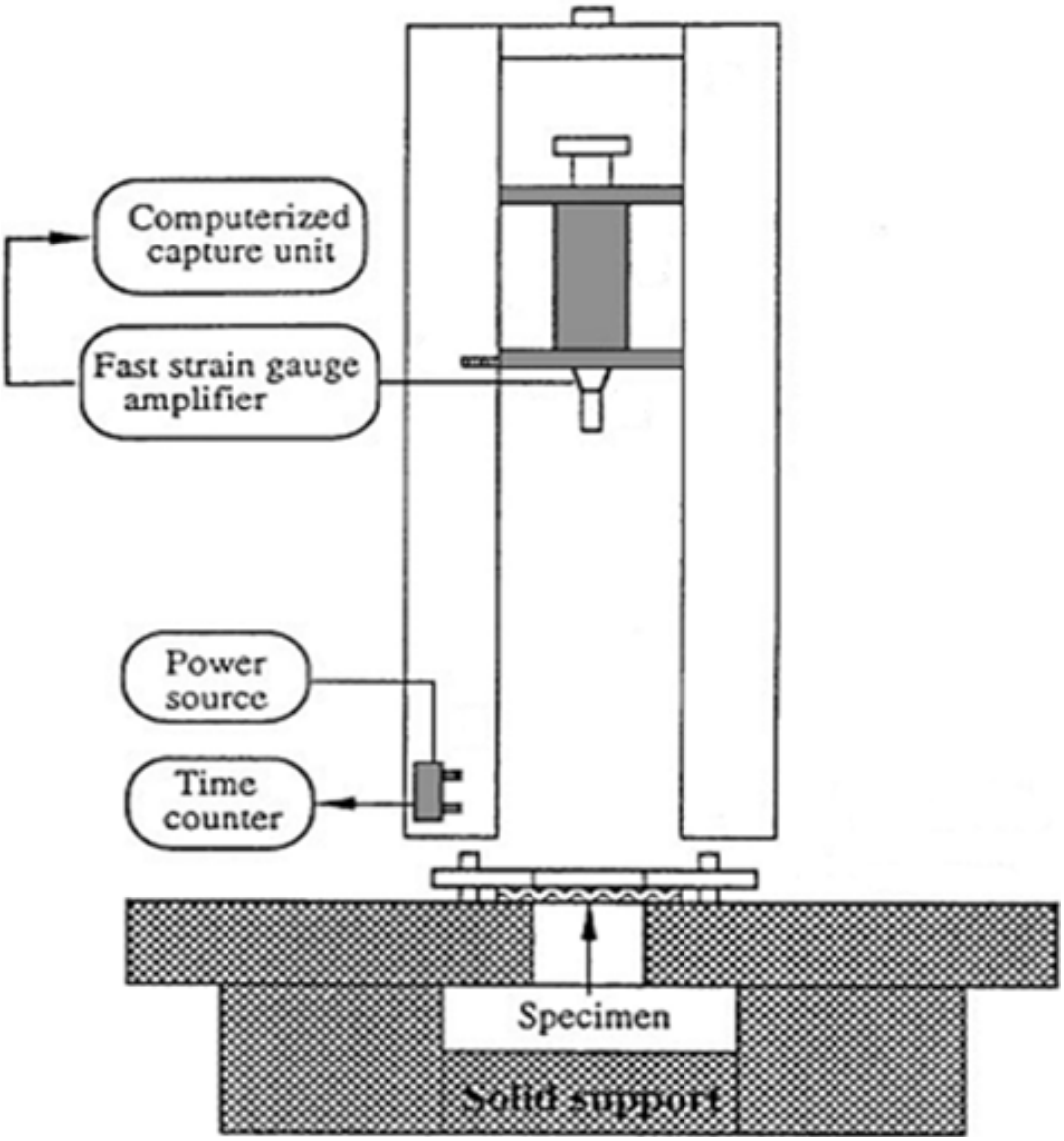

Figure 1.1. Schematic of a low-velocity drop tower [42]

An impact event is usually classified into two broad categories: low velocity and high velocity impacts. Impactor velocity is a relative term which depends upon the parameters of the composite panels as well as several other factors [9]. Such factors include the transverse stiffness in and whether the impact event is low velocity or high velocity. The higher the velocity of the striker to the composite panel the more relevant is the damage due to elastic stress wave propagation. Treatment of the low-velocity impact testing can be considered quasi-static as researchers have shown [6]. High velocity impact is governed by the propagation of the mechanical stress waves that travel through the laminate. The impactor does not contact the laminate long enough for the reflected stress waves to affect the damage area. High velocity impacted panels typically exhibit extensive fiber damage.

Ideally, the velocity should be sufficiently low enough that the entire laminate has sufficient time to react to the impact event. Elastic deformation may be used to absorb as much energy as possible before any damage is to occur. Impact may be classified by the type of damage that has occurred. Matrix cracking and delamination are considered by some [7] to be indicative of low-velocity, while fiber breakage or protrusion is indicative of high velocity. Three types of damage dominate the failure mechanisms of impacted composites. Damage types can be classified as matrix cracking, delamination, and fiber breakage. Understanding failure type and damage improvement can increase the total impact resistance of a laminated composite panel. Most research to date has concentrated on delamination resistance improvements [9]. Figure 1.2 illustrates matrix cracking and composite impact failure modes.

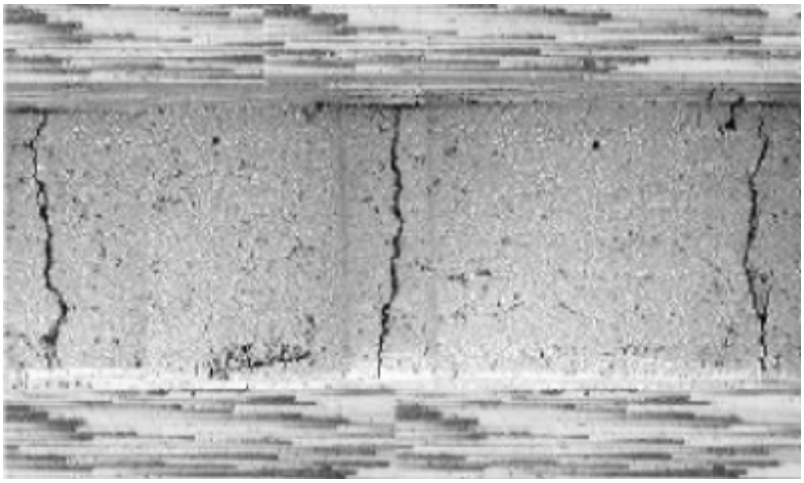

(a)

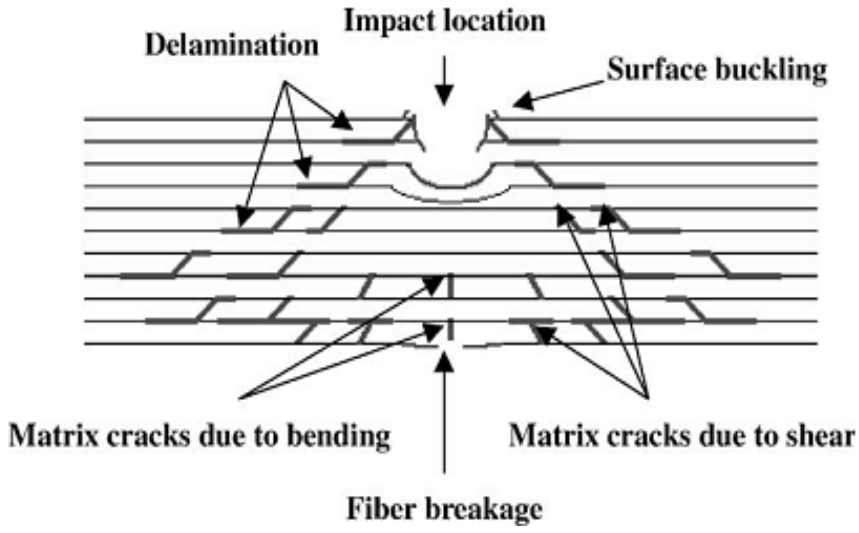

(b)

Figure 1.2. (a) Picture of matrix cracking [43] (b) Schematic of failure mechanisms [44]

Other secondary composite failure mechanisms may be designated as well. Matrix cracking generally occurs initially upon the low velocity impact event. The cracks appear parallel to the fiber and are caused by a mismatch in properties between the fiber and matrix. Matrix cracks occur due to the immense transverse shear stresses that are generated from the impactor upon the composite laminate [5]. A conical damage area

is generated under the strike zone where the impactor strikes the composite panel. This cone can be viewed in Figure 1.3 below. Research shows that a strain ranging from 0.5 to 1.0% will transition to a stress wave dominated failure mode [15].

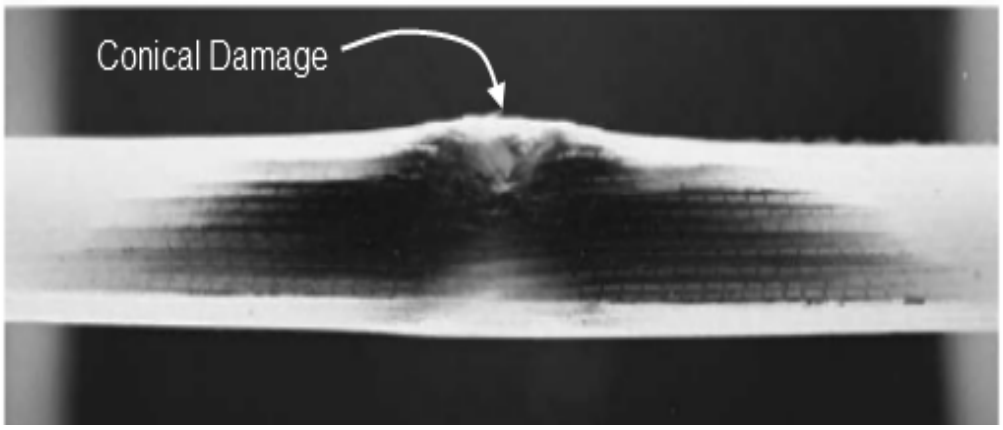

Figure 1.3. Photograph of perpendicular cross-section of impactor damage on upper surface [44]

Using different types of woven fabric may also help increase impact strength [17]. Other techniques such as fiber treatments have been investigated and experimentally tested [45]. These techniques include forming fibers with micro pores helping to increase the surface area. Increased fiber-matrix bonding results from larger surface area. Therefore, it is reasonable to expect the fiber-matrix bonding strength to increase. Comparison tests between composites with and without micro pores in the fibers were conducted to detect the final influence of the micro pores. The results show improvement with the increased micro pore density.

Delaminations are a common failure mechanism in composite laminates subjected to impact loading and are large area cracks that occur between the stacked lamina. They

extend parallel to the stacked plies. Failure of this type is dominated by interlaminar shear stresses. This interlaminar shear stress occurs typically between lamina with different stacking orientation. For example, [0,90,90,0] layup typically has the greatest interlaminar damage after impact [46]. The amount of interlaminar stresses are related to the strengths of the two different components; the matrix and fibers [8]. The major cause of the interlaminar shear stress is due to the mismatch of the bending stiffness between the lamina [47]. Stacking sequences can significantly influence the global and interlaminar bending stiffness's. Therefore, it is critical to consider the bending stiffness for impact applications. The shape of the delamination area of impacted composite panels are determined to have direct correlation with the layup orientation [8]. The delamination domain resembles a peanut shaped area. This agrees with the classical laminate theory that preceded this work. Governed by the unidirectional lamina bending stiffness component, D_{ij}, the bending stiffness is defined by the classical laminate theory represented in equation 1.1.

$$D_{ij} = \frac{1}{3}\sum_{k-1}^{n} \bar{Q}_{ij} \left(h_k^3 - h_{k-1}^3\right) \qquad 1.1$$

Delamination is almost always found in the presence of matrix cracking. It occurs once the minimum threshold energy is met. Failure due to delamination is a common problem with laminated composites currently in service around the world. It is for this reason that attempts have been made to increase delamination toughness through shear stress analysis. Of the various failure types the most significant bending stiffness degradation occurs during the delamination stage of failure [48]. Further investigations indicate that there is a strong relationship between delamination failure and matrix

cracking failure [49]. Common modern day testing practices employ the use of compression-after-impact (CAI) test following completion of impact testing. CAI is significant due to the test's ability to measure residual strength that is related to undamaged sections of the impact coupon. Impact specimens are made and cut to a CAI standard size and placed in a CAI fixture. The fixture is then placed in a mechanical loading machine where load or displacement can be controlled. The machine then compresses the specimen till the specimen fails under a compressive load of P_{ult}. Residual compression strength can then be calculated and used for comparison purposes. Some recent research have used this technique for guidance for optimization of impact toughness [50]. Ultimate residual compression strength is calculated from equation 1.2 below.

$$\sigma_{res} = \frac{P_{ult}}{A} \tag{1.2}$$

Fiber failure mechanism is the last of the primary failure mechanisms. It occurs when fiber breakage exists inside the composite laminate [4]. For the most part, there is very little local residual strength once fiber breakage has occurred. It is typically one of the later stages of failure. It occurs mainly after matrix cracking and delamination have occurred. Fiber failure, as a rule, occurs directly before catastrophic failure. Fibers break due to the local high stress surrounding them. Once fibers fail, penetration is generally inevitable during the impact event.

Penetration is another final failure mode to be considered. Penetration is considered when the striker completely protrudes through the laminated composite panel. Penetration is typically observed in high velocity impact testing. It is also observed in

ballistics modes. This type of damage is not expected to occur for the current research work. Upon penetration, there is typically no relevant residual strength available from the composite laminate.

Composite laminates consist of at least two different constituents. The constituents retain their own identity on the macro level. When the constituents form a composite, their combined properties are more desirable than the individual properties. In composite panels the constituents are characteristically composed of a fiber and a matrix. In pure tension, the fibers carry the majority of the load while the matrix acts as the binder that keeps the fibers oriented. Fibers themselves are typically very flexible and cannot sustain a bending load without support. Fibers are typically the main load bearing constituent. Common fiber materials include glass, carbon, and kevlar. Steel fibers are used in concrete composite structures. Glass is typically the least expensive readily available fiber material. Glass is the weakest fiber of the three mentioned, but also the toughest. It's typical strain at failure approaches 3.2% [51]. It provides an alternative when high strength is not always needed. Compared to fiberglass carbon's failure strain is generally within 0.5 to 2.4% range.

The other significant constituent of conventional fiber reinforced composites is the matrix. The matrix consists mainly of polymer materials. Most polymers used in conventional composites are thermosets. Thermosets are two (or more) piece mixes which chemically combine to form a polymer. The matrix transfers the external load to load bearing fibers. It protects the fibers from external damage. The matrix also keeps the fibers aligned and in the correct orientation. Epoxy also provides the composite with

one of its main flaws: cracking. Epoxy is generally brittle and its fracture toughness is very low. Therefore, it is prone to cracking under impact loading. Repeated impact to the same area will further increase damage [52].

Observations into repeated impact upon the same region have been studied less frequently. Each additional impact upon the composite laminate after the first indicates less contact force. The total amount of energy absorbed by the composite will increase with each additional impact. Certain stacking sequences of the composite will have higher number of impact-to-failure than other stacking sequences. It was noted that $[0/90/+45/-45]_s$ will have a higher number of impact failures than $[0/90/0/90]_s$. Ambient temperature typically affects impact force and total amount of energy absorbed. Compression after impact residual strength is highly dependent upon stacking sequence of the fiber reinforced composite [52].

1.2 Improvements to Interlaminar Shear Strength

Various attempts have been made to improve the interlaminar shear strength of a composite. Improving interlaminar strength is a key parameter to increasing energy absorption for composite panels. During static tests of glass epoxy specimens, shear stresses are developed as Figure 1.4 below. Common shear stress equation is provided in equation 1.3. Calculation of the interlaminar shear stress is necessary to ensure failure criterion satisfaction.

$$\tau_i = \frac{3P}{4bh} \tag{1.3}$$

Improving shear strength may come at a cost of in-plane strength performance. Therefore, it is critical to conduct research in this area to further understand the mechanisms of shear strengthening. The application of electrospinning glass nanofibers for use with mechanical enhancements is a promising field and research efforts are ongoing.

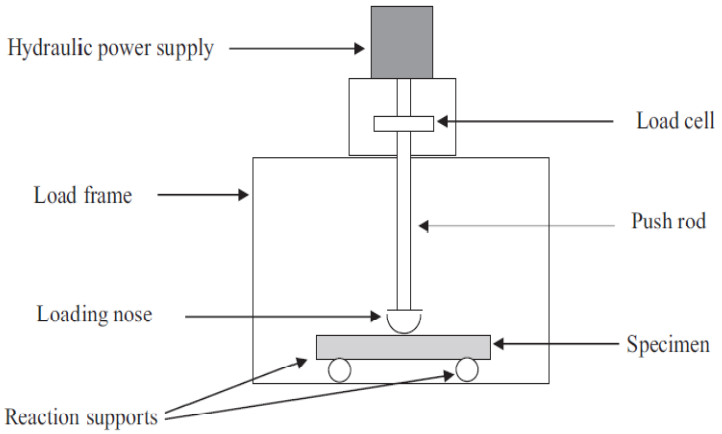

(a)

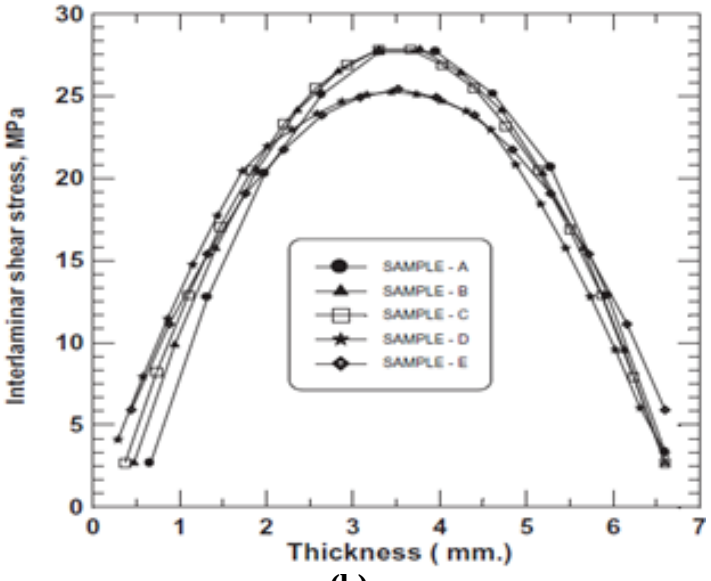

(b)

Figure 1.4. (a) Typical loading frame setup [53] (b) Example of shear stresses through the thickness of a glass-epoxy specimen under static test [53]

Strengthening the interlaminar region may have adverse effects. Researchers have reviewed the effects of z-pinning on the interlaminar fracture toughness of laminated composites [54]. Z-pinning was used to help arrest crack growth in glass-epoxy composite delaminations. Z-pins are transverse pins that are applied in variety of different ways. Most applications use ultrasonic vibrations to aid in the application of z-pins. Z-pins have been shown to significantly increase interlaminar fracture toughness. Increasing the interlaminar strength of the composite also increases its damage tolerance. Figure 1.5 shows set z-pins in the out of plane direction. Current applications of z-pinned composites include use on the F-18 Superhornet in naval applications [55]. The main advantage with z-pinning is increased interlaminar fracture toughness and shear strength in modes I and II [56-59]. Z-pinning, given their generally orthogonal direction, is highly useful in increasing strength in the z direction. Z-pinning has been shown to significantly increase fracture toughness in double cantilever beam test mode I [60]. Reductions in damage areas of 20-60% were common findings using z-pinning method.

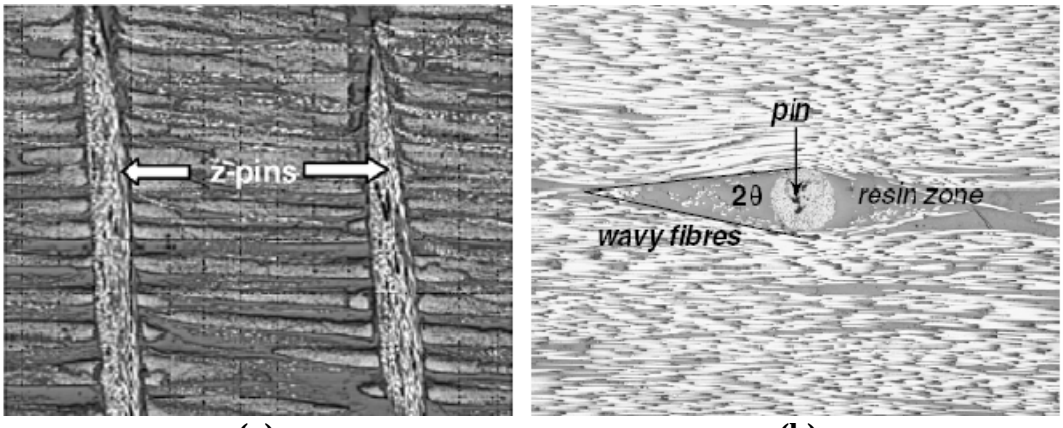

(a) **(b)**

Figure 1.5. Set Z-Pins (a) Side view [55] (b) Top view[55]

There are many disadvantages to z-pinning as well. Micro cracking can occur due to the mismatching between the thermal coefficient of the z-pins and the carbon composite. Also z-pinning is not effective at raising the threshold energy necessary to initiate damage. The energy remains the same with or without z-pins. Sufficient energy must be overcome for the z-pins to have any effect. Only when the delaminations are larger than 2-5 mm, will the z-pins inhibit maximum damage [55]. Cracking between z-pin sets can occur which may be an undesired effect. Figure 1.6 shows out of plane degradation due to z-pinning a laminated composite plate.

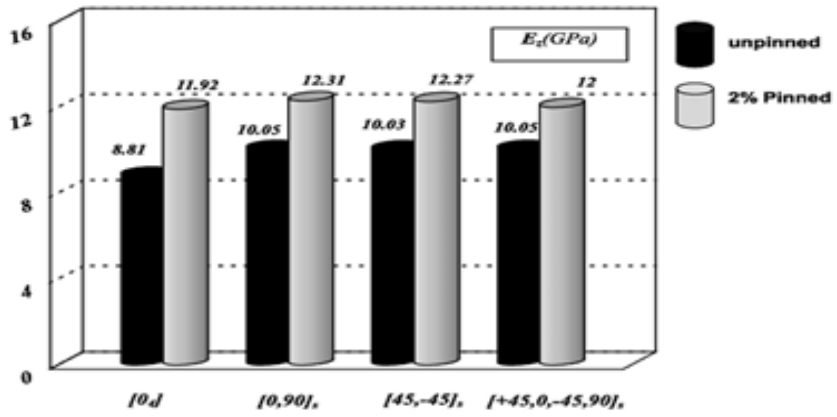

(a)

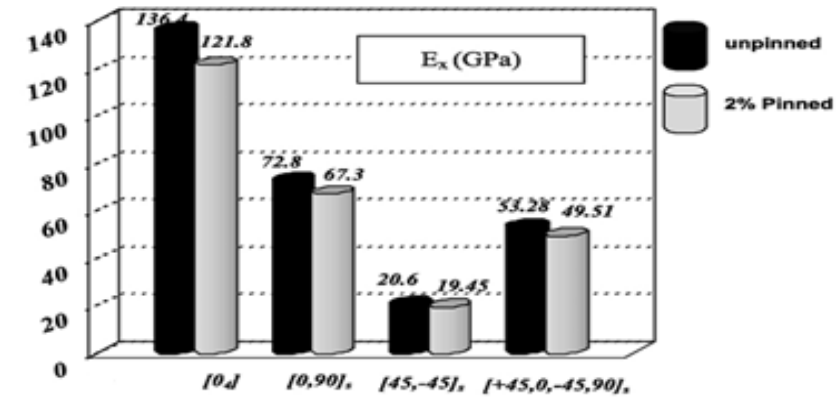

(b)

Figure 1.6. (a) Out-of-plane properties [25] (b) In-plane properties [25]

While most focus for studies of z-pinning has been on out-of-plane damage resistance, in-plane composite properties have received less attention. Finite element analysis has shown significant reduction for in-plane properties [25],[61]. Materials testing has shown the same results [62]. Z-pinning was a commonly used method for improvement of G_{IC} but its use faded over time to better systems that have lower problems with in-plane performance.

Other attempts to increase interlaminar shear strength include a method known as stitching. This is a method where the individual plies are stitched together with some binding fibers before being impregnated with resin. Stitching offers some similar advantages as z-pinning such as lowering the strain energy release rate of the stitched domain in both static and fatigue loading [63]. However, disadvantages similar to z-pinning still occur. During the stitching process fibers are damaged as the stitching needle protrudes through the multiple plies. This directly affects the tensile strength of the laminate [26]. Fewer fibers are available to carry the load. Fiber realignment occurs during needle protrusion. Both problems are evident in Figure 1.7.

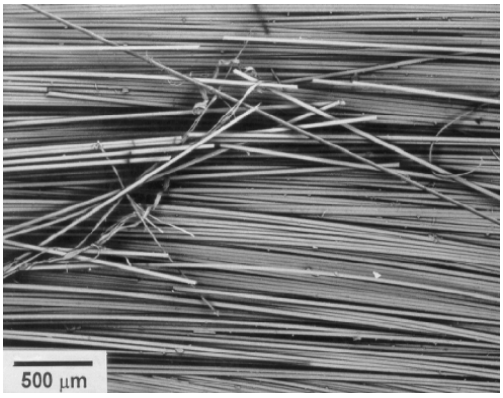

Figure 1.7. Picture of broken fibers due to stitching [26]

Research characterizing the delamination resistant in composites using stitching has been conducted as far back as 1990 [47]. Literature clearly indicated it was helpful to prevent delaminations [64]. This preserved the structure in most cases. Compression after impact residual strength tests confirmed that unstitched panels are much weaker than stitched panels [65]. Several modes of fracture toughness characterization were observed during the research into stitching. A schematic example of stitching is shown below in Figure 1.8.

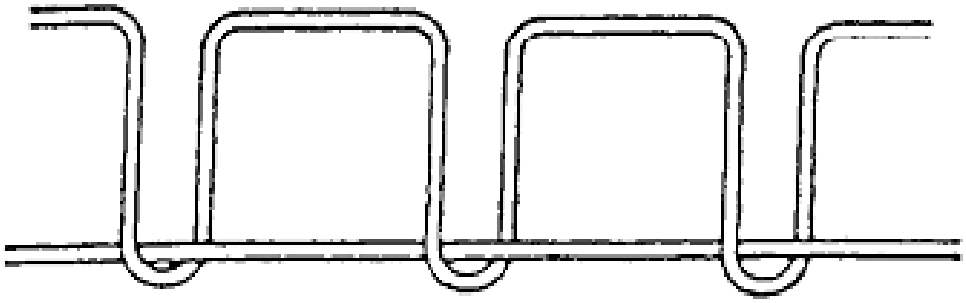

Figure 1.8. Schematic of stitching through thickness of composite panel [66]

Stitching involves several parameters that affect the resulting properties. Stitch types, stitch density, and material are a few variations that have been documented in previous research [66]. Figure 1.9 shows an example of stitched carbon composite. The flexural strength of glass reinforced composites was generally reduced by stitching. Stitching was reported to affect other materials in a dissimilar fashion when Kevlar-epoxy composites were stitched. Increases in 3-point and 4-point bending failure strengths were reported [66]. Several researchers have reported similar results in experiments [67, 68]. Stitching was also shown to increase total impact load. This was

due to decrease in impact damage area. An increase of 20% load carrying capability of stitched versus unstitched composites has been reported [69]. Degradation of modulus in both in-plane directions are generally reported by other researchers who have studied stitching. Modulus reduction above 10% has been observed [70]. A loss of in-plane stiffness can be very undesirable when attempting to improve interlaminar shear toughness.

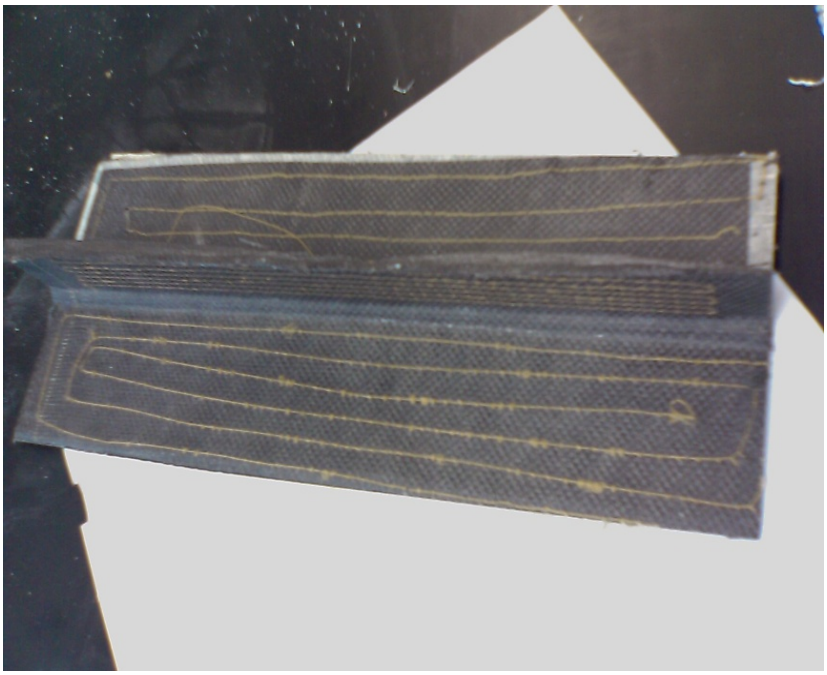

Figure 1.9. Image of carbon-epoxy T-Beam stitched with nylon threads

Delamination resistance may also be increased using other lesser known methods such as the application of small short chopped fibers embedded into the resin. A patent was filed for using this approach to help increase energy release rates as well as lower damage areas [71, 72]. Other work included the use of ultrathin fibrous sheets (UFS)

made of epoxy polymer fibers. These UFSs were created as nonwoven sheets. The sheet's thickness were varied and inserted at the interface between resin pre-impregnated composite lamina. Moderate increases in mode II fracture toughness (G_{IIc}) were reported with small amounts of UFSs applied at interfacial boundaries. Beyond a maximum thickness for the UFSs G_{IIc} dropped off significantly [73]. Comparisons between the effectiveness of stitching versus z-pinning have been examined in wide variety of applications [74].

1.3 Electrospinning

Electrospinning is a process that does not use physical contact between a spinneret and a collection plate known as the collector. An electrostatic force is applied between the two in order to draw a polymer solution from the spinneret to the collector. Under hydrostatic surface tension, electro static forces cause a droplet to extend out of the spinneret. The droplet further extends into a thick fiber where bending instability causes a whipping action resulting in elongation of the solution [75]. The whipping of the newly formed fiber continues to elongate the fiber so that the surface area to volume ratio dramatically increases. This increase of surface area to volume ratio accelerates the evaporation of solvents in the solution. This is necessary to minimize the fiber diameters.

1.3.1 History of Electrospinning

Electrospinning has evolved from observations noticed by researchers such as Bose, who in 1745 invented an aerosol, while applying an electro static force. Research into electrostatic forces for use in electrospinning type applications has been sporadic

over the past 4 centuries. Using major search engines on the internet and counting the number of papers based on the year, Figure 1.10 illustrates research frequency. Research on fundamental understanding of electrospinning physics increased in frequency in the late 1800's and early 1900's. Polymers are the most prolific type of material used in electrospinning. In the early 1880's, Rayleigh performed research determining the maximum charge any specific polymer may be induced to carry before disintegrating under the action of the electric field [76].

In the early 1900's Anton Formhals began working on what is considered to be the modern electrospinning setup. He applied a voltage to a polymer to create a fine fiber. Based on his work producing fibers using electric charge [27, 77-87], he filed several patents between 1934 and 1945. Under the patent, he used an electrostatic force to pull a very small fiber from solutions such as cellulose acetate and propionyl cellulose. It became apparent that long thin fibers were capable of being produced from this technique. His second patent filed in 1939, coined the term "Electrical Spinning" and the term "Electrospinning" was derived from that. There was significant interest in long thin fibers that were easily produced with a basic setup. Unfortunately, research on the topic slowed and little interest was shown until the later part of the century. The number of publications has increased exponentially since the early 1990's [88]. Electrospinning research continues with great intensity at many universities. However, there is little research using electrospinning technique to produce nano scaled glass fibers for the purpose of improving mechanical properties that has been reported. The current research work is unique.

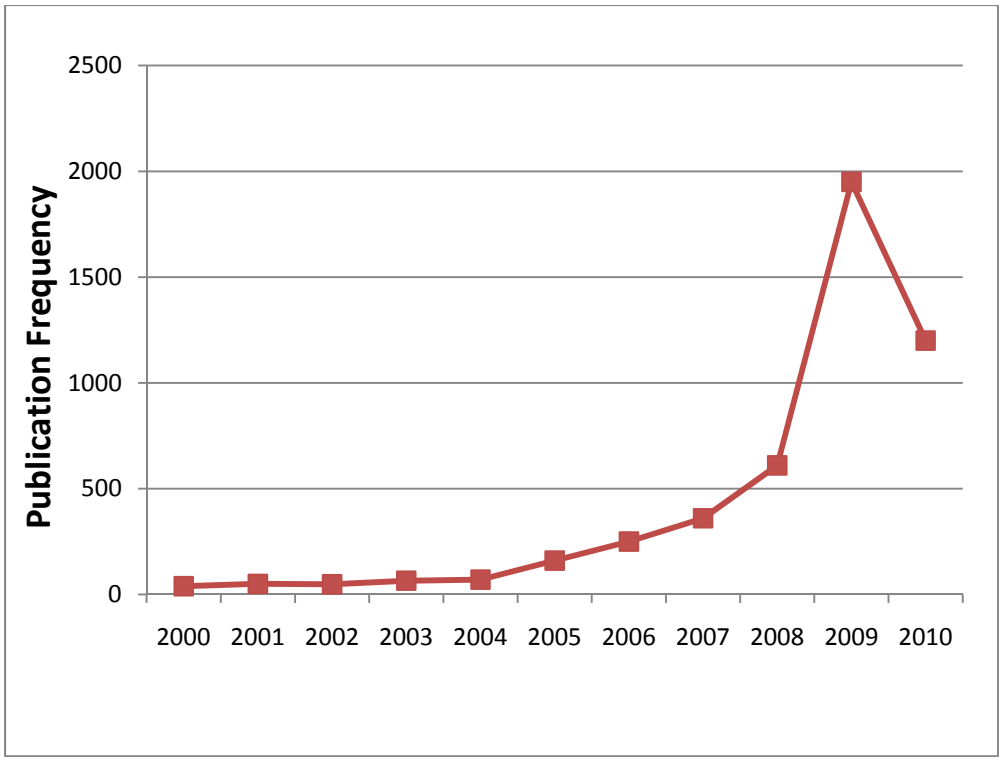

Figure 1.10. Graph of publication frequency during last decade

1.3.2 Electrospinning Setups

Various manufacturing setups have known to exist in connection with the use of electrospinning. Formation of a fiber occurs when a droplet of solution is ejected out of spinneret tube that is charged between 5-50 kV. At the tip of the spinneret, a variety of forces work against each other. When one force overcomes another multiple interactions may occur. The sol-gel is under a variety of forces when emanating from the tip of the spinneret. When the spinneret is charged, an electric field exists between the solution and a negatively charged collector plate. The electric field of the droplet overcomes the hydrostatic tension forces and elongation of the sol-gel begins to occur. One key parameter controlling elongation is the viscosity of the solution. If the solution is too thin

or inadequately viscous, droplets will tend to form and sputter themselves onto the collector substrate. If the solution is too viscous, no elongation will occur. Elongation will only occur in a small narrow range of viscosity.

Researchers initially observed mono-dispersed liquid particles early in the development of electrospinning techniques [89]. Later in 1964, Taylor noticed that a critical parameter that needed to be met in order for quality fibers to form. He noticed that a cone emanating from the end of the spinneret must be formed. For best results, the cone must have a semi angle of 49.3^{o} [90]. This became a critical finding for producing the best fibers. Once producing fibers becomes consistent, fibrous mats could be formed during production. Simons filed for a patent in 1966 when he determined a process and developed an apparatus that produced fibrous non-woven fabric mats [91]. He made a key connection between fiber length and solution viscosity which later helped researchers produce better results [89]. Researchers struggled to create fibers on the sub-micron level. Baumgarten used electrostatic means to spin sub-micron acrylic microfibers in 1971 [92]. Baumgarten's work helped to revolutionize electrospinning; he attempted to characterize many parameters such as voltage, viscosity, and solution flow rates with respect to their influence on fiber morphology. Research into electrospinning fell flat shortly after this work and was relatively idle for a while. Research interest was fairly dormant in the field while several patents were filed and used in the filtration industry. Interest emerged the field after several publications by Reneker in the mid 1990s at the University of Akron. After a renewal of interest, research expanded at an exponential rate especially when applications were observed by the bio-medical field. Today many

publications can be found using the electrospinning technique with a wide array of applications from mechanical engineering to the bio-medical field. This research work uses electrospun nanofibers for developing energy absorbing laminated fiberglass composites.

During the process of perfecting electrospinning, the issue of fiber alignment became a point of interest. The electrospinning process does not necessarily create the most proper fiber orientations. Early attempts to align fibers proved to be a challenge. Before attempting fiber alignment though, a fundamental understanding of the forces active during fiber formation was needed. With proper fiber alignment, many factors along the fiber directions may be improved such as modulus, strength, and perhaps electrical conductivity depending upon material. Using electrospun nanofibers in various applications of composites can also tremendously enhance their mechanical, electrical, and bio-medical properties. To gain the most impact with the application of electrospun nanofibers, fiber alignment needs to be ideal. In order to achieve properly aligned fibers, process control and optimization must be understood. This is a challenging task considering the non contact nature of the process used to manufacture nanofibers. While the fiber is in the transient stage between the spinneret and collector the fiber is under the control of an applied electric field. The magnitude of this electric field between the spinneret and collector plate is exponential. The electric field is defined as the force per unit charge that is experienced by a point charge at some arbitrary location. Equation 1.4 is a general version of Gauss's Law which is one of Maxwell's equations. Coulombs Law is a special case of Gauss's Law, equations 1.5. From Coulomb's equations we can

see that the electric field is nonlinearly distributed as viewed by r^2 in the denominator of equation 1.6.

$$E = \frac{F}{q} \tag{1.4}$$

$$\nabla \cdot E = \frac{\rho}{\varepsilon_o} \tag{1.5}$$

$$E = \frac{1}{4\pi\varepsilon_o}\frac{q}{r^2}\hat{r} \tag{1.6}$$

For experiments that use a very simple setup, nonwoven mats of nanofiber material is distributed over an area in a random fashion. Steps must be taken to attempt to achieve fibers in a unidirectional orientation. A whipping action occurs in the region between the spinneret and the collector. The whipping action tends to deposit random fiber orientations. The formed fiber properties of quasi-isotropic and are approximately equal in all in-plane directions. Only when alignment of fibers is in one common directions can the full engineering potential of the strength of the fibers can be realized. Figure 1.11 shows two images from a scanning electron microscope (SEM) comparing random fiber orientation to aligned fiber orientation.

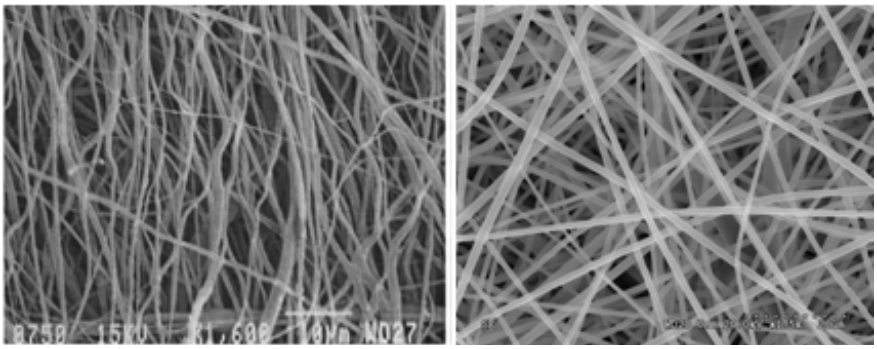

(a) **(b)**

Figure 1.11. (a) Image of aligned fibers [93] (b) Image of random fibers

The most obvious attempt to align fibers is to use a rotating drum as the negatively charged collector. The drum must be rotated to draw the fiber to the drum using the electrostatic force as well as physically winding the fiber on to itself. Some issues arising out of this method have foiled early attempts with the setup. The angular speed of the drum is critical. Angular speed must be set such that the linear speed of the surface of the drum is equivalent to the linear speed of the production of fibers out of the spinneret. If the drum speed is too slow then bunching up of the fibers occurs which becomes problematic during spinning. If the speed of the drum is too fast then fiber breakage occurs during production. Figure 1.12 shows a schematic of the rotating drum concept. This creates continuity problems and can decrease the overall strength as well as being problematic during the manufacturing stage [94].

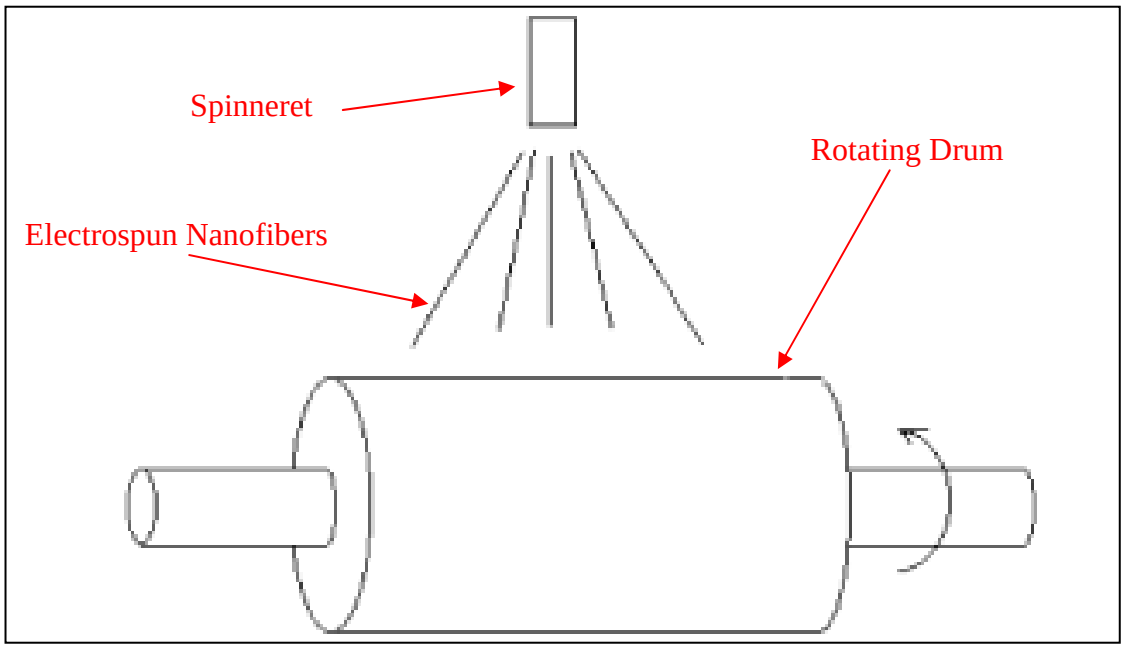

Figure 1.12. Schematic of a rotating drum collector [94]

No mechanical means of producing a half-micron diameter fiber has been developed as of date. Therefore, we must rely on non-contact methods for fiber production. Orienting electrospun fibers becomes challenging when the method is non-contacting in nature. In 1987, use of additional fields upon the manufacturing apparatus was attempted and then patented [95]. Use of a rotating drum was tested in an attempt to untangle the fibers that were electrospun onto the collector. Films of graphite were wrapped around a rotating drum covered with aluminum foil to produce a nano-fabric [96]. In this attempt, the use of the rotating mandrel drum helped to orient the fibers in a consistent direction. The fibers were then tested with medical applications such as a drug releasing agent.

Other methods such as changing collector orientation have been attempted to turn the collector into a rotating disc. By changing the shape of the rotating collector into a disc, manipulation of the electric field between the spinneret and the collector could be achieved. This in turn would change the orientation of the fiber once it has been deposited. Figure 1.13 shows an example of a rotating collector disk. The schematic drawing shows a region between the syringe/spinneret and the rotating collector disk. Within this region of bending instability, a cone shaped whipping area exists which is inverted roughly half way between the spinneret and collector. This setup proved advantageous for fiber alignment. During deposition of fiber onto the collector disk, the residual charge on the exiting fibers repelled them from other fibers thus preventing entanglement. Discrete separation of the fibers was noticed during the fiber extracting process. This process enhancement proved to be a very successful approach for discrete

fiber alignment. Lengths of up to hundreds of microns with average diameters ranging from 100-300 nanometers were achieved with the rotating collector disk setup [97]. This particular setup was only able to produce limited length fibers. Manufacturing large nonwoven mats was not possible with the cylindrical disk setup. The cylindrical disk is used for special purposes and generally is not used for bulk production of nanofibers.

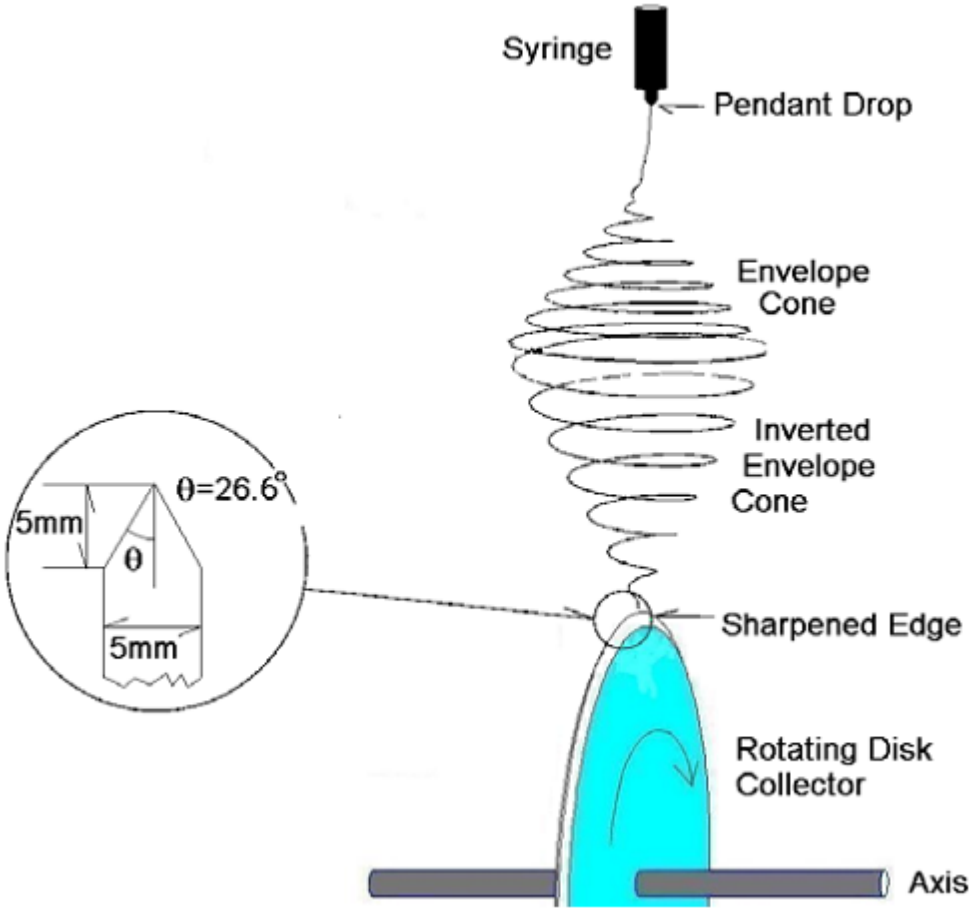

Figure 1.13. Schematic drawing of rotating collector disc [97].

A solution with a sufficient viscosity was pumped through the spinneret and formed a droplet at the tip. The applied electrical potential difference pulled the solution

towards the ground collector creating a solution jet. This action stretched the solution into very long lengths and caused bending instability [98]. The inherent instability ensured random fiber direction once deposited on the ground collector. Additional methods have been developed to provide oriented fibers on the ground collector [99]. Controlling the electric field displacement around the spinning fiber oriented the fiber in a controllable fashion. Fiber diameters down to 100 nm have been manufactured [100].

1.3.3 Process Control

The final goal of electrospinning is to produce high quality nanofibers with the intended features. Manipulating the outcome of the nanofibers is the objective of process control. Fiber diameters on the order of 10^{-9} m without defect in proper orientation are the goal of most research. The process of electrospinning is very difficult to control due to the large number of parameters involved in the process. The parameters govern the final product of the electrospinning setup. Parameters associated with the solution are viscosity, conductivity, surface tension, and concentration. Viscosity and surface tension are further reduced depending upon variables such as time, temperature, humidity, and other curing conditions. Mechanical variables in the setup such as voltage, spinning distance, spinneret diameters, collector orientation and associated mechanisms, and rate of dispensing all have a large effect on the final form of the nanofibers. Some of the variables must be adjusted slightly on a daily basis in order to produce the desirable fibers. Operator judgment must be called upon to provide the best results. Although most variables are objective, some amount of subjectivity is left to the operator to make decisions for each setup. Attempts at correlating the vast array of process variables to the

final outcome of nanofibers have been conducted. One parameter that heavily influences the fiber diameter is viscosity. Higher viscosity solutions result in thinner fiber diameters. If thin solutions are present while spinning, a phenomenon such as atomization may occur due to the spraying of micro droplets. Clogging of the spinneret may occur if the solution is too viscous. Studies have been conducted attempting to correlate surface tension and viscosity to the final diameter of the nanofibers. Viscosity of the mixed solution varies with the operating time. Spinnable solutions will not be possible if insufficient time is not given for the solution to age. Solution flow rate is also a process parameter that must be addressed. Heavy flow rates can cause fiber diameter to be too large and insufficient flow can cause discontinuities in fiber production.

Most research into process controls of electrospinning has largely been focused on controlling solution viscosity. A secondary parameter used for diameter control is applied voltage. Limited research into the influence of fiber diameter by applied voltage has been conducted. To date no known mathematical formulas exist between the applied voltage of the setup and the final fiber diameter to date. Deitzel determined a relationship between fiber diameter and the concentration of Polyethylene oxide (PEO) in the solution. When a log-log plot of concentration versus fiber diameter are plotted as Figure 1.14, a linear relationship is established [101]. Therefore, some solution concentrations will affect the final fiber diameter. It was reported that higher PEO concentration resulted in larger fiber diameters during electrospinning. Fiber diameters were reported between 0.10 and 0.60 μm. Lower PEO concentrations also helped to increase specific surface areas. High specific surface areas are desirable with glass nanofibers.

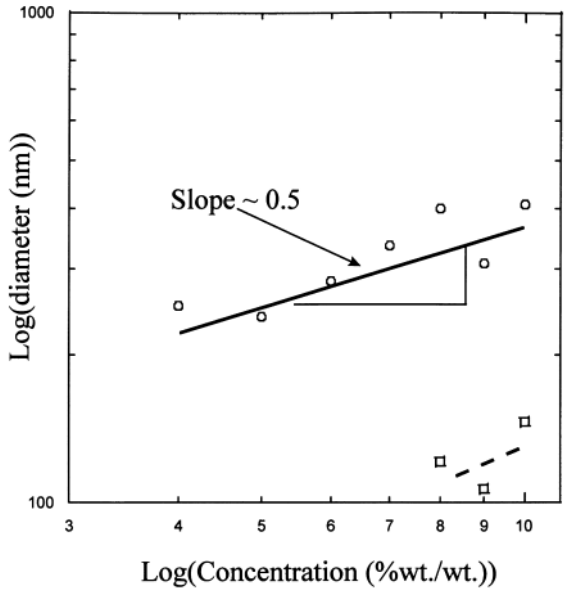

Figure 1.14. Log-Log plot of fiber diameter vs. PEO solution concentration [101]

Problems with experimental setups or solution aging may result in issues known as beading. This is one of the more noticeable problems with electrospinning. Beads are created when anomalies occur during electrospinning manufacturing. They are lumps of extra material in small sections of the continuous fiber. Therefore, understanding beads and bead formation is critical in eliminating them during conventional electrospinning. Some studies have been performed to analyze beading. Figure 1.15 shows an example of beading of different polymer mixture concentrations. Fong et al. noticed that for thicker solutions, bead frequency was lower in the final product [102]. Research that varied charge density, surface tension, as well as the viscoelasticity of the solution has also been done. Lower surface tension tends to produce larger diameter fibers or produce beads which are of larger diameters for a short length of fiber. Higher voltages were congruent with the production of smaller diameter fibers.

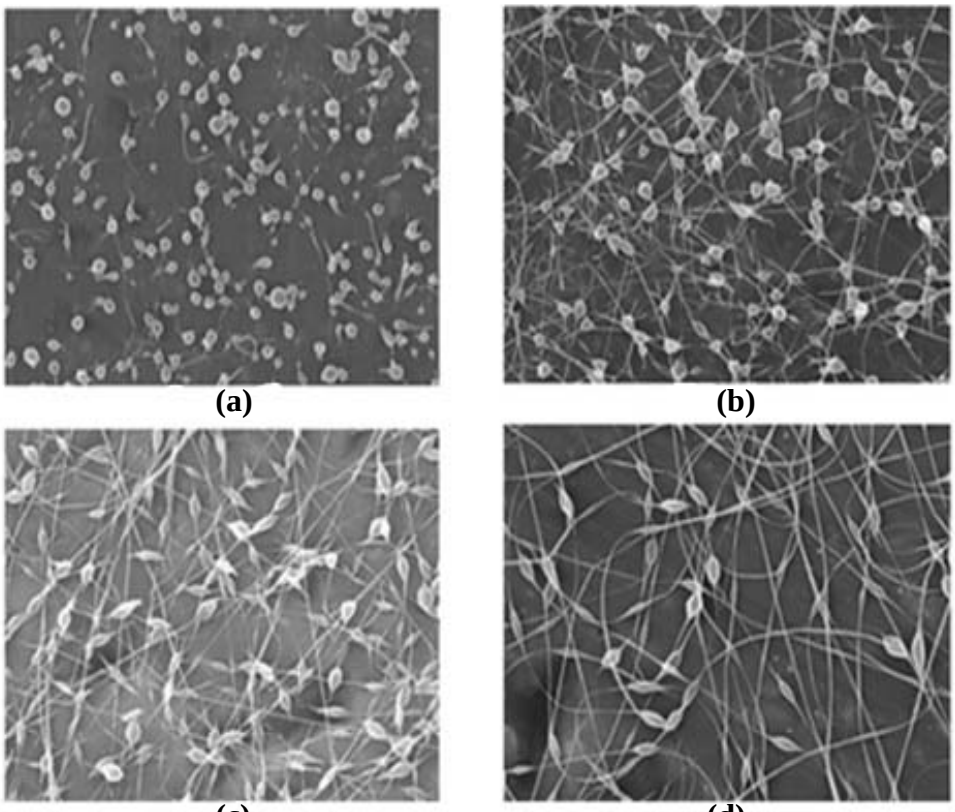

Figure 1.15. SEM morphology (a) 13 centipoise (b) 32 centipoise (c) 74 centipoise (d) 160 centipoise [102]

1.3.4 Applications of Electrospun Fibers

Electrospun fibers have a large variety of applications. Small fiber diameters lead to high surface area to volume ratio. Depending upon the material the fibers may be porous. Some fibers may or may not adhere to substrates or matrix materials. These fibers must be functionalized or treated with a surface bonding agent to bond with the matrix. One major application of nanofibers is use in composites as reinforcements [103]. Composites generally consist of a minimum of 2 different materials. Macroscopically identifiable, each material has a different purpose in the overall

objective of the final composite. Given the increased strength to weight ratio of composites, future applications of nanofibers in composites will likely grow in magnitude. Adding electrospun nanofibers to conventional composites increase the weight negligibly, but their strength and toughness may increase upon to 20% depending up application [104]. Arranging 300-500 nm diameter PBI nanofibers at the interfaces of composite panels may have a significant impact upon their relative energy release rate G_{Ic} and G_{IIc}. An increase in Mode I energy release rate G_{Ic} of 15% and an increase in G_{IIc} of 130% were reported [71]. Therefore, it is evident a small application of nanofibers at the interfaces can significantly increase the fracture toughness energy release rate.

The experimental setup of electrospinning is quite simple. The setup consists of 4 main parts: 1) a positive spinneret 2) a ground collector plate 3) high voltage power supply 4) syringe pump and solution. A previous work has attempted to discover the individual parameters that affect the fiber diameter the most [105]. Current work is also underway to further understand these parameters [106]. The effects of the electric field on the overall setup should be carefully thought out [107]. Currently there is no mechanical characterization of a single electrospun nanofiber. This is very difficult to do and must have specialized equipment to perform the task. Some mechanical properties of nano-tubes have been evaluated. A modulus of 600 GPa was estimated for nano-tubes [108]. This is clear indication that as bulk materials shrink their properties change. Figure 1.16 shows the target areas of research applications using electrospun nanofibers. Applications in the filtration field have also been investigated. This is a highly targeted field for the application of different types of electrospun nanofibers.

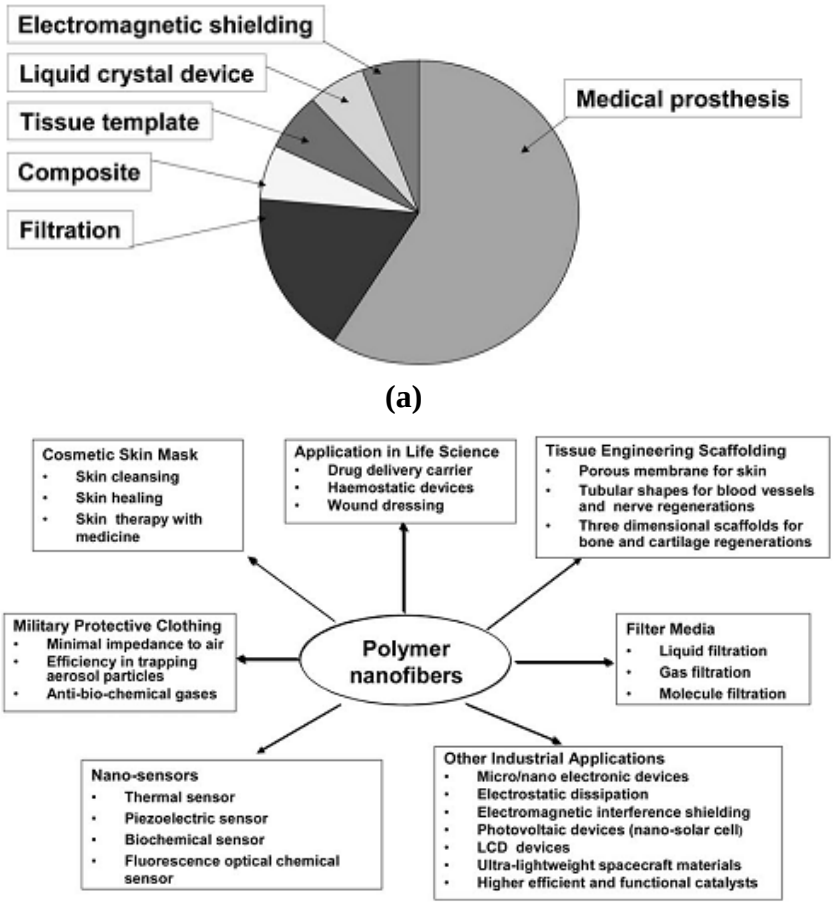

Figure 1.16. (a) Applications based on US patent filings (b) Possible applications of electrospun fibers [94]

Filtration is a large field and it is estimated that upwards of $700 billion by the year 2020 will be spent on cleaning multiple fluids [109]. Filtration efficiency is a major parameter when considering filtering foreign objects from fluids. It becomes more difficult to filter the ever decreasing size of foreign particles. Filter efficiency is a function of the diameter of the filter fibers. The smaller the diameter of the filter fibers, the smaller size particles can be removed from a medium. Nano-sized fiber diameters are rising to the challenge of filtering smaller sub-micron debris that is necessary in ever

increasing modern equipment. Air compressors are common in many manufacturing settings and compressor oil is used to lubricate the compressor mechanism. This oil poses as foreign debris in many clean laboratory settings. Filtering out oil is a priority for clean laboratories that use compressed air. Figure 1.17 shows a schematic of fiber diameter related filtration capability. It is noted that particles below half a micron can easily be filtered using electrospun nanofibers due to their large surface area to volume ratio and their high surface adhesion.

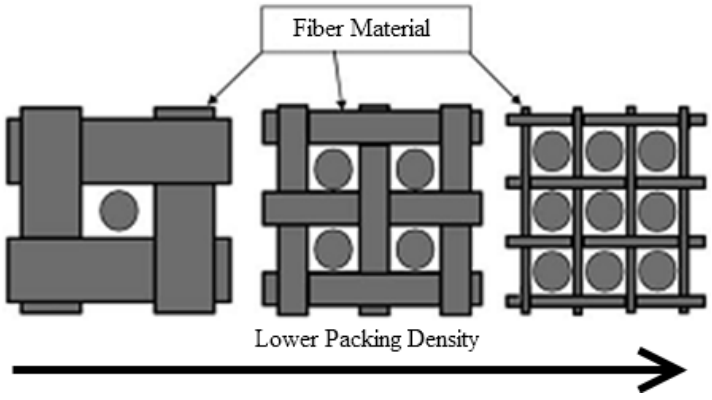

Figure 1.17. Fiber diameter: (a) larger than (b) which is larger than (c) [94]

Cosmetics seem an unlikely application for electrospinning but it may be a successful retail adventure. Many product types such as topical creams, lotions and ointments all may require some fibrous materials which ideally are invisible to the naked eye. Compatible electrospun fibrous materials serve as a substrate for the different materials used in this field. Similar to the use in cosmetology and makeup, electrospun fibrous materials also provide a good backing for the use of skin mask as skin healing

apparatuses. Smaller interstices and large surface area are several of the advantages of nanofibers [110].

1.4 Overall Synopsis

The present work has been catalogued and recorded in this dissertation. It is presented in a reasonable methodically oriented manner. The title of "*Development of Energy Absorbing Laminated Fiberglass Composites using electrospun Glass Nanofibers*" was carefully chosen to encompass most aspects of the current research. A clear understanding of most aspects of the formation of electrospun glass nanofibers and their application to composites is sought. Nanofiber applied to glass laminated composites subjected to dynamic impact forces are investigated in the present work.

Chapter 1 presents an introduction to the various aspects of the present topic. The information covers various aspects of electrospinning and their application for use in the composite materials. A review of impact damage composite materials is discussed in order to understand the history of low-velocity impact on characteristics in composites. Understanding the various forces and modes of failure is discussed. The evolution of electrospinning starts with a review of how the individual constituents of electrospinning in early history. Subsequently, individual process parameters are discussed and how they affect the fiber properties. Applications of the electrospun fibers are presented.

Chapter 2 discusses the mechanics of composites as related to the current research work. Different modes of failure of composites are discussed as well as the application of fracture mechanics to composites. Understanding the mechanics of the change in the

composites is critical to optimization of the electrospun fiber application. Delamination is particularly of a key interest in polymer reinforced composites. Efforts are made to understand why delaminations occur and how the use of electrospun fibers can change the failure mechanisms in composites.

Chapter 3 discusses the production of electrospun glass nanofibers. This chapter discusses, in detail, the individual manufacturing processes that were used in order to produce Tetra Ethyl Orthosilicate solution (TEOS) nanofibers. Further discussion of how the solution is aged and used in an electrospinning setup is examined. Processing parameters specific to manufacturing are discussed and how they affect the overall setup. During actual spinning of the glass nanofibers a process parameter optimization was used to optimize the dimensions of the fibers.

Chapter 4 discusses how the electrospun glass nanofibers are embedded into a 2 part composite laminate making it a 3 part composite laminate. Composite laminates are made of 2 or 3 continuant materials. Problems with preliminary manufacturing of electrospun nanofiber embedded composites are discussed in chapter 4. The relevant solutions to the manufacturing role are also presented. This chapter also presents the fabrication of impact test coupons.

Chapter 5 discusses the details of impact testing of the specimens. Low velocity impact tests were conducted onto the specimens to study the progressive damage in both types of composite laminates with and without electrospun nanofibers subjected to low velocity impact loadings. Impact specimens are then examined using a non-destructive testing technique known as C-scanning that uses ultrasonic sound waves to examine

damaged areas of the specimens. Damaged specimens are scanned and impact damage areas are measured for both composite laminates with and without electrospun nanofibers subject to low velocity impact loading.

Chapter 6 discusses destructive compression after impact testing on the specimens to determine residual strength. Compression after impact testing is a common approach taken to understand the residual strength after impact of the plastic reinforced composite laminated plates. Preliminary tests indicated problems that were ultimately resolved with the addition of tabs. Details of the technique are discussed in chapter 6.

Chapter 7 presents the overall conclusions of the present work and recommendations for the future work.

CHAPTER 2

MECHANICS OF COMPOSITES: A REVIEW

Composite materials are defined as the combination of normally two different materials into one final material. Macroscopically the two separate materials are identifiable typically without further inspection methods such as microscopes. The final material generally has superior properties to that of the individual components. The two individual components are generally referred to as ‘phases’. One of the phases typically is a stronger material than the other. The stronger material is generally used as reinforcement type of application. The reinforcement typically takes the shape of small diameter fibers and these fibers are grouped together in what is known as ‘tows’. The weaker material is typically referred to as the ‘matrix’. This, characteristically, is used as a structuring mechanism for the overall composite material. The interaction between the fiber reinforcement and the matrix may or may not be chemically bonded. In certain applications such as steel and concrete there is no chemical bond between the fiber and matrix. But in other applications such as carbon nano-tubes and epoxy, additional steps may be necessary to apply a chemical coating known as functionalizing.

Functionalizing of the carbon nano-tubes provide a chemical bonding interface between the nano-tube reinforcement and the matrix structuring material giving the overall composite superior properties. Figure 2.1 shows specific examples where composites are used in everyday life and play a major role in performing basic functions that go unnoticed. The Boeing Dreamliner is a modern state of the art airliner that has

extensive use of composites for a majority of its structural components. One such component is the fuselage which is filament tape wound and is produced as a whole assembly on a large mandrel. Composite's high stiffness to weight ratio and low density offer very advantageous properties to engineers designing structures. This is particularly important when weight is an issue but strength cannot be compromised. Aviation is an industry that requires low weight, high strength materials to produce an efficient aircraft.

(a)

(b)

Figure 2.1. (a) Picture of Boeing 787 Dreamliner during landing [111] (b) Dunlop tennis racquet made of fiberglass composite [43]

2.1 Lamina Properties

The most basic type of layer in a plastic reinforced composite is known as the individual 'lamina'. The lamina is a single layer which is stacked onto other individual lamina. A completed composite after stacking with more than one layer is called as a laminate. The most basic type of lamina is known as a unidirectional lamina. Fiber orientation in a single direction constitutes a unidirectional lamina. A unidirectional lamina stacked with different orientations can be considered as the stacking sequence. The stacking sequence provides a significant parameter which changes the overall global properties of the laminate. Most stacking sequences have orthotropic properties. Orthotropic properties are prefaced by isotropic properties. Isotropy is when a material property does not change with direction. Orthotropy is when a material property changes with orthogonal direction changes. Anisotropy is where the properties of the global material depend specifically on the direction from the origin. The following basic equations below show how specific parameters are related.

$$\sigma_x = \frac{E}{1-\upsilon^2}\varepsilon_x + \frac{E\upsilon}{1-\upsilon^2}\varepsilon_y \tag{2.1}$$

$$\sigma_y = \frac{E\upsilon}{1-\upsilon^2}\varepsilon_x + \frac{E}{1-\upsilon^2}\varepsilon_y \tag{2.2}$$

$$\tau_{xy} = \left(\frac{E(1-\upsilon)}{2(1-\upsilon^2)}\right)\gamma_{xy} \tag{2.3}$$

An isotropic material under uniaxial tensile loading adheres to mechanics defined by the above equations. For pure shear loading, τ_{xy}, the deformation of the material will exhibit shear deformation. For composites that are orthotropic, the material will exhibit different properties in orthogonal directions. Therefore, it is extremely important to

categorize the specific direction related to global points and local points. Local directions that are related to individual lamina are designated with 1 and 2 indicators. Global directions that are related to the overall laminate are designated with x and y [2]. An example of a 4-ply laminate with an arbitrary stacking sequence can be seen in Figure 2.2. The individual fibers of each lamina can be viewed by the cutaway rendering. Also the global coordinates (x,y,z) can be viewed as well.

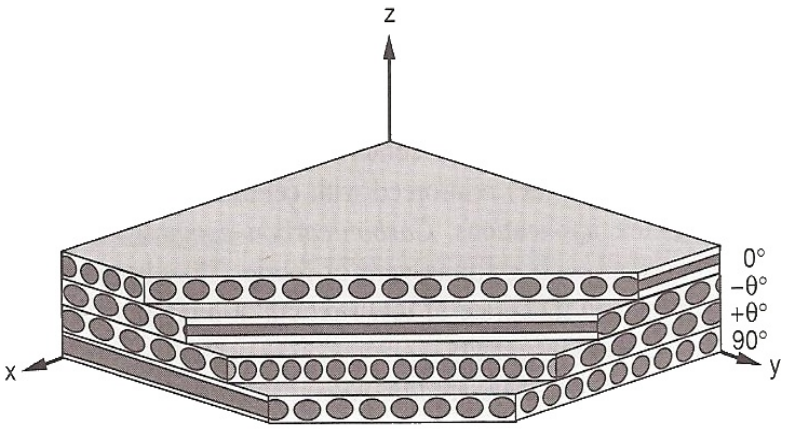

Figure 2.2. Schematic of 4-ply laminate with arbitrary stacking sequence [2]

Modeling of woven fabric materials involves a simple summation of unidirectional lamina properties. The combined result of two unidirectional lamina yields the same properties as a single lamina of a woven layer. Complete understanding of the different levels of composites is necessary for their strategic engineering applications. Figure 2.3 shows the different levels of a composite from the macroscopic use in an application down to the individual fiber. Global properties of the laminate depend upon the unit properties of the fiber-matrix micromechanics.

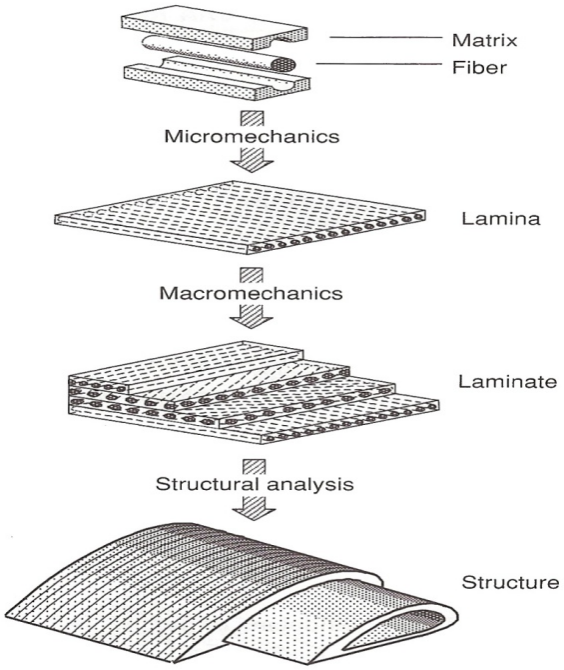

Figure 2.3. Drawing showing the different levels of a composite [2]

There are many manufacturing methods polymer fiber reinforced composites. During manufacturing, many parameters may affect the ratio of the matrix to fibers. This ratio is called fiber volume fraction (V_f). It is the volumetric ratio of fibers to entire composite laminate. Other parameters such as fiber weight ratio (W_f), matrix volume ratio (V_m), and void volume ratio (V_{void}) all affect composite mechanical performance.

$$V_f = \frac{volume\ of\ fibers}{volume\ of\ composite} \quad 2.4$$

$$W_f = \frac{weight\ of\ fibers}{weight\ of\ composite} \quad 2.5$$

$$V_m = \frac{volume\ of\ matrix}{volume\ of\ composite} \quad 2.6$$

Therefore, the volume of the voids is any volume not occupied by the fibers or matrix presented in equation 2.7

$$V_v = 1 - V_f - V_m = \frac{volume\ of\ voids}{volume\ of\ composite} \quad 2.7$$

2.2 Constituent Materials

Each phase of the composite may be made of various materials. The reinforcement phase is generally in the geometrical shape of a fiber. The fiber diameter may be adjusted to achieve specific goals of the overall composite. Table 2.1 shows some of the different available materials from which reinforcing fibers are made. Of the various materials available, carbon and glass are the two most widely used. Glass is an inexpensive strong material used in a variety of applications. Carbon is a more expensive option with very high strength and stiffness. The increased use of carbon has decreased the cost which has closed the usage gap between carbon and glass.

Table 2.1. List of various fiber reinforcement materials for plastic composites [2]

Fiber Material	Advantages	Disadvantages
E-Glass, S-Glass	High Strength Low cost	Low stiffness Short fatigue life High temperature sensitivity
Aramid (Kevlar)	High tensile strength Low density	Low compressive strength High moisture absorption
Boron	High Stiffness High compressive strength	High cost
Carbon	High strength High stiffness	Moderately High Cost
Graphite (GY-70, pitch)	Very high stiffness	Low strength High cost
Ceramic (silicon carbide, alumina)	High stiffness High use temperature	Low strength High cost

2.3 In-Plane Shear Modulus

In plane shear modulus can best be modeled with unidirectional composite lamina as a series of alternating stacking of fiber area and matrix area. For stress along the fiber direction the mechanics of the composite are dominated by the matrix. It is best to treat the composite as a series of elements. Each element is subjected to the same stress as the one above and below it. Figure 2.4 shows us an example of a typical deformation for a small section of unidirectional composites. It is imperative to remember that woven fabrics can be considered a summation of unidirectional layers. Shear deformation γ_m and γ_{12f} are different and the total amount of deformation for each element is the summation of both. For total shear deformation of the composite lamina, equation 2.8 through 2.11 shows the relationship between fiber volume fraction, matrix volume fraction and over all shear deformation.

$$\gamma_{12} = \gamma_{12f} V_f + \gamma_m V_m \tag{2.8}$$

Substituting for γ_{12},

$$\frac{\tau_{12}}{G_{12}} = \frac{\tau_{12}}{G_{12f}} V_f + \frac{\tau_{12}}{G_m} V_m \tag{2.9}$$

Canceling common term τ_{12}

$$\frac{1}{G_{12}} = \frac{V_f}{G_{12f}} + \frac{V_m}{G_m} \tag{2.10}$$

Solving for lamina shear modulus gives,

$$G_{12} = \frac{G_{12f} G_m}{V_f G_m + V_m G_{12f}} \tag{2.11}$$

Interlaminar shear modulus gives an idea of how stiff a material is in shear mode. It has significant indications when a specimen experiences multiple mode stresses.

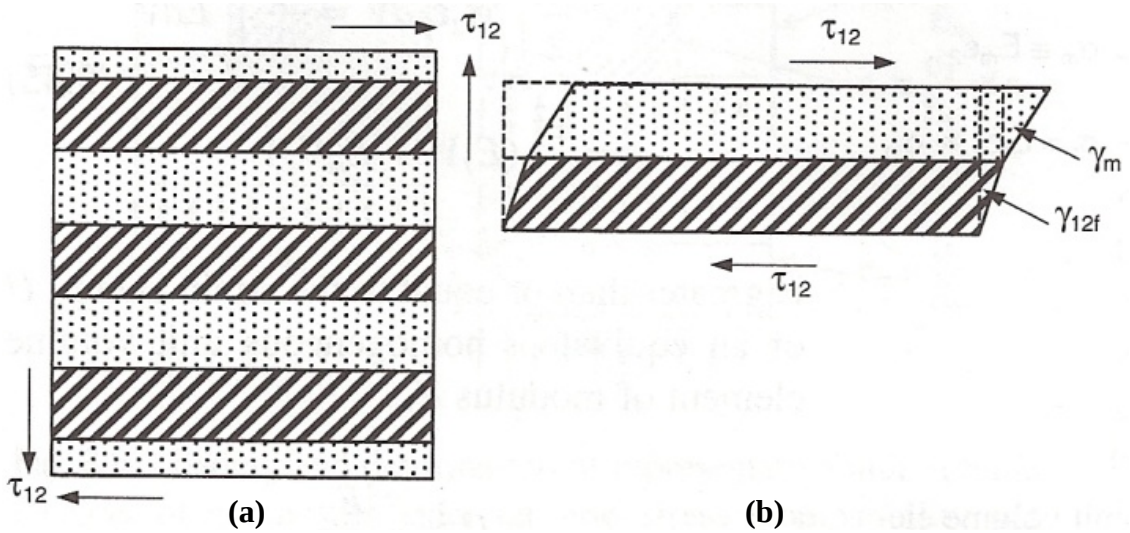

Figure 2.4. (a) Multiple layer shear (b) Single layer shear [2]

Interlaminar shear stresses and strengths are inherently dependent on the fact that there must more than 1 layer involved. When stacking multiple lamina together to form a laminated composite panel, regions between the lamina become of particular interest. These form an interlaminar region. Interlaminar stresses cannot be analyzed with ease. They may depend upon stacking sequence and shear and tensile strengths must be determined first.

Stacking sequence plays an important role in the amount of interlaminar shear stress at any given time. This is one of the few controllable variables. The orientation of shear stresses at the interlaminar interface can vary. There are 3 modes of shearing that can occur. Two of the 3 modes are out of plane, and one of the modes is in plane shearing. Figure 2.5 shows an example of these different modes of shearing with respect to a unidirectional lamina unit section. Stresses near the free edge tend to increase. The maximum shear occurs near the angle of 35^{o}.

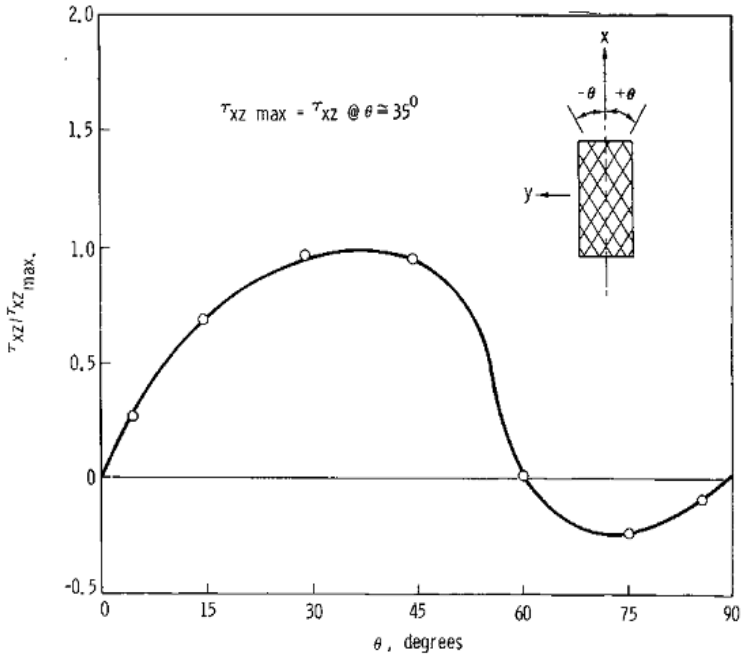

Figure 2.5. Graph of interlaminar fiber angle versus shear stress [112]

Laminate stacking sequences greatly affect the free edge interlaminar shear stresses and can give rise to stress concentrations. This is easily demonstrated on laminates with a circular hole in them. Two different laminates with two different stacking sequences each containing a hole of the same size were made. Each laminate was statically loaded while fringe stress patterns were observed. The fringe stress patterns observed indicated a difference in free edge interlaminar shear stresses [112]. Shear stress in an impact specimen causes a significant amount of damage at the interlaminar interface. Stacking sequences that increase interlaminar shears stresses due to mismatched D matrix should be avoided. Optimization of the coupling matrix may be desirable when using a laminate for energy absorption. Figure 2.6 illustrates the different orientations of interlaminar shear stresses.

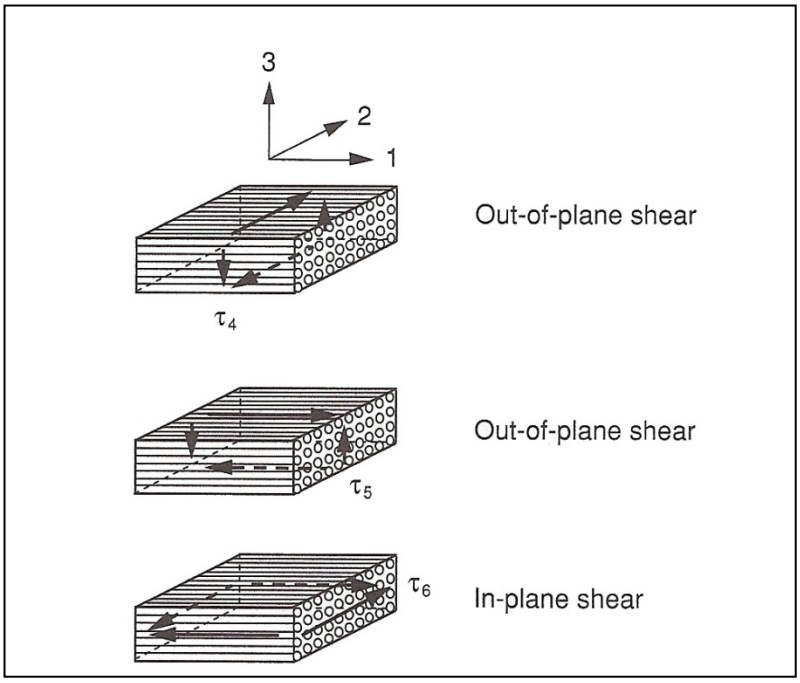

Figure 2.6. Interlaminar shear modes with respect to fiber orientation [113]

2.4 Failure Theories of Composites

Failure mechanisms of composites can occur in a variety of ways. "Failure" can have multiple definitions. It is essential that failure is well defined. Failure in terms of composites design is the nonconformance of a material system to perform in the way it was intended to perform. Therefore, if a structure were designed and intended to hold a specific amount of weight and it does not hold the weight as intended then the structure is deemed to have failed. Most of the time when an engineering failure occurs, a catastrophic event within the material takes place that causes the intended function of the part to not conform to the intended purpose. Typically a composite laminate is comprised of several constituents which usually are fibers and a matrix. The strength of the matrix is typically much weaker than that of a fiber. The matrix tends to have a much

lower modulus than the fiber therefore it is not as stiff. Failure will tend to originate in the matrix due to its lower strength. Matrix cracking is one type of failure that is likely to occur in composites. Figure 2.7 shows several types of failures in a laminated composite. This figure shows several different damage types. Delamination, matrix cracks, fiber breakage and matrix-fiber debonding are all different types of failure that can cause catastrophic failure. Matrix cracking is usually the first to occur and is a precursor to other failures.

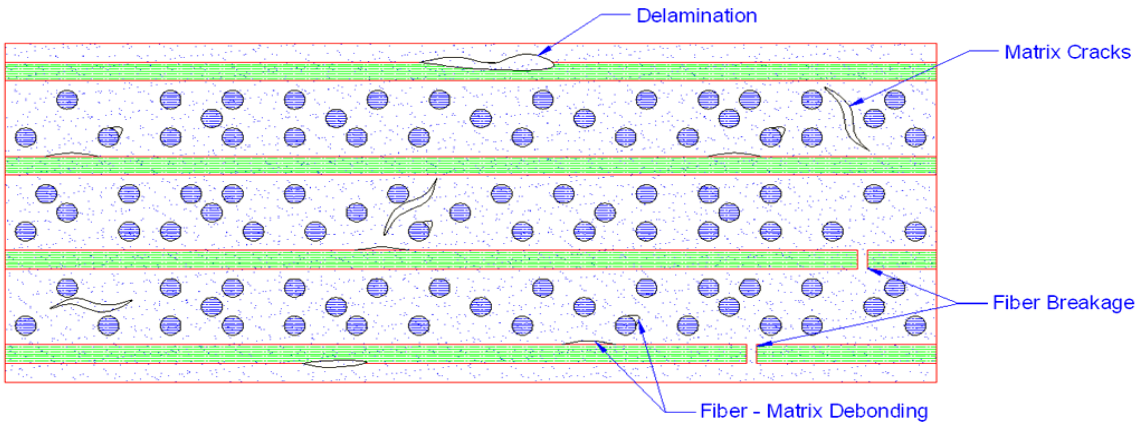

Figure 2.7. Laminated composites showing various failure mechanisms [2]

Delamination and matrix-fiber debonding occur second followed by fiber breakage. Several theories have been established over the last half century that addresses the failure of composites. Failure theories from isotropic materials were studied and developed. Initially, scientist and engineers studied these theories and adapted them to composites. Shortcomings of early theories led to an evolution of theories with more accurate predictions of catastrophic failure [114]. All of the failure theories available can be broken down into three distinct categories listed below.

1) *Non-interactive or limited theories*- These theories do not take into consideration all of the stress components in a given stress element. They simply compare each stress component to a maximum allowable. If the stress component stress state is higher than the maximum allowable the part is considered failed without regard to other stress components.
2) *Interactive theories*- These theories conglomerate all stress states into one equation. This master equation dictates whether or not a part will catastrophically fail.
3) *Failure mode based*- These theories give different failure criteria for fibers and matrices [114].

2.5 Fracture Mechanics and its Application to Composites

Fracture mechanics began as the study of cracks and abnormalities in everyday materials. Conventional mechanics of solids otherwise known as "Strength of Materials" does not take into consideration that all materials have flaws. It is well known that most all materials are not perfect. Most modern materials have inherent flaws that occur naturally or are purposely formed. The flaws may be large or small by design. In 1913, scientists noticed there must be stress concentrations around an elliptical hole in a tension specimen. Inglis then quantified the stress around the hole and this was defined as a 'stress concentration'. Figure 2.8 shows a schematic of a crack. A crack is defined as a discontinuity in atomic bonding throughout the lattice of an atomic structure. Inglis then quantified this new concept of stress concentration around the tip of the crack.

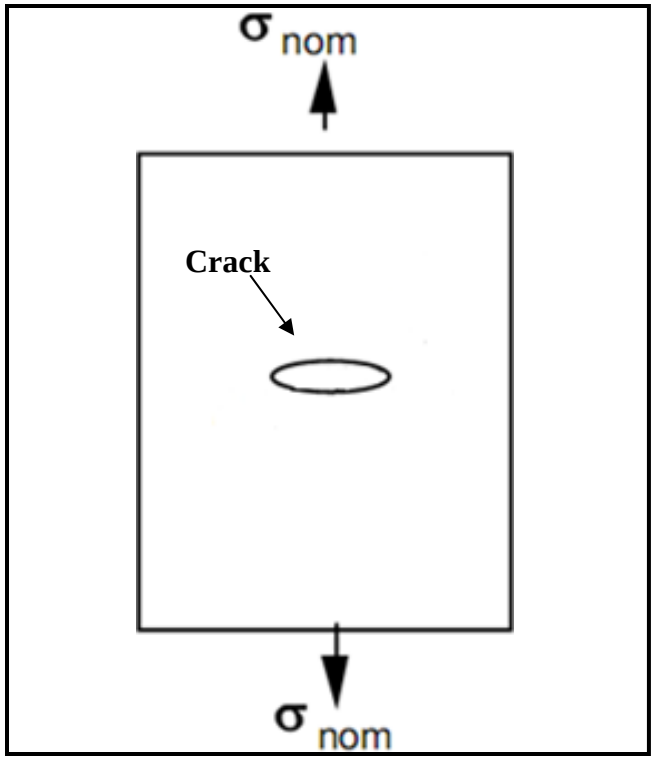

Figure 2.8. Schematic showing crack orientation [114]

It was observed that discrepancies exist between the theoretical strength in a metal and the actual strength of a metal. The theoretical strength of a metal was significantly higher than the actual strength. This sparked interest in research for answers in understanding cracks. In metals, fracture can occur in two different methods. Ductile failure is a distinctive failure mechanism that occurs with ductile metals. Brittle metals concurrently have a different mechanism that occurs. Either way, flaws within the material are present. These flaws give rise to cracks that can coalesce. Once these cracks coalesce they form a larger crack that can propagate. The stress field immediately around a crack tip is illustrated in Figure 2.9 below. It is clearly visible that the stress is highest at the tip of the crack. This is the reasoning behind the term ‘stress concentration’.

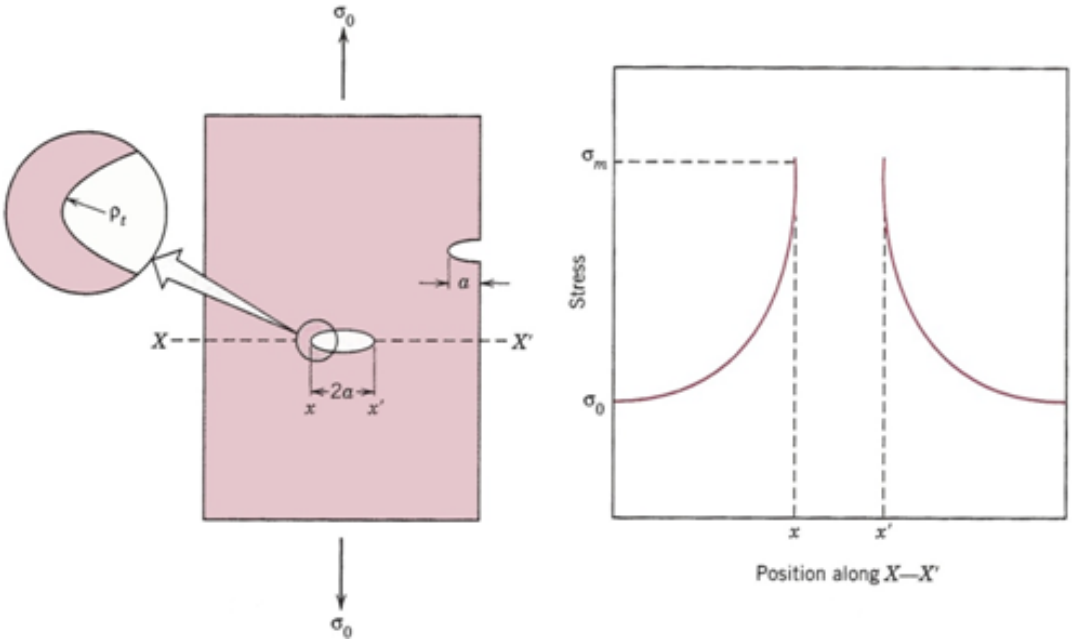

(a) **(b)**

Figure 2.9. (a) Crack proximity (b) Stress field near crack tip [2]

Irwin continued research into fracture mechanics and is known as the 'Father of Fracture Mechanics'. He developed Inglis's and Griffith's prior work into a well known modern equation that relates the stress concentration, applied stress, and crack size.

$$\sigma_f = \sqrt{\frac{E(\gamma+\gamma_p)}{\pi a}} \qquad 2.12$$

The numerator is a property of the material and can be condensed into a single variable.

$$\sigma = \frac{K}{\sqrt{\pi a}} \qquad 2.13$$

Solving equation 2.13, for K, yields equation 2.14.

$$K = \sigma\sqrt{\pi a} \qquad 2.14$$

Equation 2.14 is a well known fracture mechanic equation. K is known as a stress concentration level and can be related to residual strength. It can be characterized as the

strength of the singularity of stress at the crack tip. When stress is increased or if the crack size is increased a critical value of stress concentration will be reached. This critical value of stress concentration is known as K_{IC}. This term is the maximum stress concentration any particular material can resist before a crack will propagate at the speed of sound through the material with an applied stress (σ) [114].

2.5.1 Fundamentals of Fracture Mechanics

The origin of a new term called 'stress intensity factor' was a huge spark for the beginning of what is now called fracture mechanics. Fracture mechanics is the study of materials based on the fact that all materials contain flaws. It is unlike the strength of materials approach which neglects the fact that all materials contain flaws. The fracture mechanics approach is centered on the flaw. Stress intensity factor (K) is a variable that is used to describe multiplication of applied stress around a stress riser. Some of the concepts fracture mechanics attempts to address are as follows:

- The residual strength of a structure as a function of crack size,
- The maximum size of a crack that can be tolerated,
- Amount of time a crack grows from its initial size to its maximum size,
- The largest permissible crack size when a structure is built
- Inspection interval of the structure.

Early fracture mechanics research began with metals. After realizing that metallic materials contained flaws and they must dealt with, researchers focused their attention on quantifying the various parameters of flaw design. Eventually, the concepts developed in metals were adapted to composite materials. Similarly crack propagation can be

analyzed in various ways as has been done in metals. Most concepts of fracture mechanics for metallic materials can be adapted to composite materials.

2.5.2 Application to Composites

Conventionally fracture mechanics do not use the same parameters for composites and metallic materials. Metallic materials use the parameter K_{IC} to describe the materials ability to absorb energy in order to propagate the crack. In composite materials, an alternative parameter is used known as the strain energy release rate defined in equation 2.15.

$$G = \frac{K^2}{E} \qquad 2.15$$

G is the strain energy release rate at the crack tip field opening. It has 3 different modes of operation. Each mode has an associated critical value. The different modes are illustrated in Figure 2.10. Mode I is known as the opening mode and is out of plane. Mode II and mode III are two different shearing modes that are in plane shearing. In composites, the energy release rate of a composite typically is highly dependent on the matrix of the composite. Both K and G measure the severity of the crack tip. G is directly related to delamination resistance in a composite material. The higher the energy release rate the more resistant to delamination is that particular composite. Therefore, it may be desirable (or not) to have a high energy release rate in a particular composite. Instances where high energy release rates would not be desirable are energy absorption material situation. An example may be in an impact where the composite absorbing energy is desirable. G is determined by taking the differential of the strain energy with respect to crack length as shown in equation 2.16.

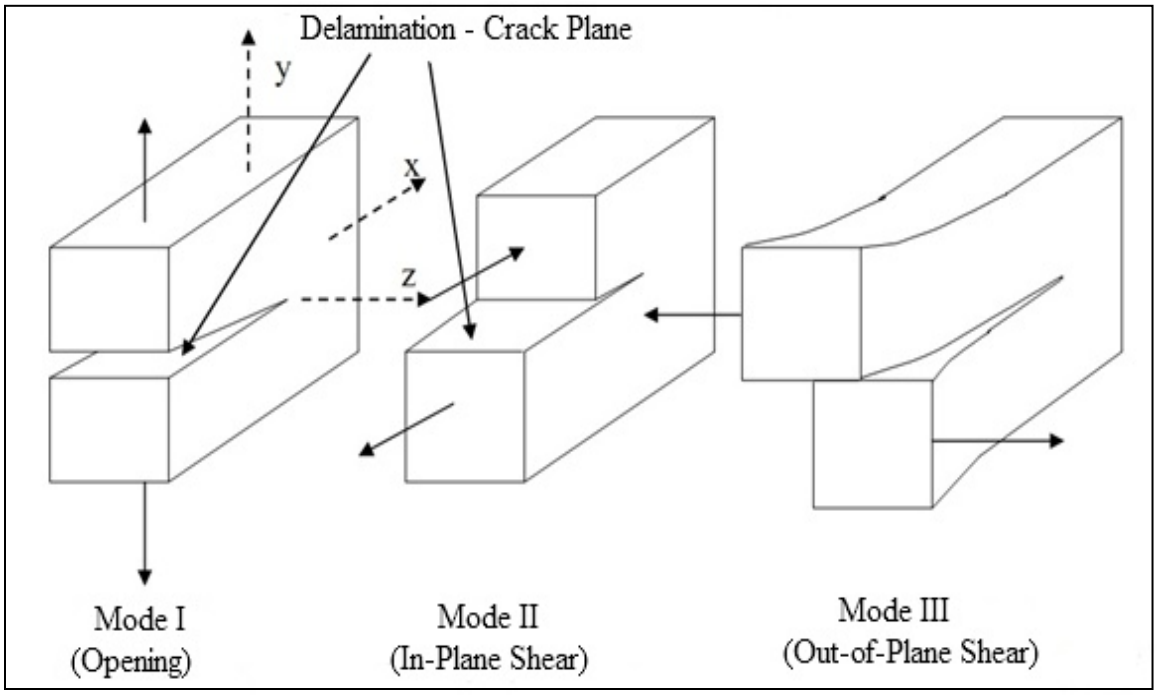

Figure 2.10. Delamination/crack plane various modes [114]

$$G = -\frac{\delta \Pi}{\delta a} = -\frac{1}{2}\left[F_x(u_{u,x} - u_{l,x}) + F_y(v_{u,x} - v_{l,x}) + F_z(w_{u,x} - w_{l,x})\right] \qquad 2.16$$

Equation 2.16 is the total energy release rate for the composite laminate. In practice though, specific tests are devised so that standards are met during actual measurement. Determination of G_I is measured by the following ASTM D 5528 standard. Figure 2.11 shows a typical piano hinged double cantilever beam that would be used in a frame machine to determine G_I empirically. Other standards are written for similar testing for in plane energy release rates. The piano hinges are pulled in a test frame and crack propagation is recorded. A sheet of Teflon is inserted into the laminate. The sheet forms the edge of the initial crack. Once pulled by the test frame, the crack begins to propagate through the material in the interlaminar region of the composite.

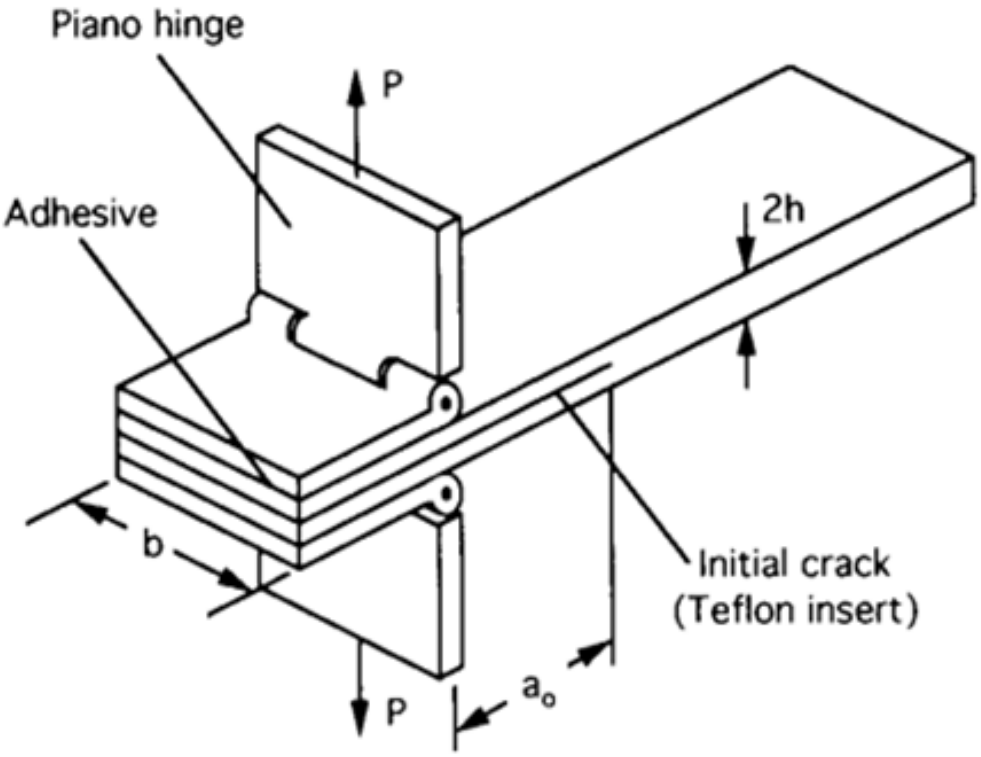

Figure 2.11. Drawing showing a double cantilever beam specimen used for G_I calculation [114]

According to ASTM Standard 5528 accounting for crack-delamination correction (Δ), G_{IC} determination is made by equation 2.17:

$$G_{IC} = \frac{3P\delta}{2b(a+|\Delta|)} \qquad 2.17$$

In fracture mechanics, analysis of the crack predicts when the crack will start to propagate. This occurs when the thermo-elastic strain energy release rate is equal to or above the fracture toughness of the matrix. Delamination fracture is a matrix dominated event. The matrix has much lower fracture toughness than the fibers. Fiber-matrix debonding is a common failure near the interlaminar interface. G_{IC} is the critical energy release rate. Mode II strain energy release rate is expressed by equation 2.18

$$G_{IIC} = \frac{9P^2a^2}{16E_1b^2h^3}\left[1 + \frac{1E_1}{5G_{31}}\left(\frac{h}{a}\right)^2\right] \quad 2.18$$

Figure 2.12 shows the type of specimen that may be used to determine the critical energy release rate of a composite specimen in Mode II.

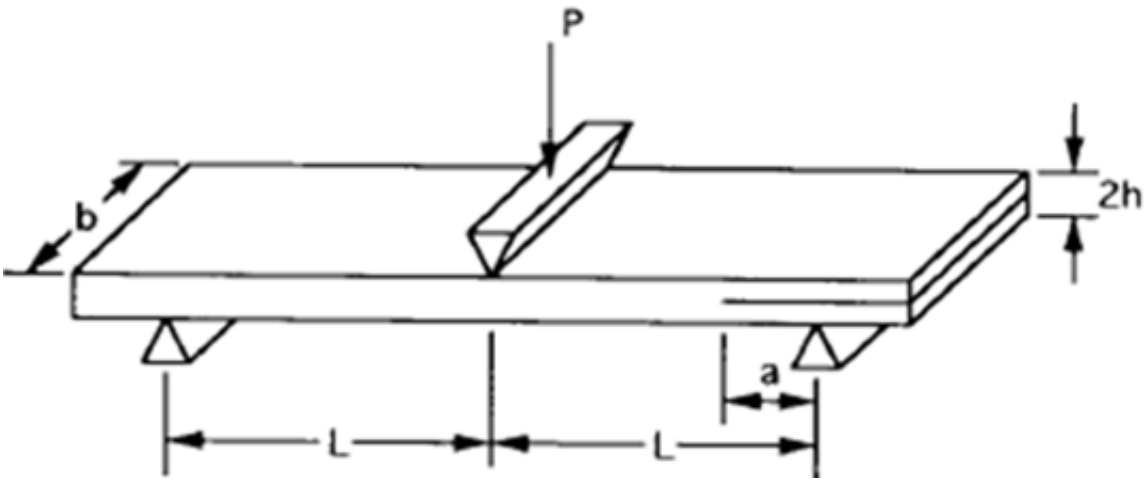

Figure 2.12. End notched specimen used to determine G_{IIC} [114].

Energy release rate is a significant parameter when considering impact energy absorption. The amount of energy that a particular composite laminate can absorb during the delamination phase of failure is highly dependent on the various energy release rates of the matrix. The amount of deflection a particular laminate experiences will also increase the energy release and may overcome the critical value. If this occurs, then the delamination crack will continue to propagate until the energy input is lower than G_{XC}. G_I is the total amount of work done by external force on the crack length.

Relevant composite material mechanics previously presented forms the basic knowledge relevant to the current research. The theories and knowledge presented will

be used for comprehensive understanding of phenomena related to energy absorption of laminated composites upon impact loading. Chapter 3 discusses the manufacturing of glass nanofibers for use in laminated composite materials.

CHAPTER 3

MANUFACTURING OF GLASS NANOFIBERS USING ELECTROSPINNING

Production of a nanofiber begins with the understanding of a solution-gelatin (sol-gel). A sol-gel is a mixture of components that, when mixed properly, achieve a final material can be electrospun to manufacture glass nanofibers. Presently, there are over 100 different polymer sol-gel combinations that may be used in conjunction with electrospinning. Glass nanofibers begin with the chemical reaction of a solution that is mixed in several stages. The solution is then aged to achieve a desired viscosity.

The motivation behind the current research is the assumption that as the dimensions of a structure become smaller, the less prone are the flaws. Certain types of flaws within the metallic structure increase the overall strength. Examples of such flaws are interstitials and grain boundaries. Both interstitials and grain boundaries restrict the movement of dislocations while increasing strength. As the overall size of the structure is reduced the probability for flaws to form is reduced as well. For a given structure such as a cable, a single flaw may prove to be fatal. In contrast, if large cables made up of many smaller fibers were to have a single flaw then the residual strength would be affected only slightly. Having multiple fibers allows the structure to change the failure mechanism. As the cable diameters are reduced and the number of cable themselves increased the overall area is kept constant. This concept is illustrated in Figure 3.1 of a cable comprised of different amount and sized fibers. With the smaller fibers, as the

fibers break, the remaining fibers take on the additional load of the broken fibers. This load transition slows down the overall failure of the cable. If a single fiber cable breaks, failure can occur suddenly and catastrophically.

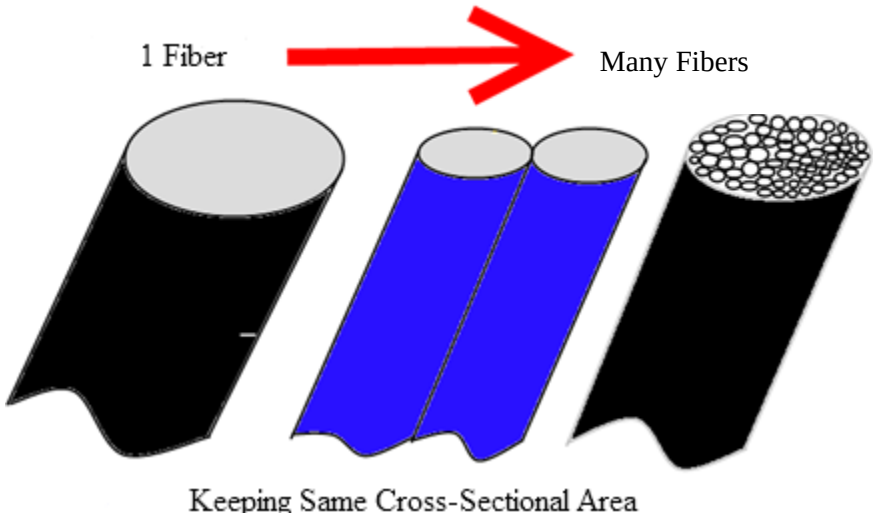

Figure 3.1. Schematic showing concept of using smaller fibers versus larger fibers

The reduction in diameter and increased number of fibers is the main motivation for making smaller fibers versus larger fibers. There are fibers on the order of billions when manufactured on the nano-diameter scale. Changing the fiber diameter in order to change the failure mechanism also has other implications. The toughness of the material may change as well. Increasing toughness is a very desirable attribute. Toughness has many definitions. It may be defined as the total amount of energy absorbed before the part fails. Another way to define toughness is the area under the curve of a stress-strain ($\sigma - \varepsilon$) graph. Therefore, increasing the total amount of energy absorbed is highly desirable. Figure 3.2 shows the concept of increasing toughness by viewing the area

under the curve of a sample stress-strain graph. From this it is clearly evident that as strain increases as well as stress, toughness correspondingly increases.

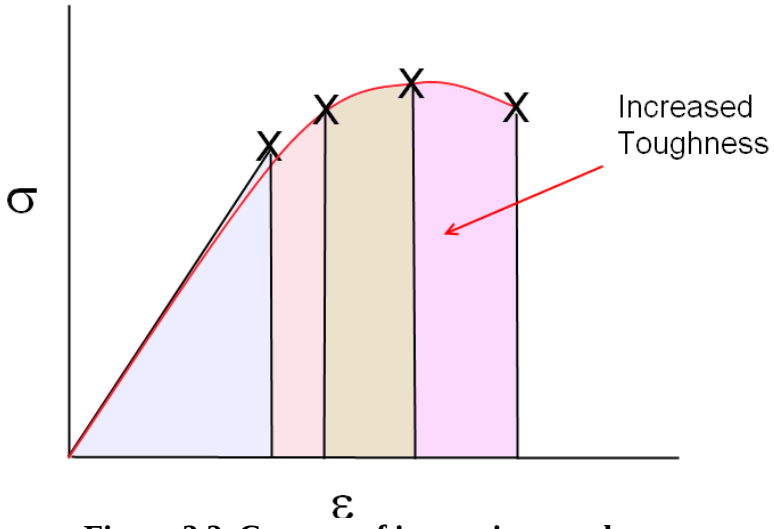

Figure 3.2. Concept of increasing toughness

Reduction in glass fiber diameters increases toughness. There are a variety of ways to form fibers with nano-scale diameters. One-dimensional fiber formation is very limited with its ability to scale up production wise [115]. Electrospinning provides an inexpensive and very scalable means to provide excellent nanofibers on a large scale. Nanofibers formed using the electrospinning procedures are used in a variety of ways. The dominant use of most electrospun fibers is in the biomedical field. Several parametric issues became clear as the experimental setup was being initiated. These issues will be discussed in detail and a clear understanding of the causes will be provided. For the current research work, the flow chart in Figure 3.3 was used as a guide for all the experimental work.

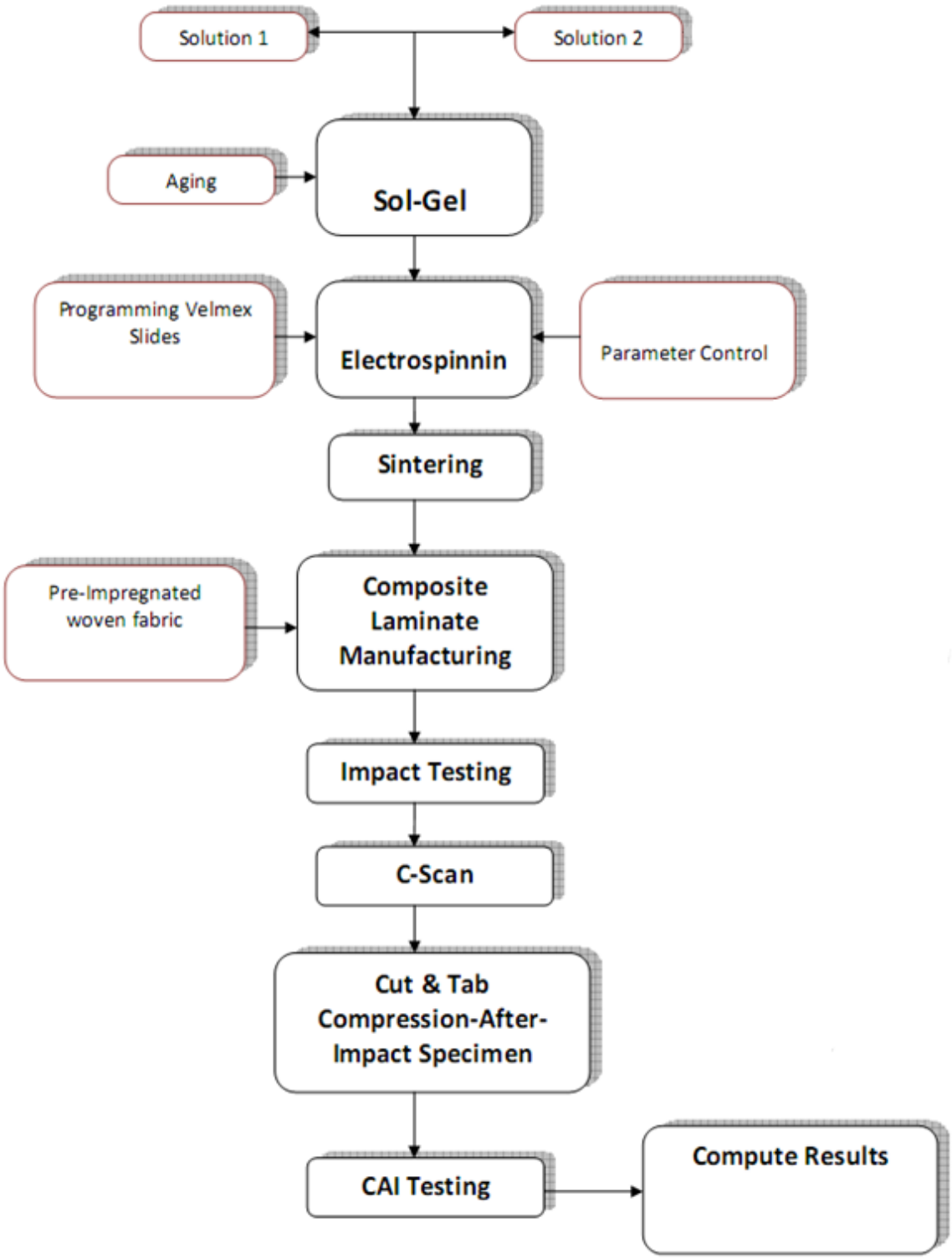

Figure 3.3. Flow chart of work

3.1 Tetraethylorthosilicate Sol-Gel Formation

Glass nanofibers were produced using a four part solution. The components were mixed and aged. The main ingredients for the mixture were Tetraethylorthosilicate (TEOS), ethanol, hydrochloric acid, and deionized water. TEOS sol-gel formation began with the individual constituents. The following chemicals were used to prepare TEOS sol-gel.

1) *Tetraethylorhosilicate* 98% made by Acros Organics. Purchased from Fisher Scientific website item number AC15781-0010. The TEOS purchase had the following properties: Molecular Weight: 208.33, $C_8H_{20}O_4Si$, Freezing Point: 45°C, Boiling Point: 166°C
2) *Ethanol Anhydrous (EtOH)* 95.27% histological grade, clear, and colorless. The ethanol was also purchased from fisher scientific item number: A405F-1GAL. Contents consisted of Et-OH 95.27%, Methyl Isobutyl Ketone, 1.0%; Ethyl Acetate, 1.0%; Hydrocarbon, 1.0%.
3) *Deionized Water (H_2O)* The deionized water was supplied by fisher scientific. Item number: 23-751-628.
4) *Hydrochloric Acid (HCl)* Hydrochloric acid 500mL (certified ACS Plus) was supplied by fisher scientific. Item number: A144S-500.

The Tetraethylorthosilicate solution was first mixed into two smaller sub-solutions given as:

Solution A: TEOS (95.5g) + EtOH (10.425g)

Solution B: EtOH (10.425g) + Deionized Water (4.125g) + HCl (0.0825g)

For solution B, the deionized water was first mixed with HCl that was slowly dripped into EtOH. For A and B, both solutions were mixed in 200mL beakers using an OHAUS Scout Pro 2000g scale. Solution B was dropped into solution A at a rate of 1 drop every 20 seconds. A 50ml burette was used to control the speed of the droplets. Solution A was placed in a 200ml plastic flask. The flask was placed on top of a magnetic stirrer. The stirrer speed was set such that there was a slight vortex of approximately 6mm deep. Figure 3.4 shows the setup for the mixing operation. Mixing was conducted in a closed vented hood in compliance with local safety codes.

Figure 3.4. Picture of burette mixing solution B to solution A

Most sol-gel solutions weighed approximately 200-215 g after final mixing. Figure 3.5 shows an example of a solution after being mixed with all 4 components. Solution mixing occurred at room temperature and ambient humidity levels. If mixing

occurred too fast, white flocculent precipitates were formed and became evident. This was an undesirable effect. Slowing the drop rate prevented the solid precipitates from forming. After final solutions were mixed they were kept at ambient temperature of 22-25^{o}C. They were stored in a dry container that prevented air currents from flowing over the top of the flask.

Figure 3.5. Picture of final mixed solution

3.2 Hydrolysis and Polycondensation of $Si(OC_2H_5)_4$

The hydrolysis and polycondensation of tetraethylorthosilicate have been studied over the past several decades by various researchers. Conversion of $Si(OC_2H_5)_4$ into SiO_2 can be achieved with different techniques. The transition of gels into oxides has

been investigated using techniques such as thermal analysis, x-ray diffraction, and electron microscopy and so on. One specific mixing formula has proven to achieve better spin-ability rates than others [116]. The reaction occurs as follows:

$$n\mathrm{Si(OC_2H_5)_4} + 4n\mathrm{H_2O} \rightarrow n\mathrm{Si(OH)_4} + 4n\mathrm{C_2H_5OH} \qquad 3.1$$

Equation for hydrolysis,

$$n\mathrm{Si(OH)_4} \rightarrow n\mathrm{SiO_2} + 2n\mathrm{H_2O} \qquad 3.2$$

Equation 3.2 above illustrates the occurance of polycondensation. Notice the formation of water molecules.

$$n\mathrm{Si(OC_2H_5)_4} + 4\mathrm{H_2O} \rightarrow n\mathrm{SiO_2} + 4n\mathrm{C_2H_5OH} \qquad 3.3$$

Equation 3.3 illustrates the net overall reaction that occurs. Hydrogen chloride was found to be a very good catalyst for the reactions. Ethanol was used to dilute the mixed solutions such that there were no precipitates during mixing of solution B to solution A. The formation of chain-like polymers during the hydrolysis of titanium alkoxide has been reported by other researchers [117, 118]. It is assumed that a similar type of hydrolysis polycondensation occurs for tetraethylorthosilicate catalyzed by hydrochloric acid. If this is true the hydrolysis of $\mathrm{Si(OC_2H_5)_4}$ catalyzed by HCl is shown:

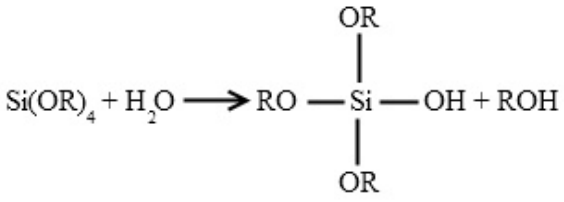

Where R = $\mathrm{C_2H_5}$ and hydrolysis begins to occur.

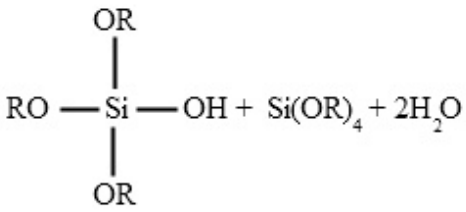

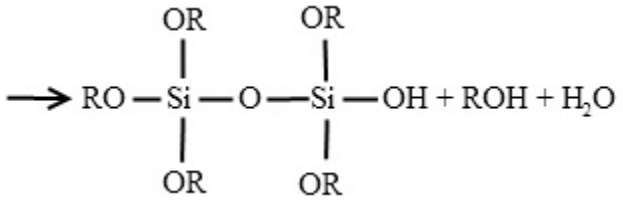

Polycondensation is observed by the chain of OR-Si monomer as it begins to grow in size.

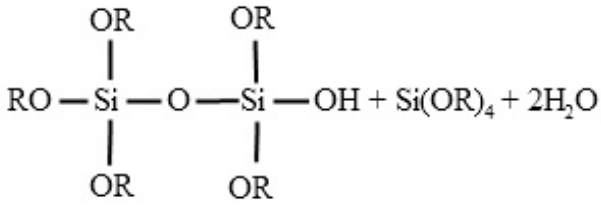

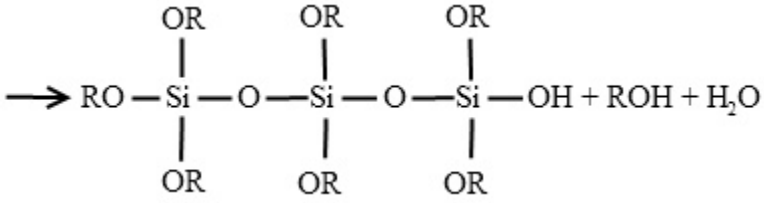

The addition of the polymer chain is larger, so polycondensation continues to occur.

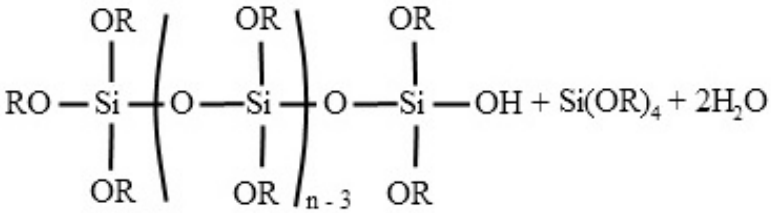

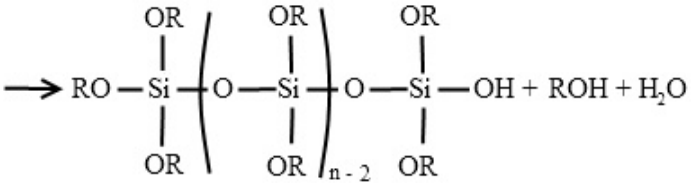

The previous chain illustrates the reaction in the late stages of sol-gel formation.

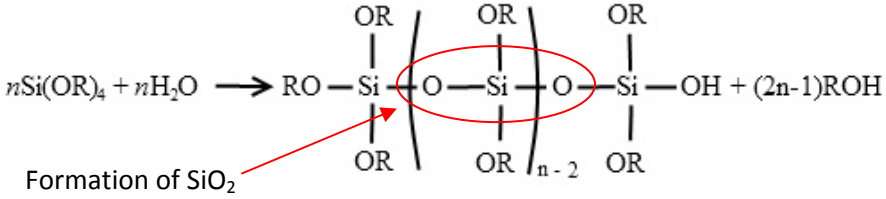

The SiO_2 formation shows the net result of hydrolysis and polycondensation catalyzed by HCl [116]. Equation 3.4 shows the net balanced chemical equation for the sol-gel reaction.

$$nSi(OC_2H_5)_4 + 4H_2O \rightarrow nSiO_2 + 4nC_2H_5OH \qquad 3.4$$

Aging of the solution is a necessary step because the above chemical changes do not progress rapidly. The reactions occur at a relatively slow rate. It takes varying amounts of time to achieve the final product of SiO_2. The amount depends on the temperature and surface area of the container holding the sol-gel. During preparation of the sol-gel, data was recorded in order to establish the rate at which the solvents evaporated. Ten different solution's weights were recorded during the aging process and their data averaged to establish an evaporation rate. Figure 3.6 shows the solution weights as a function of time. Their evaporation rates were subsequently calculated. Humidity levels of 30 – 70% were observed at different periods and season in a year. During the curing stage the sol-gel was placed in an area in which the building's ventilation system would have little influence.

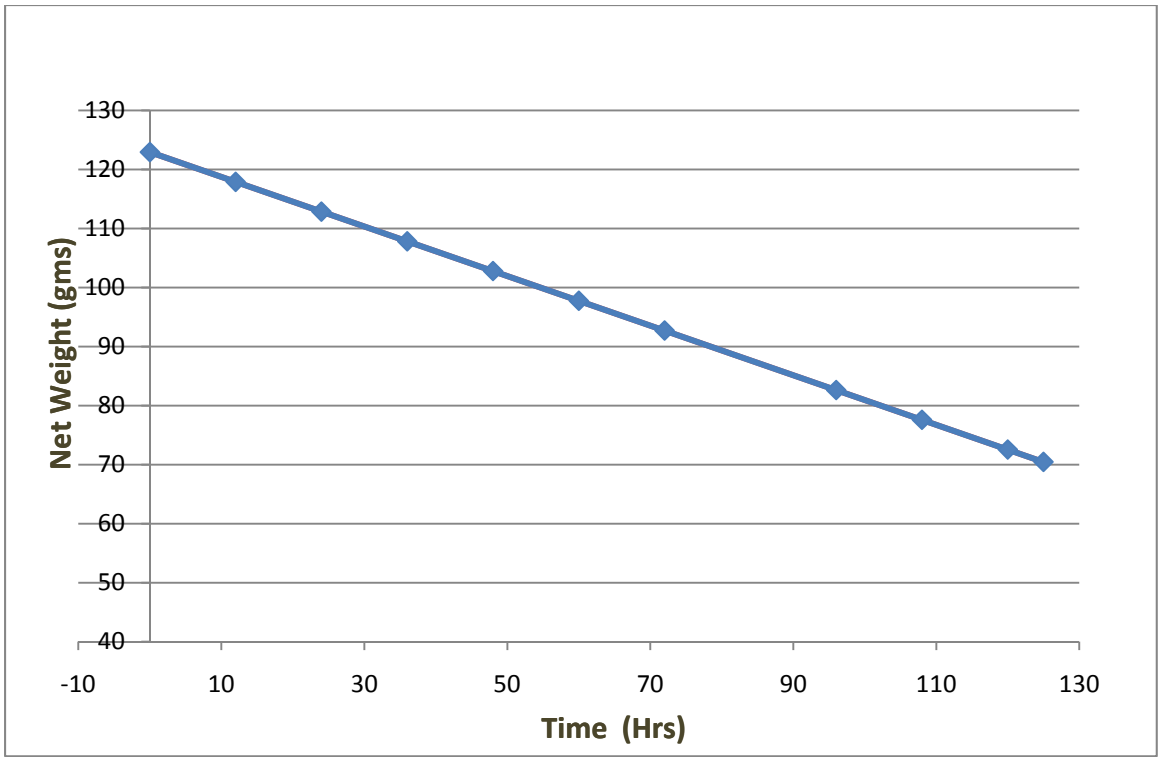

Figure 3.6. Graph of average weight loss during curing state of sol-gel

Freshly mixed solutions took approximately 5 days at an ambient temperature of 23 ^{o}C to reach a spinnable state. Several steps were taken to extend the life of the spinnable sol-gel once it reached the spinnable state. One technique implemented was to cover the plastic flask with aluminum foil very tightly. This helped timing control by preventing the evaporation of additional ethanol and thus kept the sol-gel diluted so that spinning may occur. A second technique implemented was to freeze the sol-gel slightly prior to reaching the mature spinnable state. This would also slow down the chemical reactions occurring in the solution. It also slowed the evaporation rate as well. Both techniques were used in manipulating the sol-gel such that spinning could occur at a preferred interval of time.

3.3 Experimental Setup of Electrospinning Production

Electrospinning is the process in which an electrostatic potential charge is applied to a polymer solution. The solution is then attracted to anything at ground potential. This attraction pulls the sol-gel into a very small diameter fiber. Once the fiber is out of the spinneret and in the electric field region it is dominated by the electric field. The electric field causes a whipping action due to bending instability. This action further decreases the diameter of the fiber. If all the various parameters are approximate then a non-woven fabric mat of glass nanofibers would be deposited onto the ground collector. Four main components are needed for electrospinning production. Table 3.1 describes the function of each component for the production of glass nanofibers.

Table 3.1. Description of electrospinning setup components

Item Number	Component	Description of Component
1	Power Supply	Provides electrostatic charge to the polymeric sol-gel
2	Syringe Pump	Pumps sol-gel at a prescribed rate through the spinneret
3	Spinneret	Provides a small orifice through which the sol-gel is pumped
4	Collector Plate	Collects deposition of the un-sintered glass nanofibers
5	CNC controlled table	Moves collector plate to obtain even deposition

The sol-gel is placed into a 30ml syringe with an inside diameter of 26mm. The syringe was then loaded into a Model NE-1000 Multi-Phaser dispensing pump supplied by New Era Pump Systems Inc. This model syringe pump has a capability to hold a

variety of different syringes. It must be programmed in order to display accurate dispensing rates. The interior diameter of the plastic syringe was correctly programmed into the NE-1000 syringe pump. The pump can be programmed to dispense an allotted volume or programmed to dispense a rate. The NE-1000 syringe pump has the capability to dispense at a rate between 0.1 μl/min and 10 ml/hr. A schematic of the electrospinning setup can be seen in Figure 3.7 below.

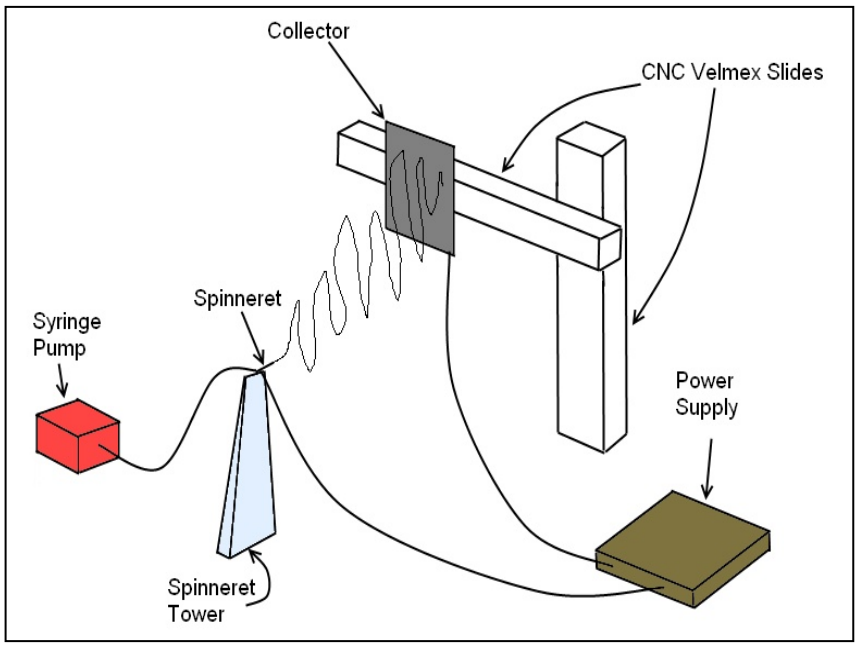

Figure 3.7. Schematic of electrospinning setup

Once the solution was pumped into the spinneret, it becomes charged. The charged fluid was attracted to a surface which had a lower potential. While the sol-gel was pulled toward the collector, the internal viscosity and surface tension were resisting the pulling action by the potential difference. To charge the spinneret, a FC series 120

watt regulated high voltage power supply was used. The power supply was capable of supplying up to 30 kV. During the electrospinning process it was noted that virtually no current was flowing between the spinneret and collector. An integral ammeter on the power supply indicated current flow. However the current, during the process, was very low and the indicator did not indicate any current flow. The attraction of the sol-gel in the spinneret towards the collector plate was inhibited by the inner hydrostatic forces of the viscous fluid. These intrinsic forces caused the sol-gel to form a 45^{o} angle cone. This cone formation was initially discovered by Geoffrey Taylor. The cone is now referred to as the 'Taylor Cone' [119].

The Taylor cone emanates from the tip of the spinneret. After the Taylor cone forms, the electrostatic force on the sol-gel overcomes the combination of internal viscosity and surface tension elongating the sol-gel into a fiber with several microns diameter thick. Bending instability occurs roughly 1 to 2 mm from the Taylor cone which triggers a whipping action of the fiber. The whipping action continues to elongate the fiber further decreasing the diameter. Fiber diameter also decreases across the gap due to the evaporation of solvents. The evaporation of solvents is accelerated by the area-to-volume ratio increasing significantly. Evaporation of the solvent during the transitional stage between the spinneret and collector is a necessary step. In addition to creating smaller diameter fibers, the excess solvent prevents the nanofibers from sticking to one another between the spinneret and collector plate resulting in a smoother deposition. The actual experimental setup is shown in Figure 3.8 for electrospinning operation in the present study.

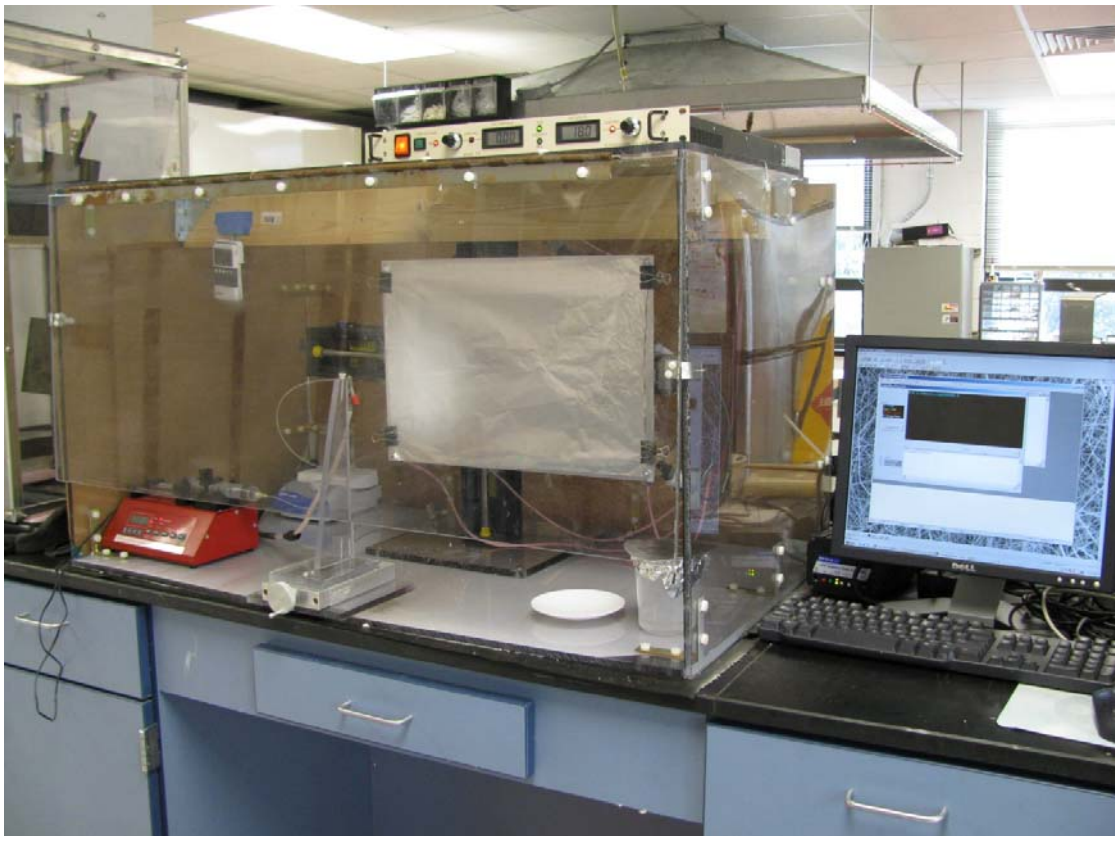

Figure 3.8. Picture of experimental setup

Figure 3.9 shows an example of the Taylor cone and the bending instability immediately after the Taylor cone. Once the fiber reduces in diameter the surface-to-volume ratio decreases significantly. The reduction in the ratio increases the fiber's ability to easily evaporate any remaining solvents. The reduction in evaporated solvents further decreases the fibers diameter. The whipping action of the fiber ensures a random un-woven mat deposition. Therefore, it is assumed that in-plane properties are quasi-isotropic. Deposition occurred onto a collector plate made of aluminum. The aluminum collector's dimension is 14 in. x 17 in x 0.25 in. The collector is grounded to the power supply.

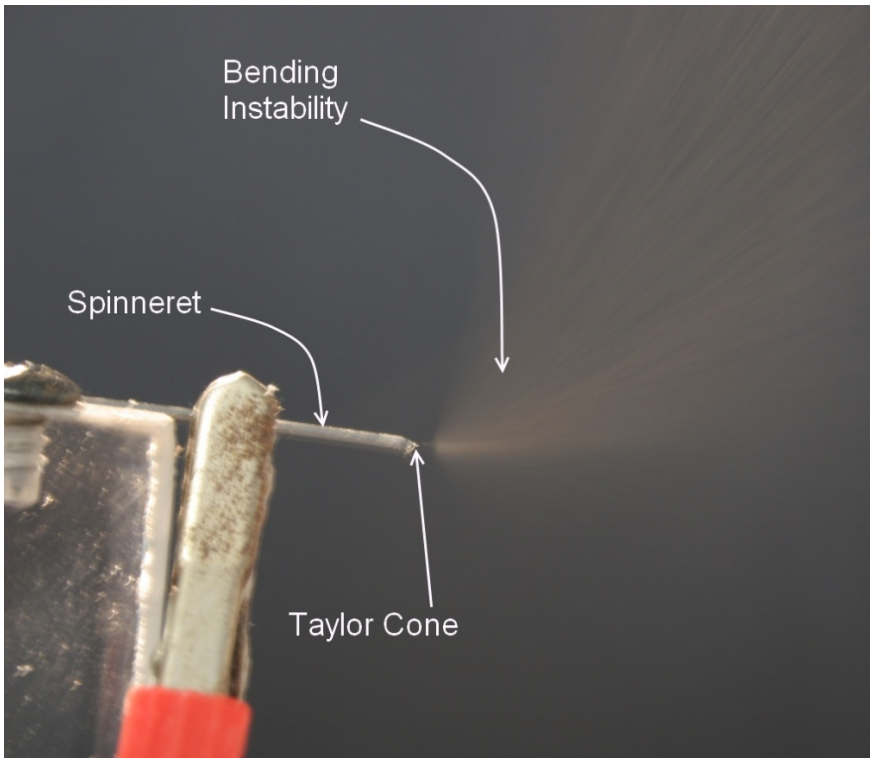

Figure 3.9. Picture of spinneret, Taylor Cone, and bending instability

In order to create a 'sheet' of nonwoven electrospun glass nanofibers, the collector plate was attached to a computer numerically controlled (CNC) screw slide. Two slides were used in conjunction with one another to give a 2 degrees-of-freedom motion. The height and lateral position of the collector plate could be controlled. The two linear slides were fastened to one another and the collector plate fastened as well. The linear slides were connected to a computer that was programmed to control the motion of the collector plate. Figure 3.10 shows an example of a slide from Velmex that was used in this work. Programming of the slide was performed with a computer control program named COSMOS. COSMOS was used to control the position and trajectory of the collector plate.

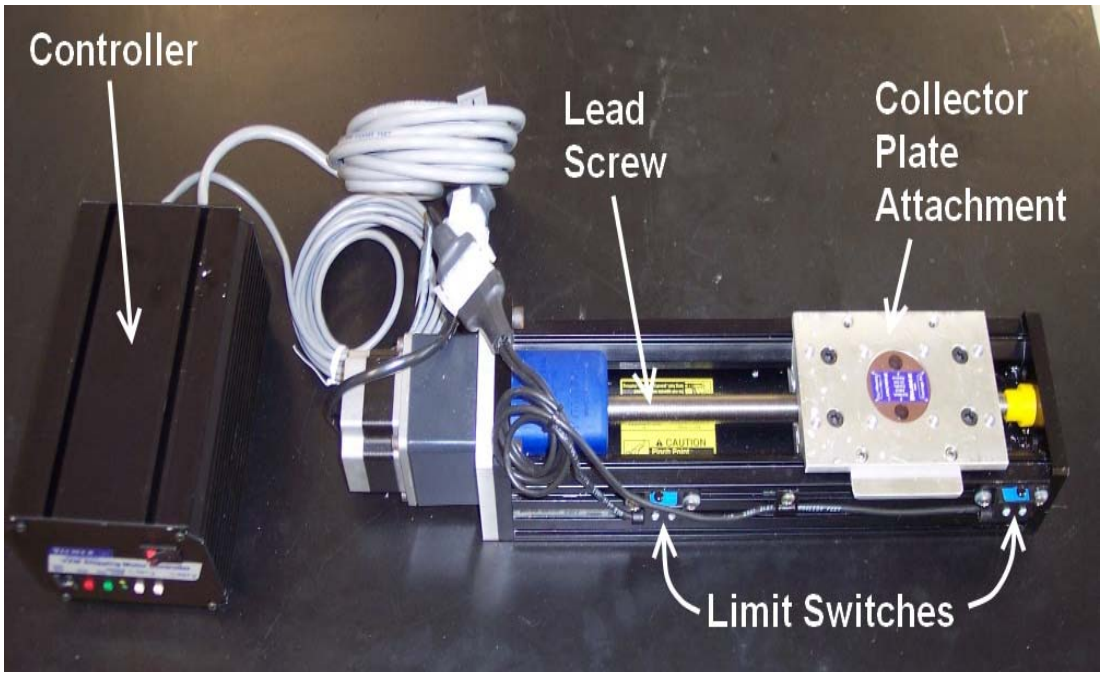

Figure 3.10. Picture of 12 in. Velmex linear slide

The deposition area of static collector plate was approximately 3 inches in diameter. Therefore, a deposition plan was developed with the most efficient use of time and the least amount of overlap between the depositions. Figure 3.11 shows a screen shot of the Velmex program and the deposition plan. The plan was developed to achieve the proper thickness and consistent results across the various runs. The total height of 12 in. allowed for three deposition loops in order to achieve total coverage of the collector plate. The three deposition loops were evenly spaced. The program has a very simple graphical user interface so that operators of various skill levels may be able to use it. Two different instructions were used within the COSMOS software. The first instructions return the collector plate to a home position. The "home position" is the starting point to run program.

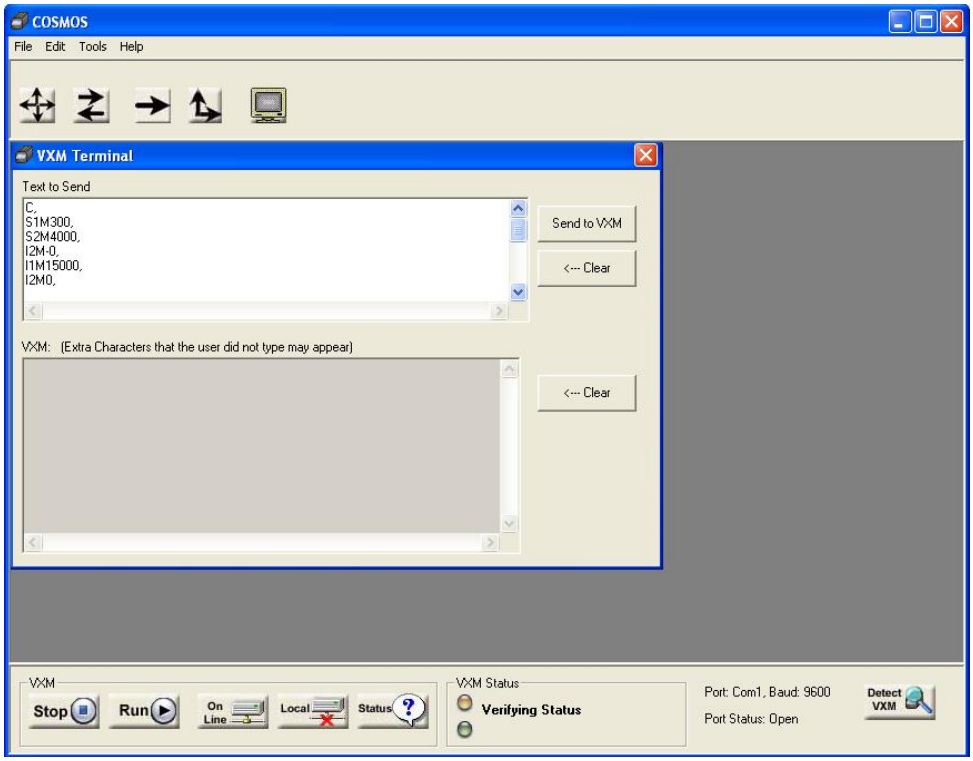

(a)

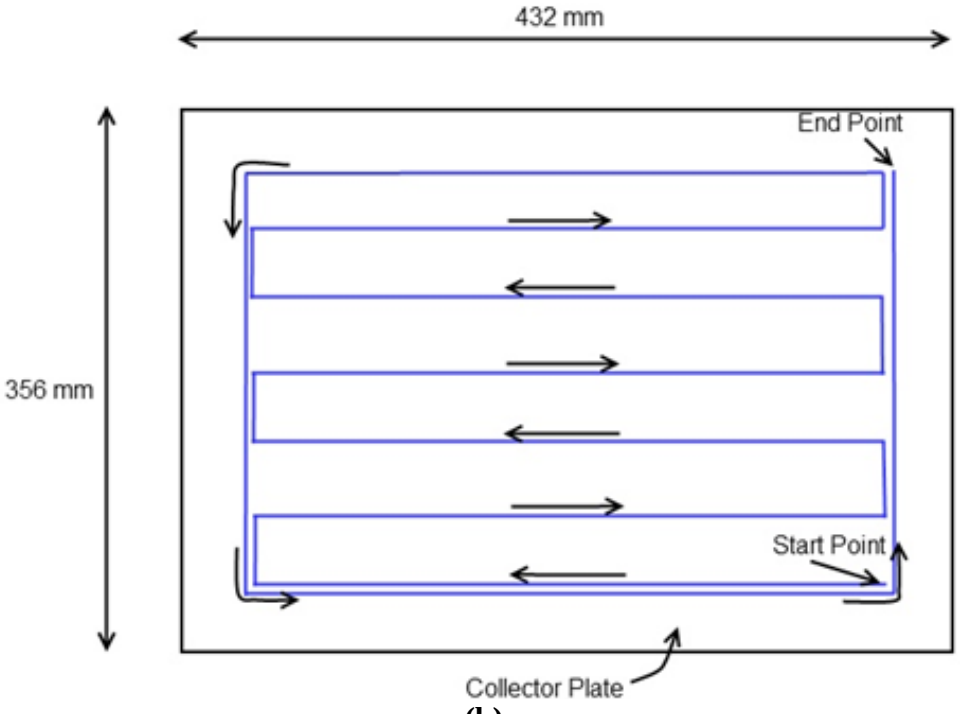

(b)

Figure 3.11. (a) Screenshot of the program COSMOS used to control deposition plan, (b) Deposition plan used for collector movement

The optimal selection of the experimental parameters was crucial in obtaining quality glass nanofiber sheets. Every effort was taken to minimize the number of defects such as beading and fiber breakage. Controllable parameters of the process were viscosity, surface tension, applied voltage, spinning distance, collector position and velocity, as well as conductivity of the sol-gel. Maximizing the spinning time by extending the spinnable viscosity was discussed previously in section 3.2. Controlling the parameters over the entire process required meticulous concentration and it was difficult, at times. The objective of this portion of the work was to manufacture the smallest diameter nanofibers possible while controlling quality and quantity.

3.4 Deposition Voltage and Distance

Deposition voltage was carefully selected in order to achieve the smallest diameter fibers. Concurrent research was to determine how the voltage correlated with the diameter of the fibers produced. Shendokar conducted tests to determine the voltage and distance that would result in the smallest diameter fibers. Four voltage levels between 15 kV and 18 kV were selected in a systematic fashion. The distance between the spinneret and collector plate was varied from 70 mm to 100 mm. Multiple glass nanofibers sheets were spun at each setting and inspected with a scanning electron microscope [120]. Figure 3.12 shows the samples taken from each of electrospun sheets. The SEM images were inspected in imaging software to determine the diameter of the glass nanofibers at each setting and the average diameter at each setting was calculated using software.

Figure 3.12. SEM sample to determine fiber diameter [120]

Figure 3.13 (a) shows the average diameter of the glass nanofibers at each setting. From this diagram, it is clear that the combination of voltage of 18 kV and a distance of 70 mm provide the smallest diameter fibers. SEM images of the sample used for analysis purposes are also shown in Figure 3.13 (b). The SEM images show that the glass nanofibers are free from defects and the diameters are consistent throughout the deposition area. The fiber orientation show no set pattern and are deposited in such a manner that makes them quasi-isotropic. The increase in the distance between the spinneret and the collector plate tend to increase the diameter of the fiber due to lower electric field strength. Increased spinneret distance also tends to increase the area of deposition so there must a balance between the two parameters. The optimal setting seems to be at high voltage and a relatively short distance of 70 mm.

Distance / Voltage	70 mm	80 mm	90 mm	100 mm
15 kV	669 nm Sheet 27	903 nm Sheet 20	1.165 um Sheet 19	740 nm Sheet 12
16 kV	1.495 um Sheet 16	1.029 um Sheet 22	978 nm Sheet 18	1.2 um Sheet 11
17 kV	806 nm Sheet 10	723 nm Sheet 24	1.78 um Sheet 17	939 nm Sheet 13
18 kV	515 nm Sheet 26	493 nm Sheet 03	1.24 um Sheet 15	665 nm Sheet 09

(a)

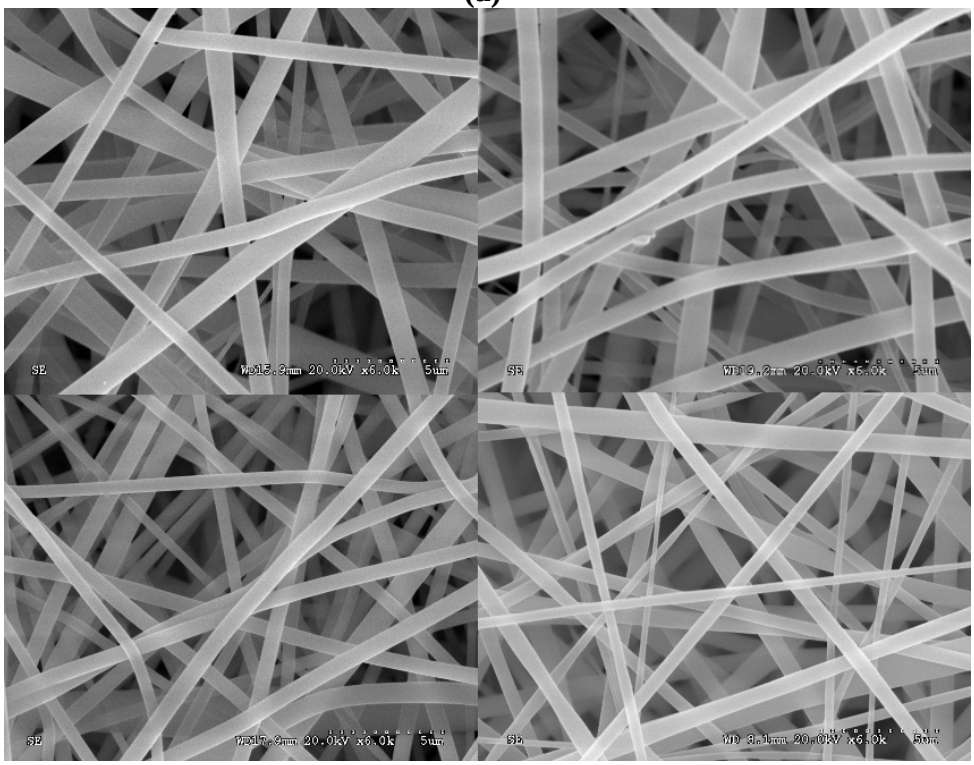

(b)

Figure 3.13. (a) Diagram indicating average fiber diameter at each setting, (b) SEM example images used for analysis [120]

Sol-gel was injected into a 30 ml syringe from the 200 ml plastic flask. Care was taken not to introduce any solids into the syringe. A small needle was placed on the tip of the syringe. Air was then purged out of the syringe to ensure a constant flow of sol-gel. Tubing was connected to the syringe needle and cut at approximately 12 in. length. The other end of the tubing was placed on the backside of the spinneret. The spinneret was fastened to the spinneret stand. The spinneret stand was made of non-conductive plexi-glass. This ensured that the high voltage did not conduct to ground. The spinneret stand was approximately 8 in. tall. The syringe pump purged the plastic tubing line so that no air was present. When the presence of sol-gel detected at the spinneret the high voltage power supply was turned on.

Deposition can be visually seen usually within the first 1-2 minutes. Once the sheet was completed, the voltage supply was turned off to prevent accidental electrical shock. A Teflon coated release film was attached to the collector plate so that deposition would accumulate on it. It was undesirable to allow deposition to accumulate on the collector plate. Peeling of the glass nanofibers sheets resulted in no noticeable damage to the nanofibers if deposition occurred on the Teflon release film. Early attempts to spin onto glass fabric resulted in damage to the electrospun sheets during peeling. Several substrate materials were used in optimization test runs to determine the best material for the future deposition. Figure 3.14 shows the experimental setup for depositing SiO_2 glass nanofibers. It is clear from the photo that the deposition of white substance (glass nanofibers) onto the brown Teflon coated release film. The electrospun deposition has a very smooth and silky appearance during proper nanofiber deposition.

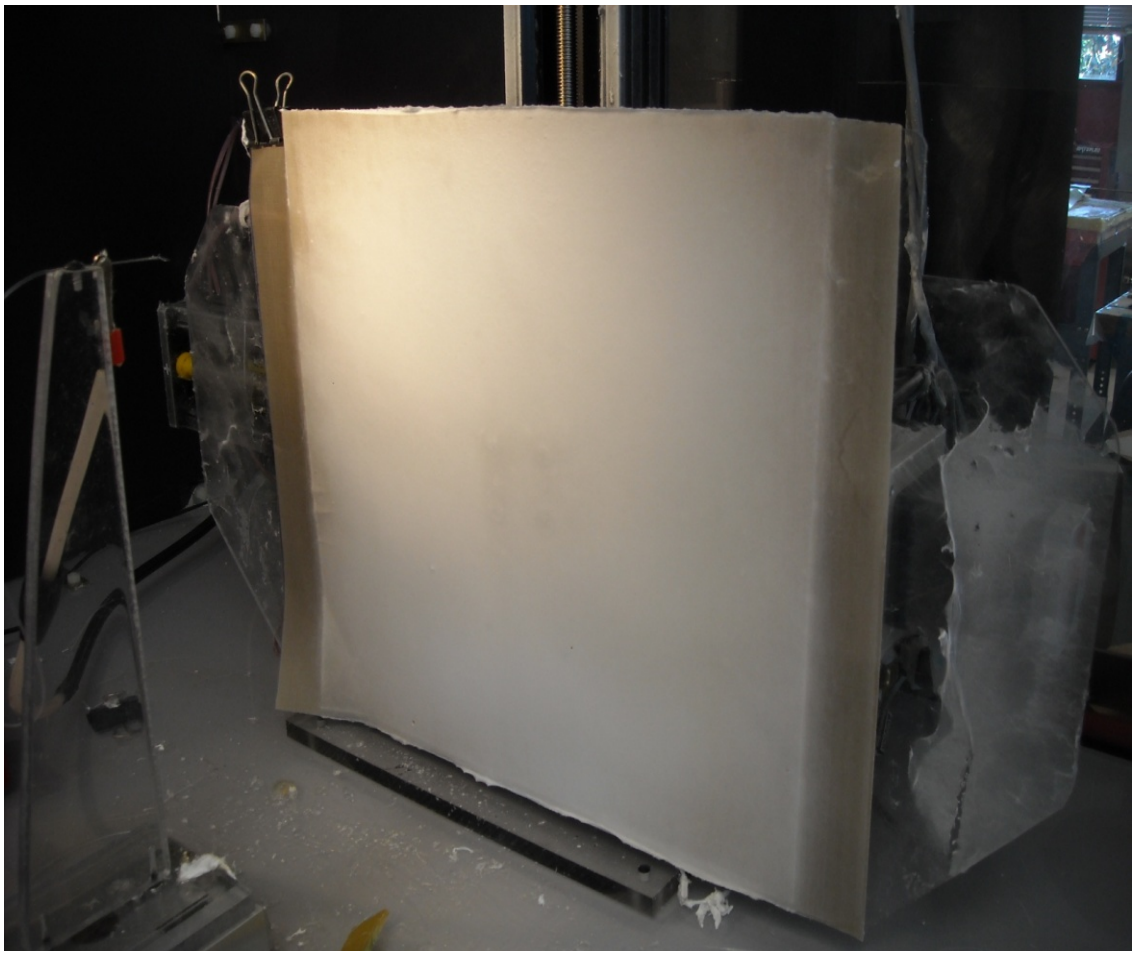

Figure 3.14. Picture of deposition of glass nanofibers

3.5 Sintering the Electrospun Nanofiber Sheets

Before the electrospun nanofibers could be implemented in mechanical systems they must be post-processed. Post processing consisted of sintering. The electrospun sheets were sintered at 600 ^{o}C in order to remove any remaining solvents within the fibers. After electrospinning but before sintering, the fiber diameters tended to be relatively large. The fiber diameters ranged from 500nm – 5μm. Figure 3.15 shows a SEM image of the fibers before sintering. There is significant solvent left within the

fibers. Sintering the sheets significantly reduced the diameter of the fibers. Approximately 30-50% fiber diameter reductions have been observed in a prior work using sintering [121]. A similar reduction of 35-50% in fiber diameter was observed in the present study. Fiber diameters were determined using a SU-8000 scanning electron microscope (SEM). Still images were captured and analyzed using the SEM's computer software to determine the average fiber diameter and their variations.

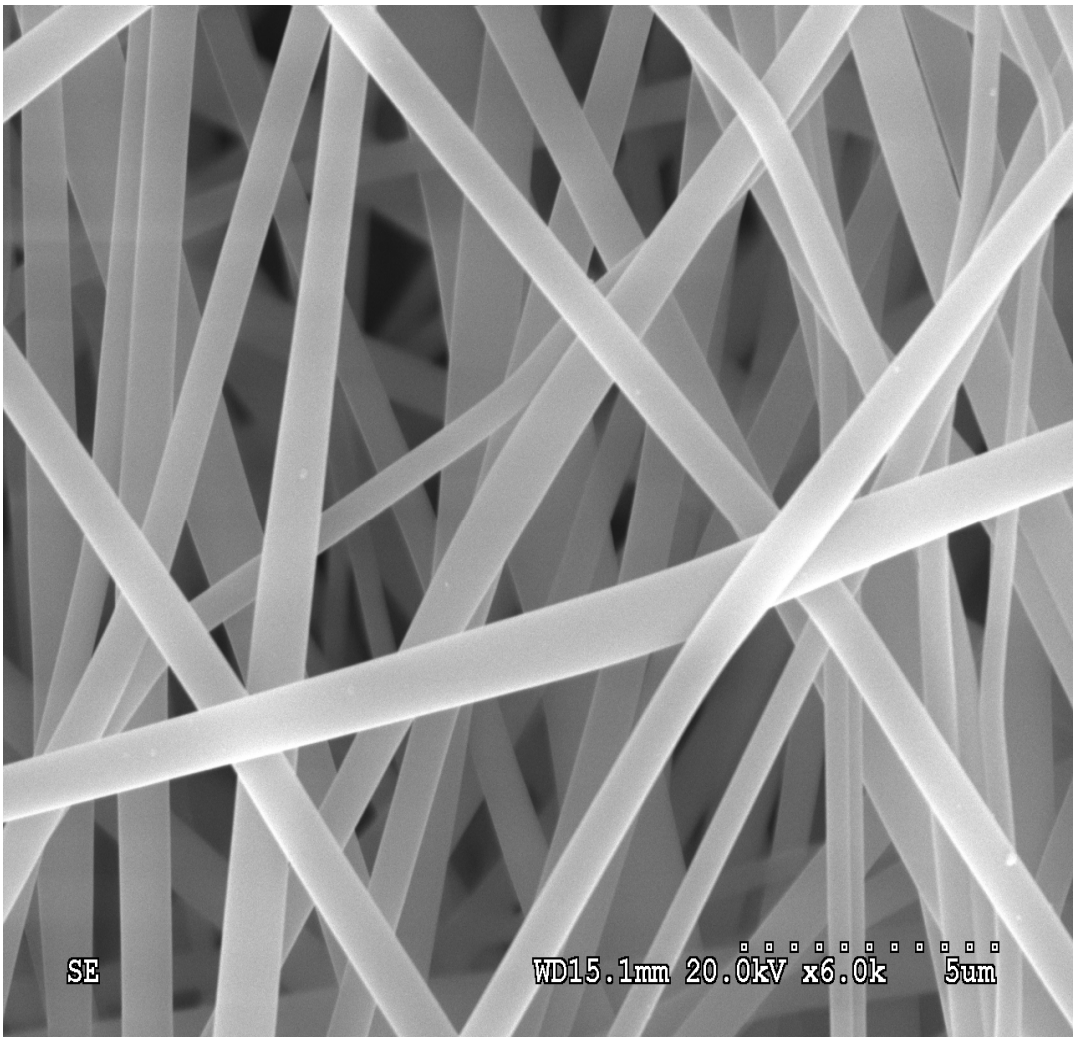

Figure 3.15. SEM image of un-sintered glass nanofiber

Scanning electron microscopes also have the ability to detect chemical compositions through Energy Dispersive X-ray Spectroscopy (SEM/EDS). This function makes high energy electrons collide with the glass nanofibers components inner electron shell. An inner electron shell electron is ejected from an atom. The second electron shell then donates an electron to the first electron shell orbit. This process gives off energy in the form of electromagnetic radiation. The electromagnetic radiation given off is an x-ray. The x-rays are captured by the SEM and analyzed for their energy content. Every element in the periodic table has very specific x-ray energy ejection during this event. Elements can accurately be determined with the SEM. The chemical composition of the glass nanofibers was determined to be 98% SiO_2 [120]. Figure 3.16 below shows a single layer of electrospun fabric and the sintering temperature profile used.

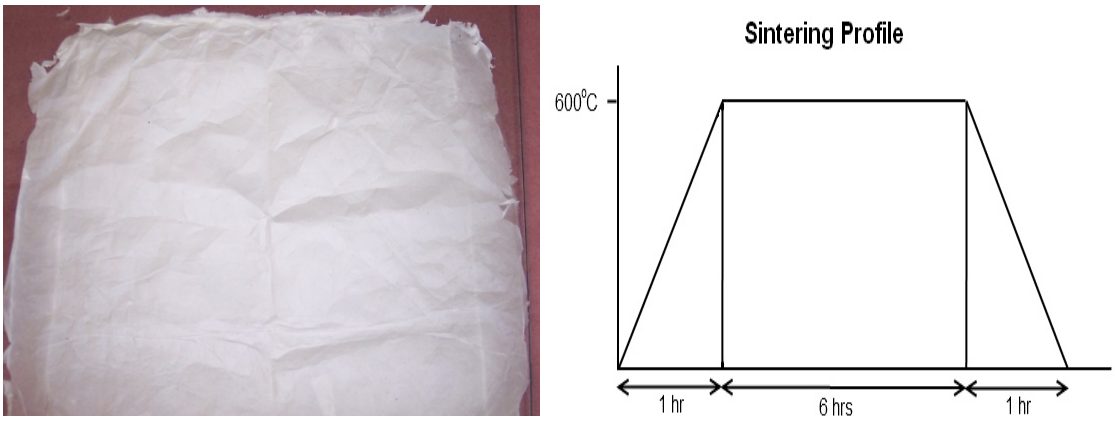

(a) **(b)**

Figure 3.16. (a) Electrospun nanofiber sheet, (b) Sintering temperature profile

CHAPTER 4

COMPOSITE MANUFACTURING

Most modern composites are comprised of two or more materials which retain their individual identities in the complete structure. Their individual properties complement one another and enhance the overall properties of the integrated composite material. This may be referred to as a two-phase composite material. The matrix is usually the weaker component and fibers are generally used for reinforcement. The combined comprehensive performance tends to be better than either one of the individuals. After completing the mixture of the TEOS sol-gel, aging of the sol-gel, and spinning electrospun sheets, the electrospun sheets are applied to the composite laminate's interfaces. Initially, it was considered that application of electrospun sheets to the interfaces of the lamina would enhance the overall performance by enabling the composite to absorb more energy. Application of the electrospun fibers at the interface could affect the ability of cracks to travel between the lamina. It could inhibit the crack growth and propagation between the lamina. Determining this is one of several objectives of this current research.

Handling the electrospun sheets is very tedious and application to the interfaces is difficult. This chapter discusses to the manufacturing process of the composites with and without electrospun sheets. Heated Vacuum Resin Transfer Method (HVARTM) was initially used to manufacture the composites until credible problems were acknowledged in the formed composite panels. This method was changed to using pre-impregnated

(prepreg) woven composite fabric. Specimens were prepared for materials with and without electrospun fibers to set a baseline and to determine if there are dissimilarities.

4.1 HVARTM

Initial efforts of the current research focused on making electrospun nanofibrous sheets with the intention of applying it to interfacial regions of plastic reinforced composites manufactured using Heated Vacuum Assisted Resin Transfer Method (HVARTM). HVARTM is a patented pending process developed by Bolick and Kelkar [122] at North Carolina Agricultural and Technical State University. This manufacturing technique produces high quality low cost composites with semi-high viscous resin systems. HVARTM differs from VARTM because of the use of a heated blanket that preheats the mold. The mold is also kept at an elevated temperature during resin infusion. A heated blanket was placed under the mold and used to heat the process. This process also produces high fiber volume fraction composites. HVARTM uses simple materials and can be adapted for various applications. HVARTM can also be readily scaled up. HVARTM uses vacuum as a source for resin transfusion. Premixed resin is inserted into a container and then forced into the woven fabric through the existence of pressure gradient. With high viscosity resins, steps must be taken to lower the viscosity such that it would flow through the HVARTM setup. Compression during the vacuum stage provides an obstacle that must be accounted for. The resin choice for the present study is EPON 862 mixed with the curing agent ‘W’. This unique system requires elevated temperatures during resin infusion.

The mixing ratio of resin to curing agent was 100:26.4. The resin was too viscous to flow through the setup at the room temperature. After the resin was mixed with the curing agent, it was stirred for approximately 30 minutes. Mixing introduced air into the resin. In order to use the resin for infusion, the viscosity has to be much lower. Subsequently, it was placed in a 100 ^{o}C oven for approximately 30 minutes to lower the viscosity. After heating, the resin's viscosity was such that is was capable of flowing through the HVARTM setup and to wet the fabric in the specimen. The setup consisted of a glass mold which was free from defects. The glass mold was treated with a release agent to assist in post curing release. E-glass plain weave fabric was chosen and was cut to a dimension of 12 in. x 12 in. and consisted of ten layers.

Resin breather material was cut to a dimension of 15 in. x15 in. It was placed directly into the mold. Release film cut to a size of 14.5 in. x 14.5 in. and was placed on top of the resin transfer media. The release film aids in releasing bagging material from the specimen. The release film produced a nicely textured surface that was even and free of defects. The 10 layers of cut woven fabric were stacked with a consistent stacking sequence keeping the same warp and weft direction in all the lamina. Release film was placed on top of the fabric followed by breather material. A sealant was applied to the glass mold and a vacuum bag placed on top of the mold. A vacuum line and resin distribution line were placed inside of the sealant. The mold was placed on top of a high temperature preheated blanket. The heated resin was placed into a preheated flask connected to the resin distribution tubing. Resin was then infused using a vacuum pump attached to the vacuum bag. Figure 4.1 shows a schematic of a typical HVARTM setup.

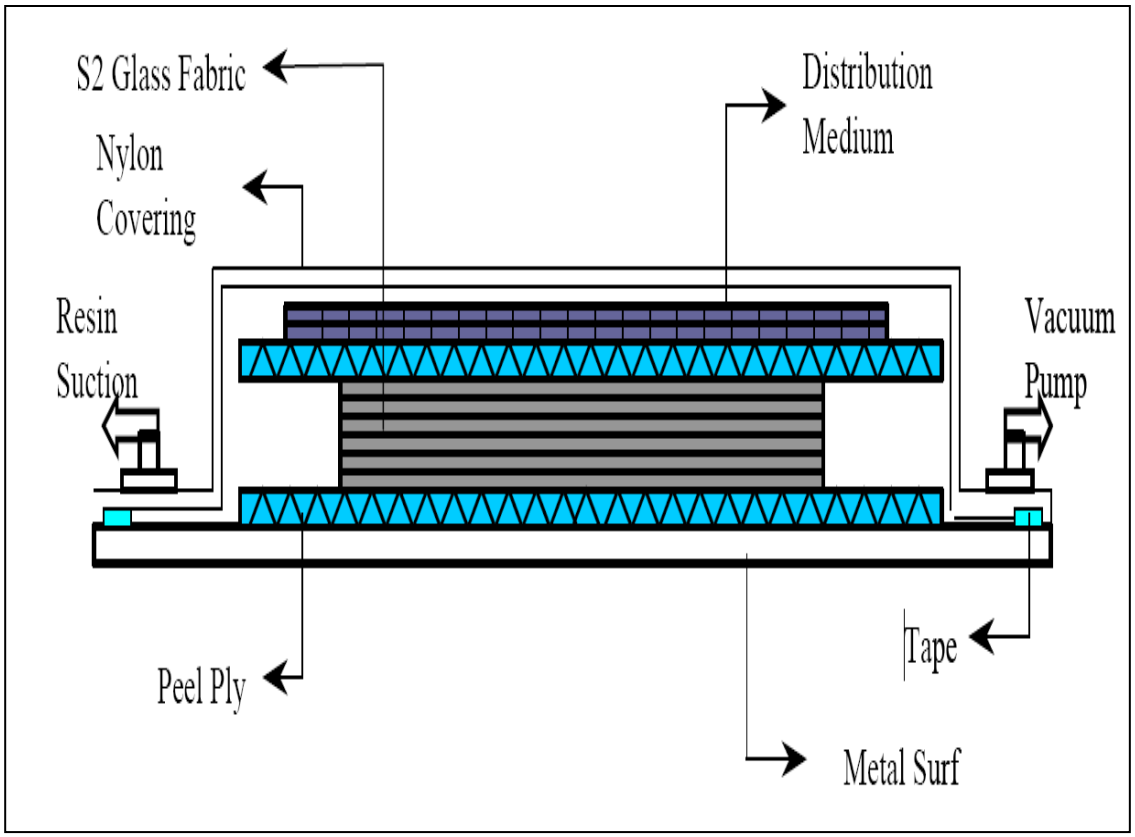

Figure 4.1. Schematic of layup of HVARTM [120]

Resin was controlled such that wetting occurred at a infusion rate of 1 in./30 secs. across the pre-form. This rate was designed to ensure complete wetting before gelatin occurred. Once the resin was infused into the fabric completely, the vacuum line and resin supply line were capped. The entire mold was then transferred into a walk-in oven for curing. The oven was programmed to have two different curing cycle temperatures. Figure 4.2 shows the temperature curing cycle for the HVARTM setup. A multi-temperature curing cycle time was chosen for the resin system used in this study based on the manufacturer's data. Recommendations from the resin manufacturer data sheet lead

to the decision of using a two temperature curing cycle. However, it was determined that problems existed with the second stage of the thermal curing cycle. Bagging material and sealant melting problems were encountered during curing. Vacuum holes in the bag lead to vacuum release allowing air to enter the bag. Air entered the bag forming bubbles in the resin and laminate resulting in voids. Voids are unacceptable in laminated composites. High temperature bagging material and sealant were used in an attempt to alleviate the problem.

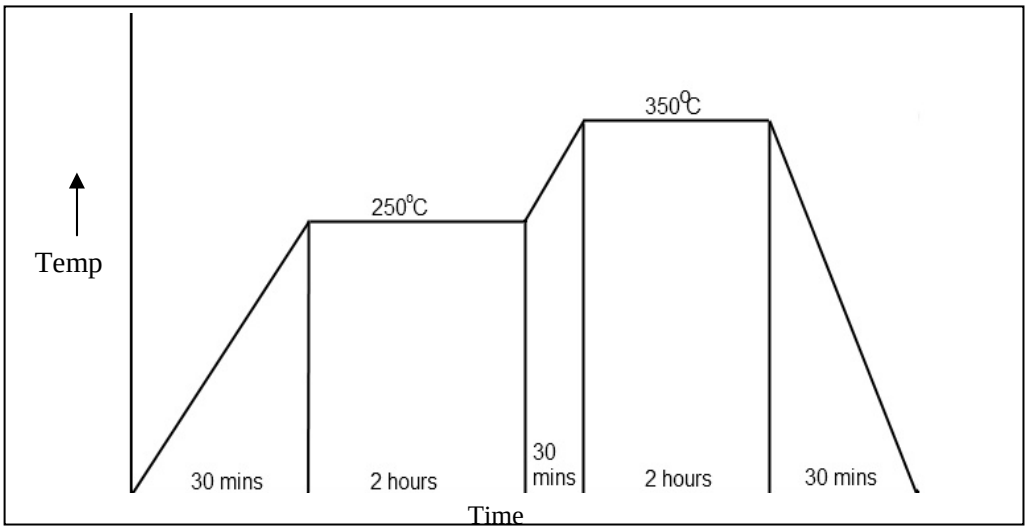

Figure 4.2. Curing cycle of HVARTM specimen

The entire curing cycle took about 6 hours to complete. The mold was then removed from the oven and inspected for vacuum leaks during the curing cycle. After passing inspection, the laminate was removed from the mold. Figure 4.3 shows a picture of a completed raw specimen after curing. Manufacturing of the HVARTM specimens for use in the current research was halted due to the results from concurrent research

which indicated that the HVARTM specimens may not be appropriate choice for comparisons of highlighting the use of electrospun nanofiber sheets. Shendokar's research on the characteristics of G_{IC} indicated little change in G_{IC} of specimens with electrospinning treatment compared to the laminates without electrospinning treatment. Problems included insufficient wetting of the electrospun fibers as well as fiber bridging. Wetting of the electrospun fibers was insufficient and thus resulted in a 40% drop in G_{IC} value [120]. Although the intention of this research was to compare the mechanical properties of electrospun nanofibers under impact loading, it was decided to use an alternate material system for the manufacturing of two and three phase composite panels based on the previous results. For comparison purposes it was decided to use pre-impregnated (prepreg) woven plain fabric.

Figure 4.3. Picture of complete raw specimen before cutting

4.2 Prepreg 2 and 3 phase manufacturing

Manufacturing of new specimens was to avoid dry nanofibers in the composite. VTM264/7725 prepregs were chosen. A product known as Variable Temperature Molding was chosen due to its flexibility of curing temperatures and its compatibility to prior purchased products. Properties for VTM264/7725 can be found in the APPENDIX A. Problems with peripheral equipment were known to occur during high temperature curing (350 ^{o}C) with the use of EPON 862/Curing Agent "W". Therefore, during the selection of a new laminated composite system, it was a priority to choose a curing system with a wide range of curing temperatures. The curing cycle of the newly chosen laminate material system had wide curing range which was ideal in the use of the current research. Curing capability of the new laminate material system ranged between 90 ^{o}F and 300 ^{o}F.

A glass mold that was free from defects was selected. For production of the laminates with electrospinning interface layers all steps remained the same except for the addition of the electrospinning sheets and an additional layer of resin film. For production of prepreg laminated composites, the following steps were taken:

1) *Mold preparation*
2) *Fabric layup*
3) *Vacuum bagging*
4) *Application of electrospun sheets*
5) *Curing cycle*
6) *Post processing (Specimen cutting)*

4.2.1 Constituents of 2 and 3 phase laminated composites

During the manufacturing of prepreg laminated composites the following materials were acquired and used:

1) Plastic film was used for two different purposes. It was placed directly onto the mold to aid in the cleanup during post curing as well as the forming the vacuum bag. The plastic film must be flexible enough not to tear in areas where excessive straining occurs due to the vacuum and sharp corners. Plastic film with a thickness of 3 mil was utilized.
2) Teflon coated release film was used in direct contact with the fabric. Due to its nonstick nature the release film aided in the release of the bagging materials with the specimen after curing.
3) Resin flow media was used to provide a near uniform vacuum to all parts of the bag as well as to provide a relief area in which excess resin may travel. This was a very important aspect for the specimens that had the electrospinning sheets applied. Additional excess resin was applied to each interface to ensure complete wetting of the electrospinning sheets inside the specimen. This additional resin was squeezed out under the vacuum.
4) Sealant (mastic) was placed around the mold. The plastic bagging material was attached to the sealant to create an air tight vacuum bag.

Prepreg fabric was manufactured with VTM264 resin film that was B-staged. B-staged was characterized by a resin and curing agent that were mixed together and then carefully applied to the fabric. The fabric was then refrigerated or frozen in order to slow

the curing of the resin. VTM-264 has an ambient temperature shelf life of 30 days. If kept frozen, it has approximately one year shelf life. Mold preparation was conducted by applying a release film agent directly to the mold. A small piece of bagging plastic was laid down to aid in post curing clean up. The stacking process involved the breather material followed by Teflon coated release film. The prepreg was then stacked with a stacking sequence as mentioned earlier. After two lamina were stacked upon each other, the combined laminate went through a process known as debulking. Debulking compressed excess air out of the two layers and condensed the lamina into a more compact and dense laminate. Every time an interface was joined it went through debulking. Debulking was performed in a vacuum debulking unit. Figure 4.4 shows two different laminates prior to debulking. Debulking resulted in higher quality laminates. Its overall goal was the reduction of void content. Void content of the laminate allowed matrix cracking to occur more easily. Further reduction of void content would require the use of an autoclave. The use of an autoclave tend to increase production costs

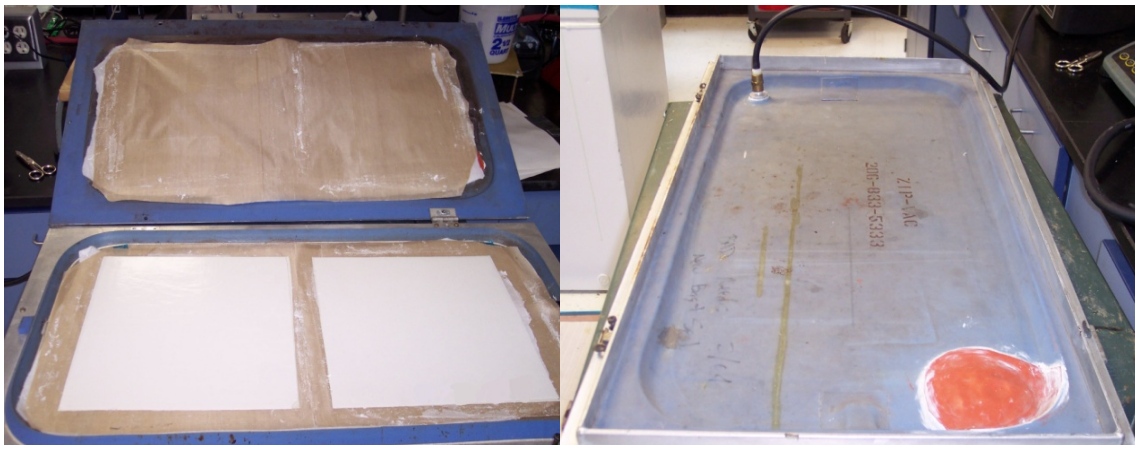

Figure 4.4. Debulker

Release film, resin flow media, and finally the top bagging material were all laid down as part the final debulked uncured laminate. Sealant was placed around the perimeter of the mold to seal off the vacuum bag. Figure 4.5 shows a picture of the actual layup after vacuum application prior to curing. The mold with completed bag was then placed inside an oven. A high temperature vacuum line was inserted through the oven wall and installed onto the molds vacuum port. A vacuum pump was placed outside the oven and used to pull a vacuum of 29 in. of mercury during the cure cycle.

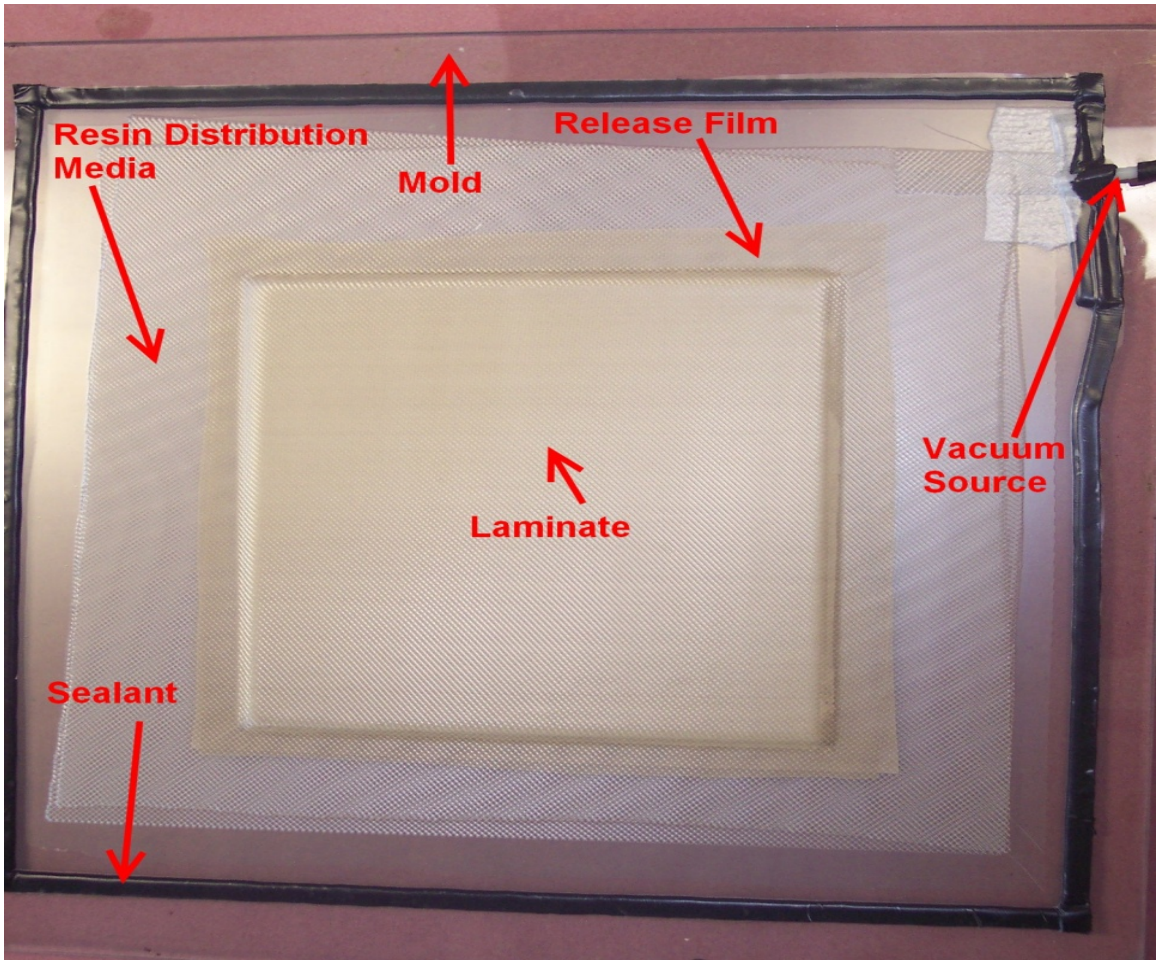

Figure 4.5. Picture of laminate layup prior to curing

4.2.2 Electrospun Fiber Embedded Composites

Electrospun sheets were applied to half of the specimens. Application of the sheets to the specimens was conducted with extreme care. Wax paper was peeled from the prepreg material. This exposed the B-staged film which consisted of a very high tack. A sheet of sintered electrospun nanofibers was removed from storage and placed onto a lamina interface as shown in Figure 4.6. Care was taken not to make wrinkles in the application of the sheets. Due to the high quality manufacturing of prepreg composites excessive resin was not available to wet the glass nanofibers at the interfacial region. Additional neat resin film was applied to the interfacial region. The additional resin film ensured proper wetting of the glass nanofiber upon curing.

Figure 4.6. Picture of application of electrospun sheet to interface

During curing, the resin heated up which lowered the viscosity. Under compression, the excess resin flowed through the laminate and escaped to the resin distribution media. Electrospun sheets were applied to every interface between the prepreg lamina. The entire laminate was comprised of 10 lamina. This resulted in 9 interfaces. Therefore, for each laminate 9 layers of electrospun sheets were required. Each electrospun sheet weighed approximately 0.8 grams prior to application. The total weight contribution of the electrospun fiber sheets was 7.2 to 7.5 grams. Each laminate measured 12.3 in. x 12.3 in. after curing. The total weight of each laminate was approximately 448 grams. The addition of the electrospun fibers added approximately 1.5% to the weight of the laminate. Curing of the laminates was performed at 250 ^{o}F for 2 hours. After the curing cycle was complete, the mold was removed from the oven and was cooled for approximately one hour. After cooling to the ambient temperature, the vacuum bag was discarded and the formed laminate removed. Figure 4.7 shows a final cured specimen. Chapter 5 discusses the preparation and sizing of the smaller specimens from the large cured laminate prepared in chapter 4.

Figure 4.7. Cured prepreg 12 in. x 12 in. with electrospinning treatment

CHAPTER 5

IMPACT TESTING AND C-SCANNING

Impact testing is a dynamic destructive test that characterizes the ability of a material to absorb energy. Impact testing has evolved from a crude form to a highly accurate scientific test. The current impact tests generally use a drop test impact tower. Energy calculations are derived from the conversion of potential energy to kinetic energy.

The impact test applies a force over a very short period of time which has different effects on the material than if applied over a long period of time. The type of damage largely depends on the velocity of the impact. Impact testing can be categorized into two categories, low velocity and high velocity impacts. The present work focuses on low velocity impact. Determination due to low velocity or high velocity type test involves the comparison of the velocity of the impactor with the speed of sound in the impacted coupon. Generally, if they are of the same order then the impact is considered to be high velocity. If the impactor velocity is less than 1/10th of the velocity of the speed of sound, the test is considered to be a low velocity impact. There is no industry standard on how to determine if the impact test is considered low velocity or high velocity.

A force applied to an object at very slows speeds will cause the material to elastically deform first. An impact event in which the force is administered over very short amount of time is known as impulse. The mechanics of how the impacted material may change depend upon how fast the force is applied. The faster the force is applied,

the more the material may tend to react in a brittle manner. In a classical sense, impulse is defined as the integral of a force with respect to time. Equation 5.1 mathematically defines the relationship between impulse and the time rate change of the force for a given time period.

$$I = \int_{t_1}^{t_2} F dt \tag{5.1}$$

Newton's second law states that a time rate change in momentum equals force applied as shown by equation 5.2.

$$F = \frac{dp}{dt} \tag{5.2}$$

Substituting equation 5.2 into 5.1 gives equation 5.3

$$I = \int_{t_1}^{t_2} \frac{dp}{dt} dt \tag{5.3}$$

Simplifying equation 5.3 results in equation 5.4.

$$I = \int_{t_1}^{t_2} dp \tag{5.4}$$

Therefore, impulse equals a change in momentum of an impactor identified by equation 5.5.

$$I = \Delta p \tag{5.5}$$

Impulse can be characterized as a change in momentum from t_1 to t_2. This is otherwise known as the impulse-momentum-theory. Common units of energy are expressed in either Joules or ft-lbs. Units of impulse are expressed in force. For measurement of energy, the test must measure the deflection of the test coupon or velocity of the striker head. Energy measurements are generally more desirable but more difficult to acquire.

5.1 ASTM Standard D 7136/7136M

Impact testing begins with specimen preparation. Raw composite laminate specimens were manufactured as described in chapter 4. The raw laminated specimen dimensions measured 12 in. x 12 in. x 0.1 in. The composite laminates were cut using a diamond tipped ceramic wet tile saw. Water was used during cutting to prevent the epoxy matrix from melting and altering the mechanical properties. The ASTM standard D7136 specifies 4 in. x 6 in. specimens. However, it was decided to use a Boeing fixture that supports the use of a 6 in. x 6 in. specimen. Reasoning for this fixture's application is its wide usage in the aerospace industry, where the present impact characteristic results have the most significance.

The ASTM standard dictates the use of a drop weight tower that has a crosshead affixed to guides with proper instrumentation. For the current research an Instron 8250 drop weight impact tester was used. Figure 5.1 shows an image of the impact tester. The impact tester uses a data acquisition system that acquires data at a high rate of speed. The impulse test generally occurred in less than 20 milliseconds. The crosshead of the impactor weighs 11.91 lb_m. The crosshead was mechanically raised and lowered using a pulley system. The striker is a 1 in. diameter hemispherical shape. The higher the drop height of the impactor, the larger the amount of energy applied to the specimen as indicated by equation 5.6.

$$Energy\ Input = mgh \tag{5.6}$$

The mass of the crosshead as well as the gravitational parameter are both constants. Therefore, energy input to the specimen is a direct function of the height of

the cross head. Increased or decreased energy can be obtained by addition or subtraction of weights to the crosshead.

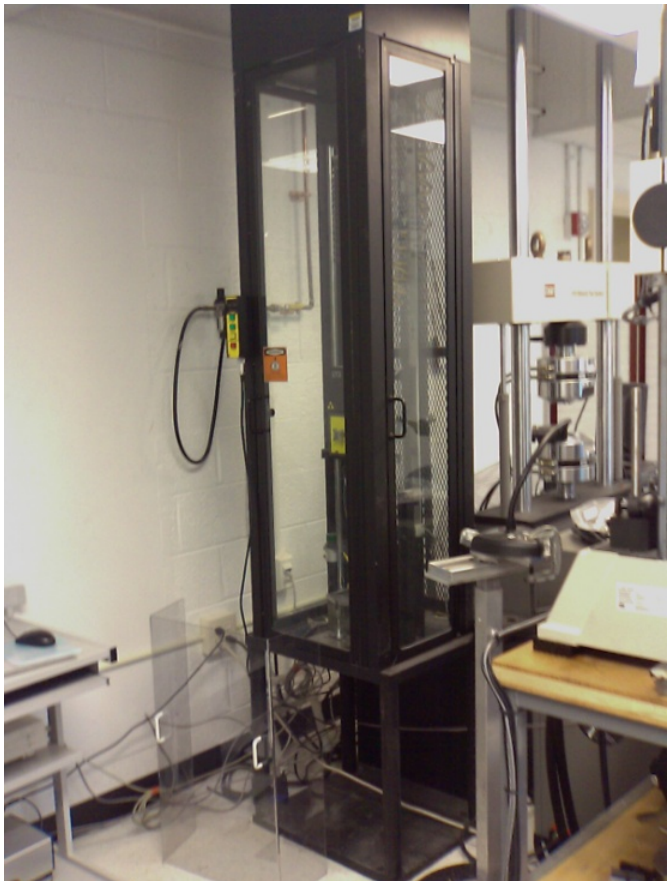

Figure 5.1. Picture of Instron 8250 impact test machine

5.2 Impact Testing

Specimens were secured into the test fixture. The top plate was affixed to the test fixture through the use of two screws. Prior to each test, the screws were hand-torqued to 40 in-lbs. This was performed to ensure an even clamping force at the boundaries. Figure 5.2 shows the test fixture with the impact test coupons. The test coupons were

used to determine incipient and maximum drop heights. Incipient damage is a term to describe a height at which damage begins to occur. An initial height of 3 in. was chosen to begin incipient damage inspection. After completing the initial test, the specimen was visually examined only to determine the extent of the damage.

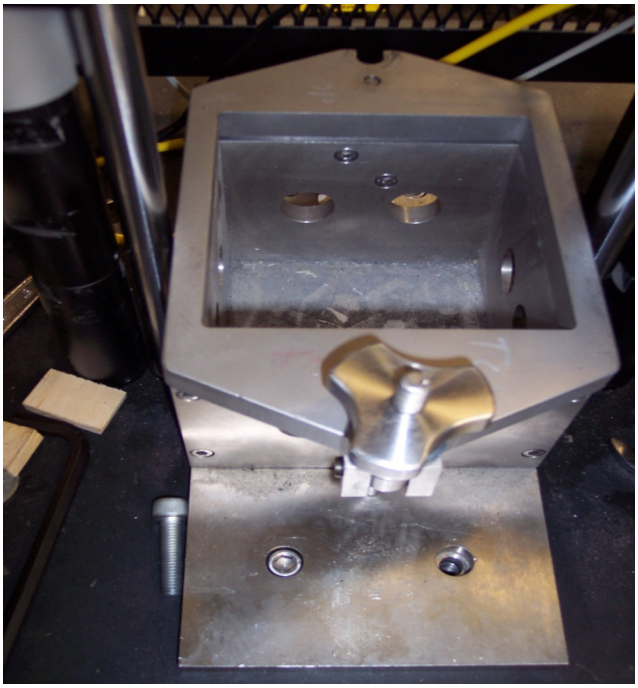

Figure 5.2. Picture of drop test fixture

Several iterations of preliminary incipient damage with varying drop heights were performed before deciding on 5 inches as the first drop height. The maximum drop height was determined in the same manner. The drop weight crosshead was increased until the impulse program indicated that no load carrying capability remained in the specimen. A drop height of 29 in. was determined to be the maximum height at which no additional load could be sustained by the specimen. Drop heights were divided evenly

into 5 intervals. Intermediate drop tests were performed at heights of 5 in., 11 in., 17 in., 23 in., and 29 in. Three specimens were impacted at each drop height. This resulted in a total of 15 drop impact tests that were conducted without the electrospinning treatment at the interfacial layer. A total of 15 impact drop tests were also conducted with the electrospinning treatment at the interfacial layer at the same drop heights. The software program Impulse was used to collect data from the impact machine. This is based on ASTM standard D7136 protocol. Figure 5.3 shows a screenshot of the Impulse program. Coupons were randomly chosen and placed into the test sequence. The specimens were subsequently numbered for archival and record keeping of the test results.

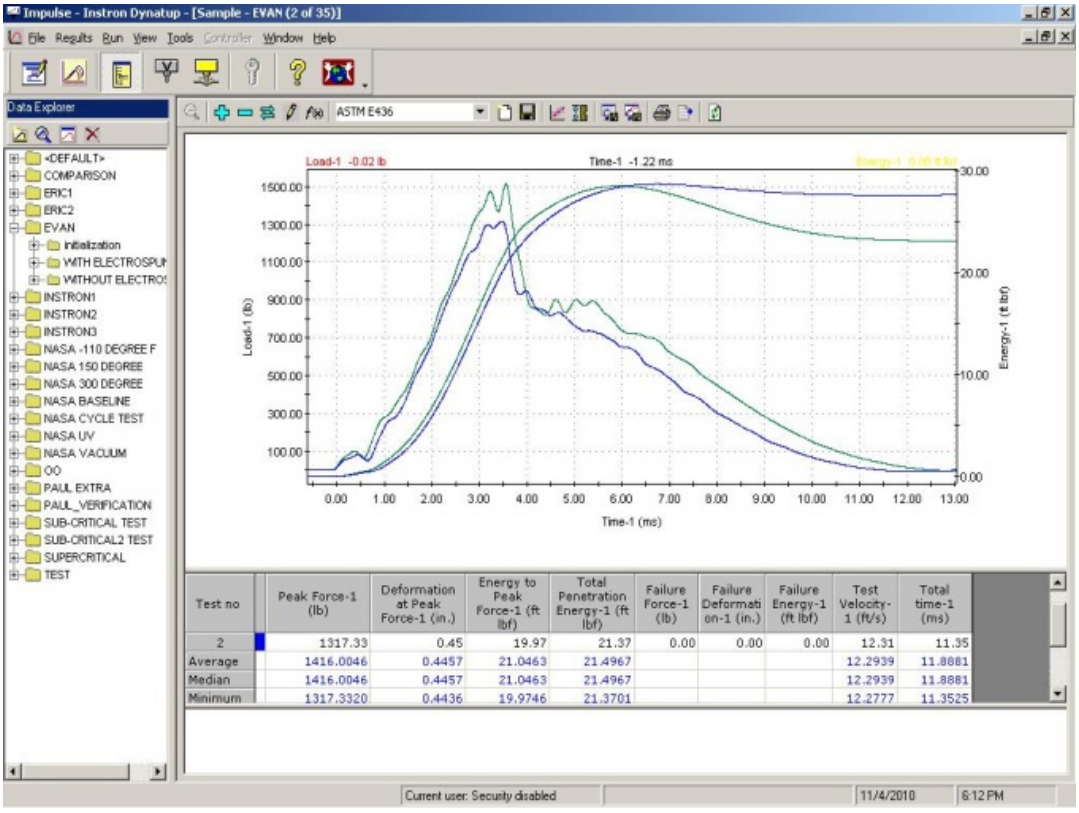

Figure 5.3. Impulse software program output

5.3 Data Acquisition

The Instron impact test machine automatically triggered the data acquisition process. The first round of tests included the specimens without the electrospinning treatment. The specimens without electrospinning were randomly selected from the pool and numbered 1 through 15. The specimens were tested in that respective order. After completion of the specimens without electrospun nanofibers, the specimens with electrospun nanofibers were conducted. Figure 5.4 is an example of data collected from the Instron impact test machine. Load versus time is plotted to compare the first 3 specimens without electrospun nanofibers tested at the 5 ft-lb energy level. All remaining drop test data can be view in Appendix B for comparison.

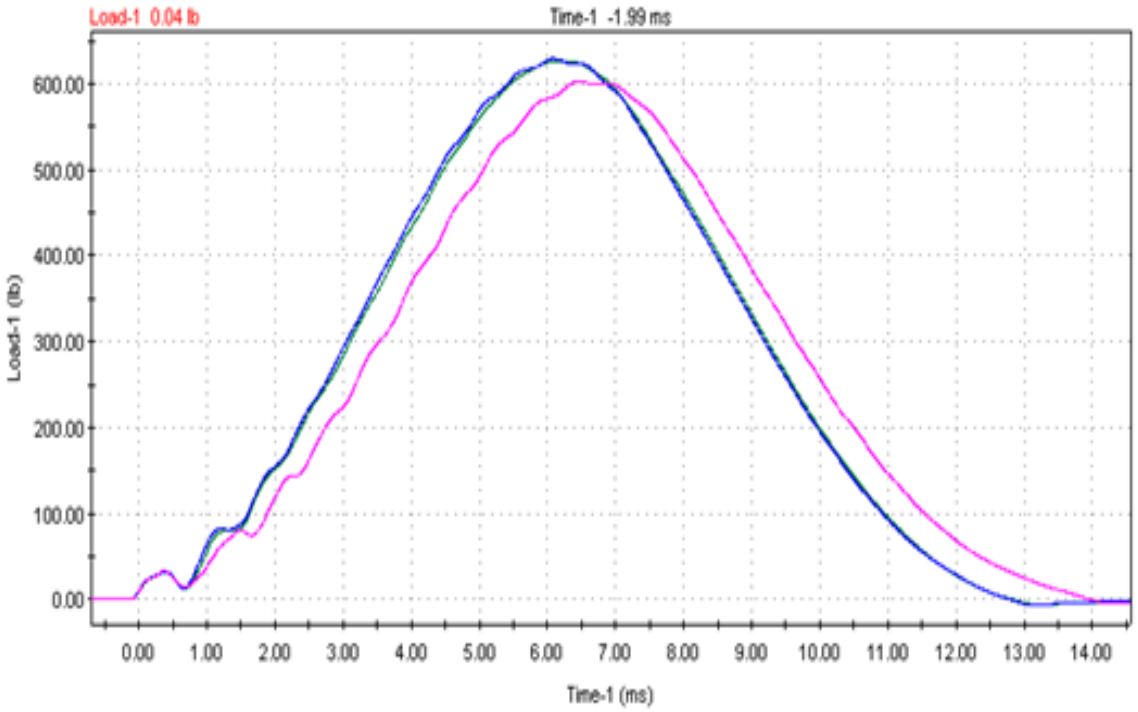

Figure 5.4. Impact test data; load vs. time at 5 in. drop height

Absorption of energy by coupons with glass nanofiber application occurs due to the additional resistance of the nanofibers. The additional crack surface created by the impact event is an indication of an additional amount of energy absorption. Figure 5.5 shows additional cracking that absorbs more energy for samples with electrospun glass nanofibers.

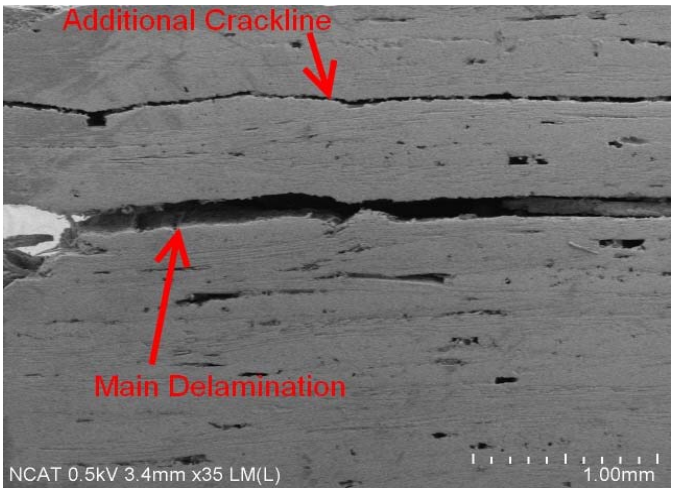

(a)

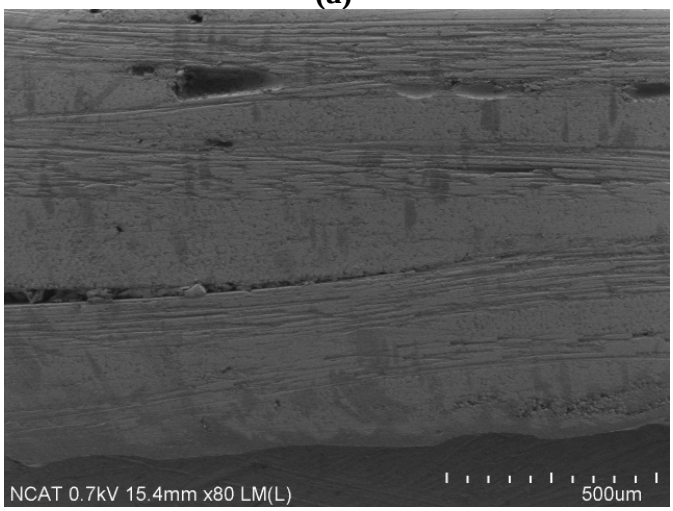

(b)

Figure 5.5. Differences in additional crack (energy absorbed) at 17 ft-lbs energy level: (a) Specimen 28 with nanofibers (b) Specimen 9 without nanofibers

It was observed that after testing, specimens with electrospun nanofibers had additional layers of delamination as indicated in Figure 5.5. Figure 5.6 shows the details of the crack line in specimen 9 which was impacted at the 17 ft-lb energy level. Noticeable crack propagation at the interfacial region can be seen. Delamination cracks always propagated through the interface of two stacked lamina.

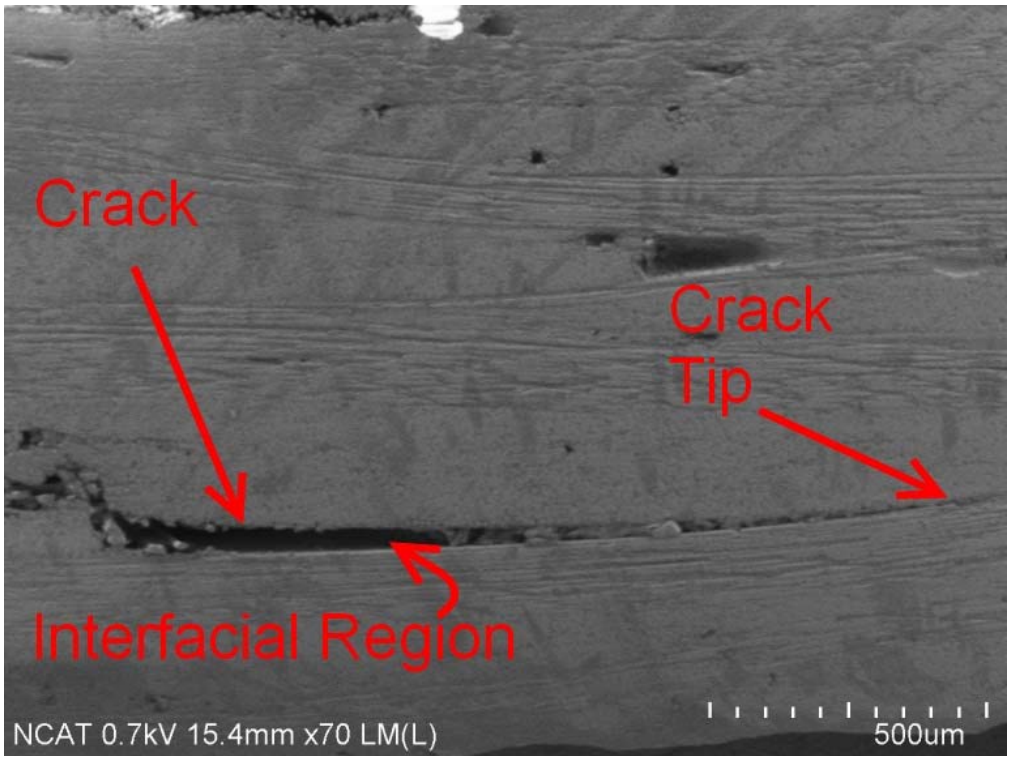

Figure 5.6. SEM image showing crack tip in specimen 9

In the case of crack propagation during the impact, the specimens with glass nanofibers had additional obstructions for cracks to propagate through. The interfacial layers contain glass nanofibers that must be broken, pulled, or de-bonded for the crack to propagate further. Figure 5.7 shows the upper edge of a crack surface in which the crack

must overcome additional obstructions such as the glass nanofibers. Glass nanofiber, broken glass nanofibers as well as the upper crack surface are visible in the figure. Additional energy is required to de-bond the glass nanofibers from the matrix as well as to break the glass nanofibers.

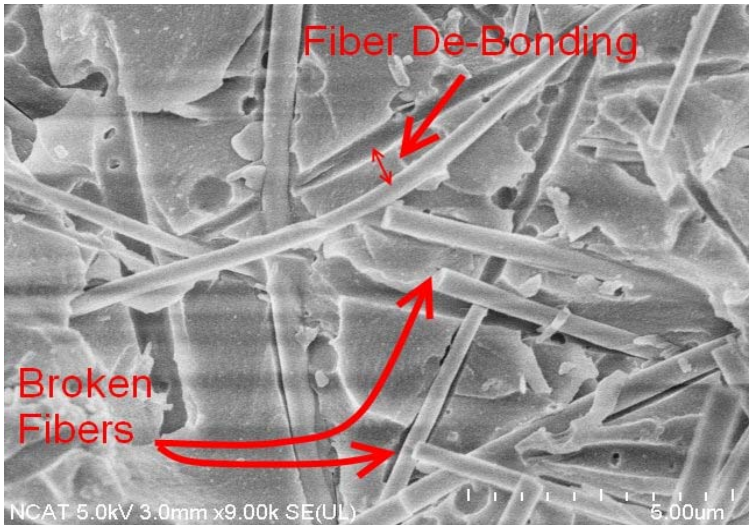

Figure 5.7. Crack surface showing broken fibers and fiber-matrix debonding

In some regions of crack propagation the layers of resin around the interfacial glass nanofibers was thick enough for the crack to propagate through. These resin areas raise concern. These areas need to have lower resin content so that the required energy release rate would be higher than that of the glass nanofiber areas. Figure 5.8 shows an area where the impact crack propagation occurred on top of the thin resin film above the glass nanofibers. The figure displays the layer of nanofibers in between the different lamina. In the upper right of Figure 5.8 is the upper lamina with a resin rich area. The lower lamina is clear due to the peeling of the resin that exposes the fibers. The

interfacial layer is located between the two adjacent lamina layers. Resin peeling is believed to be a localized event that caused the resin to crack in this manner. Further investigations of this type of damage may be necessary. Local increased resin content is believed to have caused this type of fracture surface.

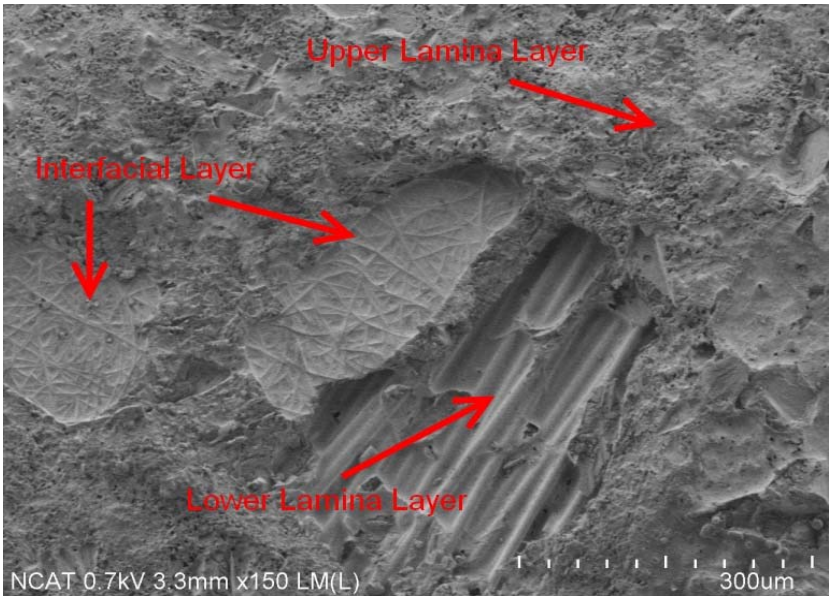

Figure 5.8. Glass nanofibers between different lamina

A typical comparison of the crack surface with and without glass nanofibers can be made as in Figure 5.9. Figure 5.9 (a) shows the upper edge of the crack surface at 13000x magnification. Evident from the picture are broken fibers and fiber-matrix debonding. Fiber debonding, which requires additional energy for crack propagation to continue, can also be seen. This mechanism also helps to absorb additional energy. Figure 5.9 (b) shows the upper edge of the crack surface in specimen 7. The absence of nanofibers is evident and thus, cracks propagate without interruptions.

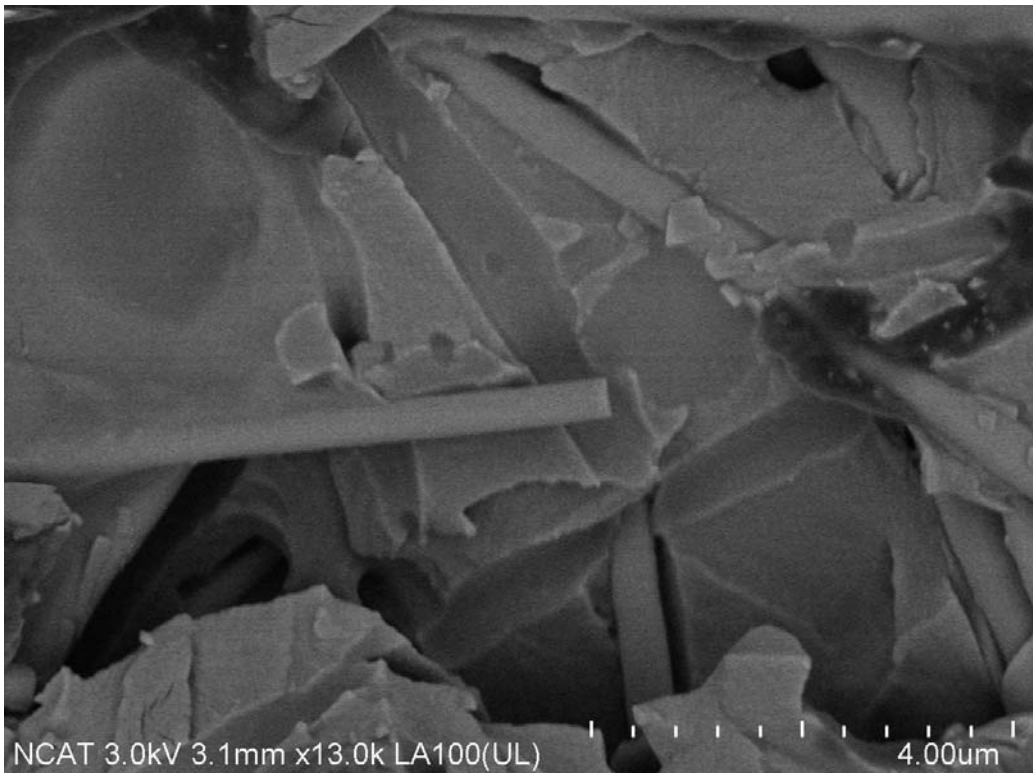

(a)

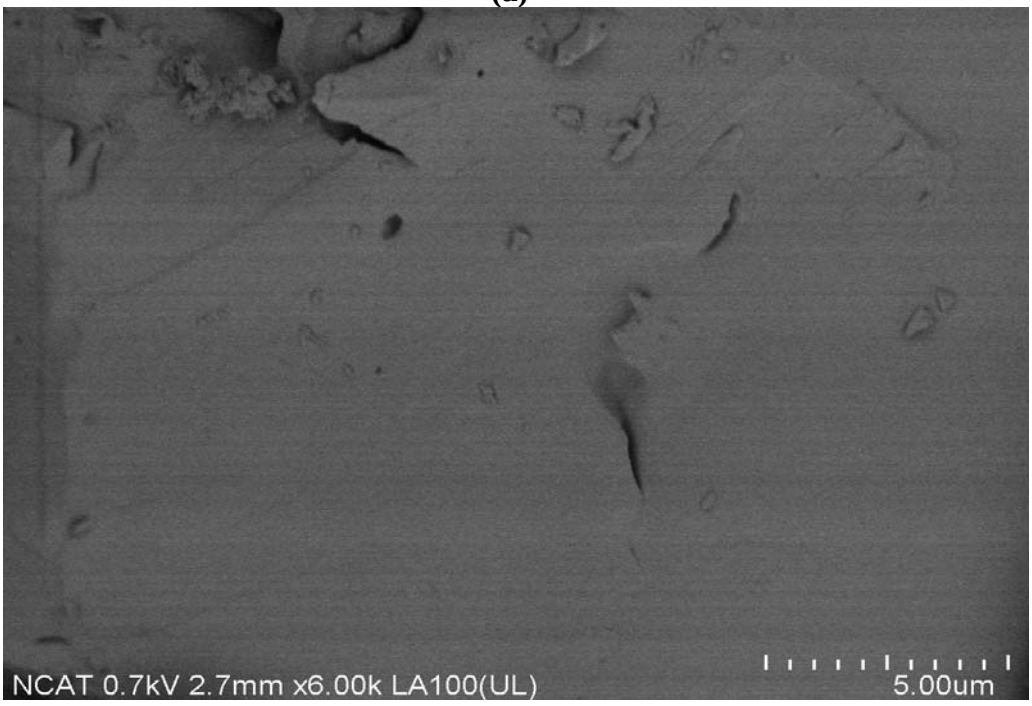

(b)

Figure 5.9. (a) Sample 27 crack surface with nanofibers, (b) Sample 7 crack surface without nanofibers

5.4 C-Scan

C-scanning is a non-destructive test that can non-destructively evaluate defects in a material. C-scanning is an extension of ultrasonic scanning that has evolved to be a very useful tool in determining laminated damage or possible flaws that lie within a material. C-scanning uses a transducer to produce an ultrasonic sound wave used to evaluate a specimen's integrity.

There are two modes of operation of a C-scan. The two different modes are pulse echo and through transmission. The pulse echo mode uses a single transducer for both transmitting and receiving. Through transmission uses two different transducers. One transducer pulses and the other transducer receive the ultrasound. The transducer produces a mechanical sound wave using a piezo-electric crystal. This transducer resonates at a specific frequency. In the present work, a 5.0 MHz transducer was used. The sound wave propagates through an intermediate medium to the coupon. A water medium is typically used to avoid the incompatibility of impedances between the different materials. An impedance mismatch may occur if a liquid is not used. The specimen is oriented such that a maximum amount of energy is absorbed by the specimen.

Pulse Echo: The transmitted and reflected waves are produced at the front edge, any anomaly, and back edge of the laminated specimen. The reflected wave within the boundary of the material gives an indication of damage. The absence of a reflected wave indicates continuity of the material, and indication of no flaw. Figure 5.10 illustrates a schematic of a signal of a reflected wave due to the presence of delamination.

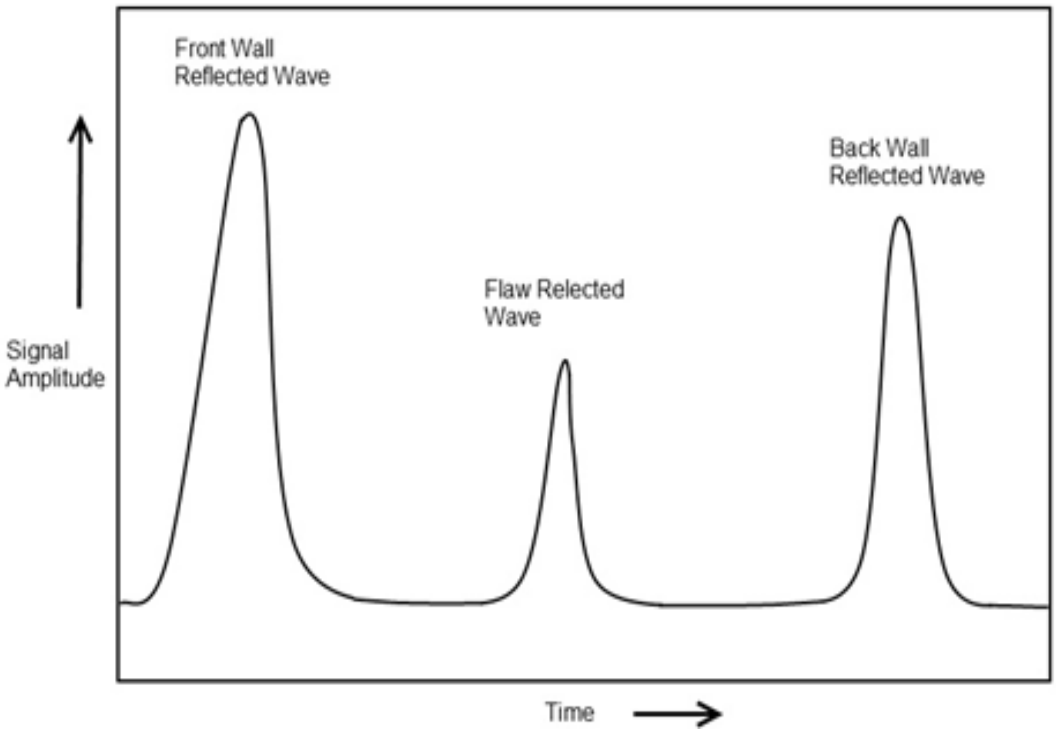

(a)

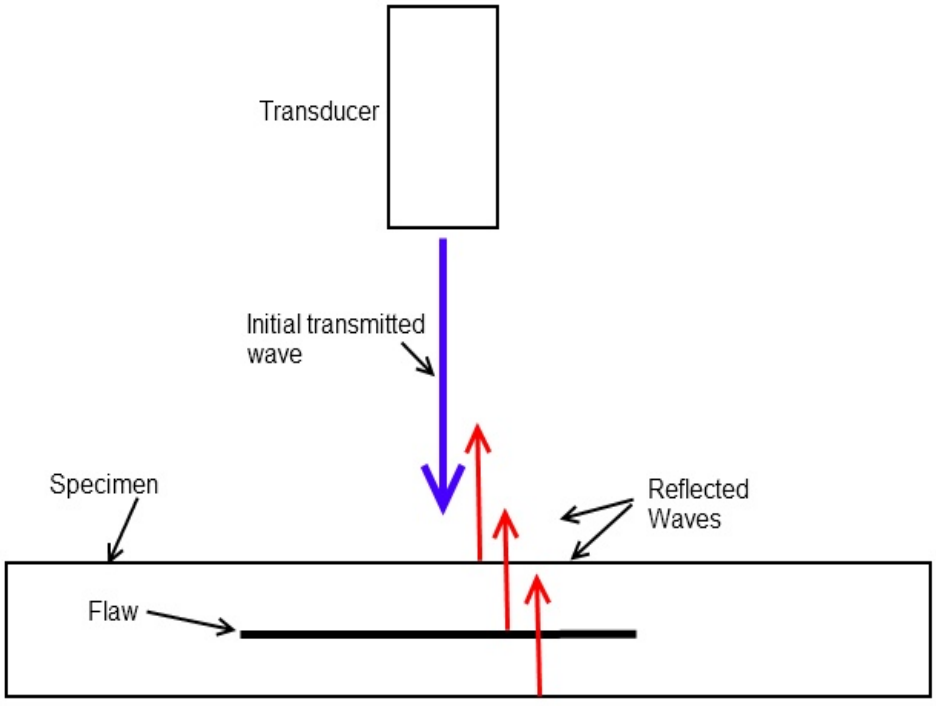

(b)

Figure 5.10. (a) Pulse-echo signal return (b) Pulse echo physics schematic

Through-Transmission: in through transmission technique, two transducers are used to produce an image of the quality. One transducer produces an ultrasonic sound wave that propagates to the specimen, enters the specimen, and leaves the specimen on the other side to be intercepted by a second transducer that acts as a receiver. The attenuation of the signal is an indication of the quality level (or damage presence) in the specimen. Figure 5.11 (a) and (b) shows a schematic and picture respectively of a through transmission system. Both through transmission and pulse echo modes require that the transducer(s) scan over the specimen in order to produce a two dimensional image.

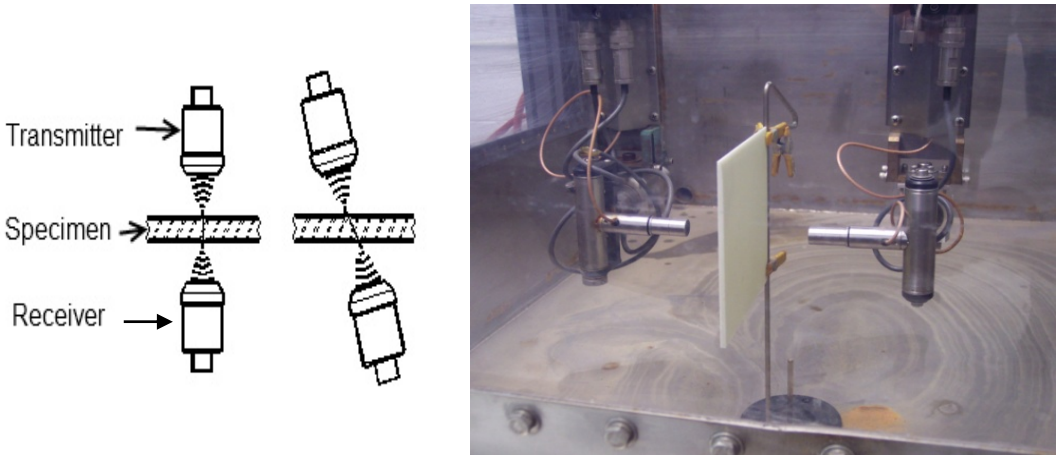

(a) **(b)**

Figure 5.11. (a) Schematic of through transmission, (b) Actual setup for through-transmission

Coupons are typically arranged in a fixture that keeps the orientation and spacial dimensions. Amplifiers are connected to the pulser and receiver augments the amount of energy that enters the material. Figure 5.12 shows the settings for the amplifiers as well

as the graphical user interface for the C-scan. A 3 in. x 3 in. area was scanned with the center of the area containing the impact zone. The scan speed of the C-scan was set to 1.5 in./sec. The scan index was set to 0.040 in. The scan time was approximately 15 minutes for each specimen. The computer software automatically acquires and stores data.

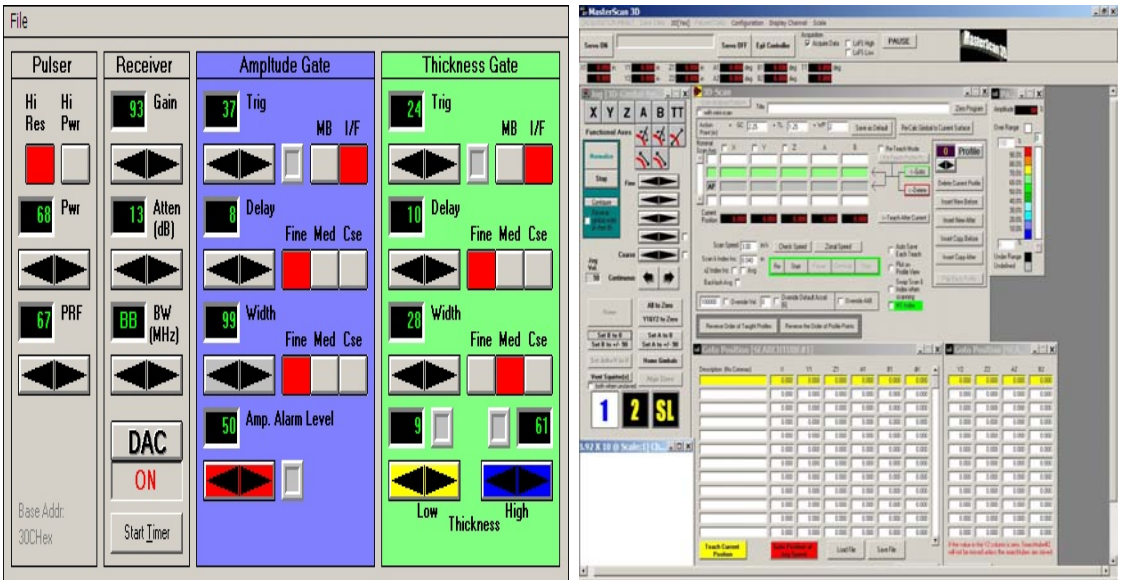

(a) **(b)**

Figure 5.12. (a) Power settings, (b) Master Scan 3D software output

Figure 5.13 illustrates the response from all 30 scans. The middle column shows the scans of the specimens produced without the electrospun material in between each layers. On the right are the specimens with electrospun nanofiber at the interfaces. The observations from the C-scan show that the electrospinning treatment causes more delamination at the interfacial layers. This allows delamination cracks to propagate further allowing more energy from the impactor to be transmitted into the specimen.

Therefore, more energy is transmitted into the specimen from the impactor to coupons with electrospun nanofibers than the ones without them. Also, the damage tends to be more severe showing signs of deeper penetration by the striker. Fiber breakage is evident in both treatments for the higher drop heights.

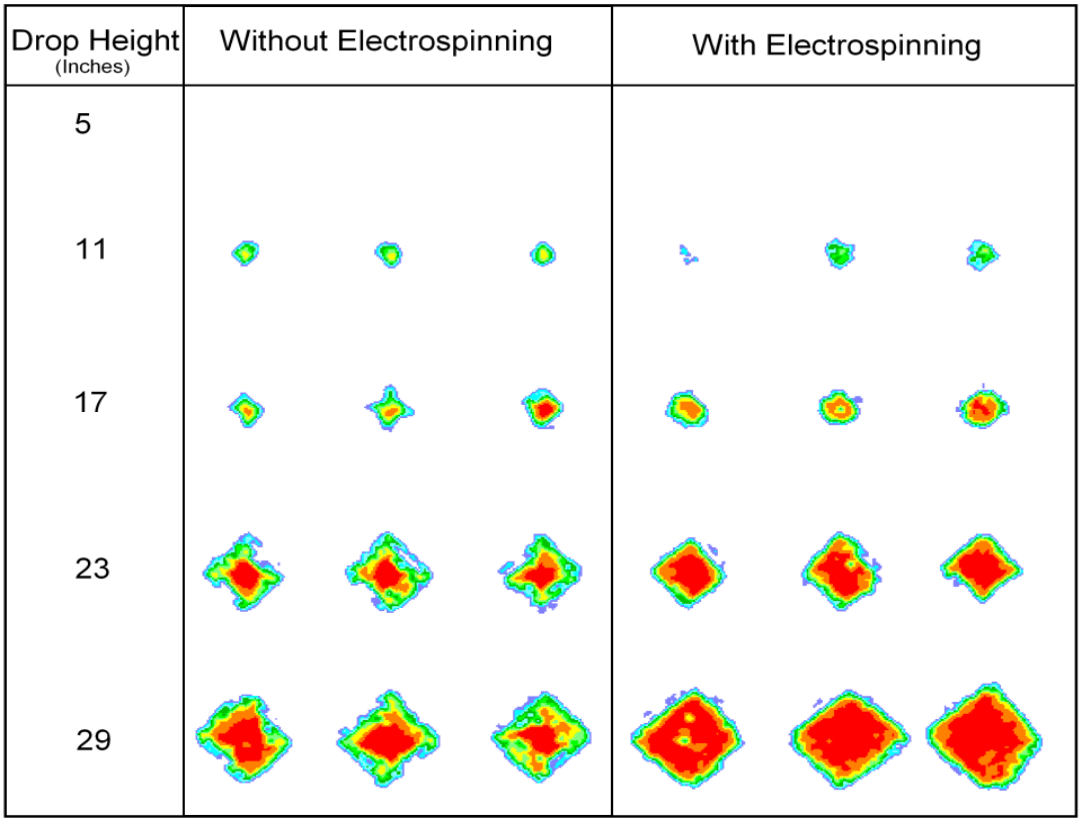

Figure 5.13. C-Scan comparison of impacted specimens

Using the SDI C-scan software, an accurate damage area was calculated using a histogram of the color of each pixel in the scan. Specimens that had electrospun interfacial treatment indicated larger damage areas than those that did without the treatment. The C-scan software calculated the damage area of an impact specimen. Each

damage area was divided into different colored pixels. The software summed up the number of pixels for each given color. A histogram was used to calculate the damage area of a specimen. Figure 5.14 show the screenshot of the software implementing the histogram feature. The damage area calculation is circled in Figure 5.14.

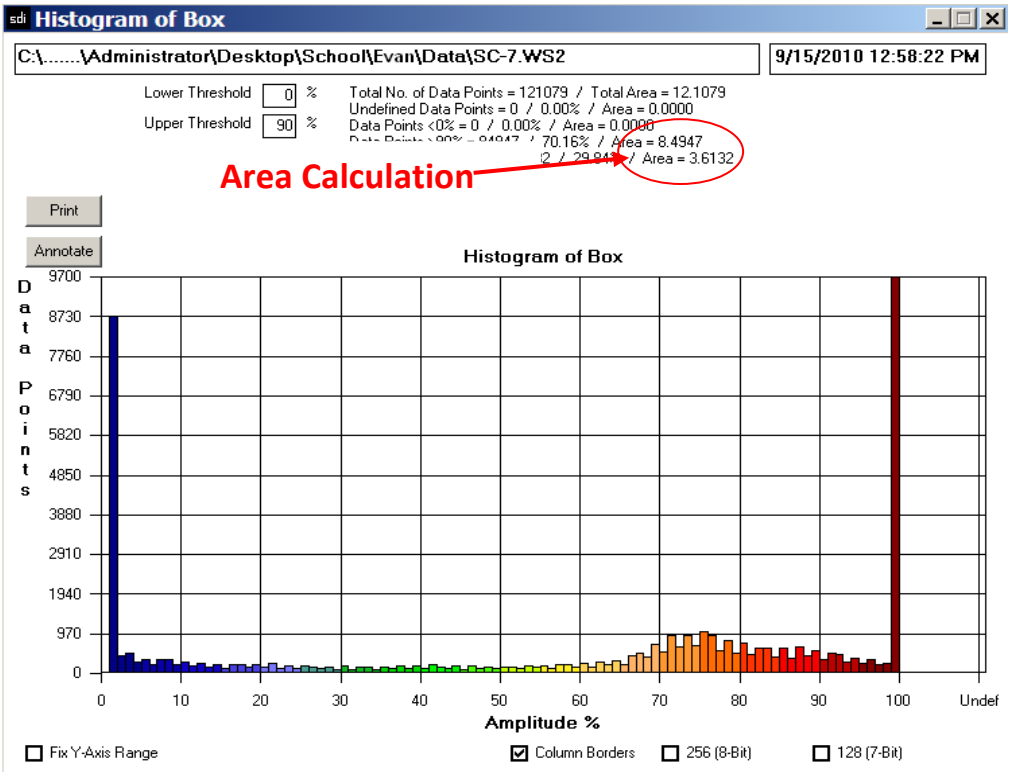

Figure 5.14. Histogram example of a given sample

From the histogram box, area calculations are tabulated. Background amplitudes are neglected with transmission amplitude above 96%. Table 5.1 tabulates the comparison of the damaged area for electrospinning and without electrospinning. It is observed from the table that there was larger damage for specimens that were treated with electrospun nanofibers. From the data in the table, an average area increase of 9% was

observed. This implies from the literature review that, if G_{IC} and G_{IIC} were higher with electrospun nanofibers, then the specimens with nanofibers absorbed significantly more energy than those without.

Table 5.1. Damaged area of specimens

Drop Height	Without Electrospun	With Electrospun
(Inches)	Damaged Area (inches^2)	Damaged Area (inches^2)
5	0.0000	0.0000
5	0.0000	0.0000
5	0.0000	0.0000
11	0.0508	0.0144
11	0.0568	0.0672
11	0.0500	0.0652
17	0.0844	0.1276
17	0.1196	0.1200
17	0.1220	0.1520
23	0.4340	0.3656
23	0.4340	0.4348
23	0.3868	0.3712
29	0.5848	0.7996
29	0.6056	0.7876
29	0.6088	0.8468

CHAPTER 6

COMPRESSION AFTER IMPACT TEST

Compression after impact testing is a common method used to determine the residual strength of materials after damage. A common strategy for impact specimens is as follows: ASTM standard D7136 test, followed by C-scan, followed by ASTM standard D7137 compression after impact test. Compression after impact testing is a destructive test that renders a specimen unusable for further testing. Residual strength of the specimen will be dependent upon the amount of cross-sectional damage that has occurred. A larger cross-sectional damage will result in a lower residual strength.

ASTM designation D7137 is the standard procedure for testing for the residual strength of plastic reinforced composite laminated plates. The test coupon dimension is 4 in. by 6 in. A minimum thickness of 0.200 in. is required for the test. The current research test coupons did not meet the minimum required thickness and samples were tested for indications of noncompliance or anomalies. During preliminary testing, indications of failure in non-critical areas required adjustments to the coupons. Tabs were affixed to each test specimen approximately 2.25 in. inches from the top and bottom on both sides. This prevented failure in non-critical areas due to bending of the specimen in the test fixture. Figure 6.1 shows a coupon with tabs affixed to the test coupon. Plastic gripping material was used for tabbing. Tabs were affixed using structural epoxy adhesive. The specimens were heated to 120 ^{o}F to fully cure the tabbing adhesive.

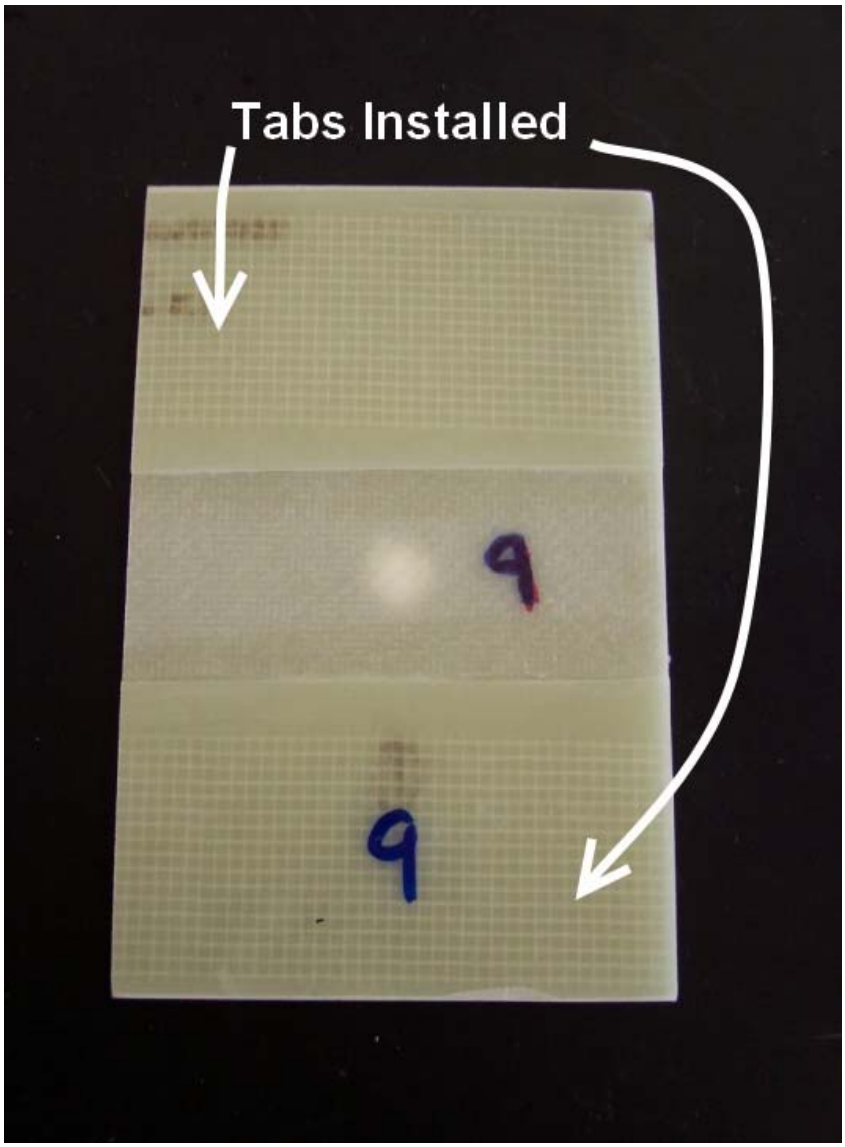

Figure 6.1. Tabbed specimen

The specimens were removed from the oven and adhesive overflow was trimmed so that the required 4 in. x 6 in. specifications were complied with. They were reduced from the impact size dimension of 6 in. x 6 in. to the required size of 4 in. x 6 in. A tile saw with water coolant was used to properly size the coupons. The coupons were then loaded into the D7137 test fixture pictured in Figure 6.2. The test fixture was designed

specifically for compression after impact testing. Once loaded into the test fixture, guides were adjusted to orient the specimen properly without applying a clamping force. Care was taken not to place a clamping force on the specimen that could alter the result. The guides prevented bending from occurring during the actual test. The test fixture was loaded into an Instron 30 kip load frame. Blue Hill software was used for writing the test method according to ASTM standard D7137/D7137M – 07. Strain gauges were not used during testing. The Instron testing frame was controlled with Blue Hill 2 software. Data was collected at a rate of 50 Hz.

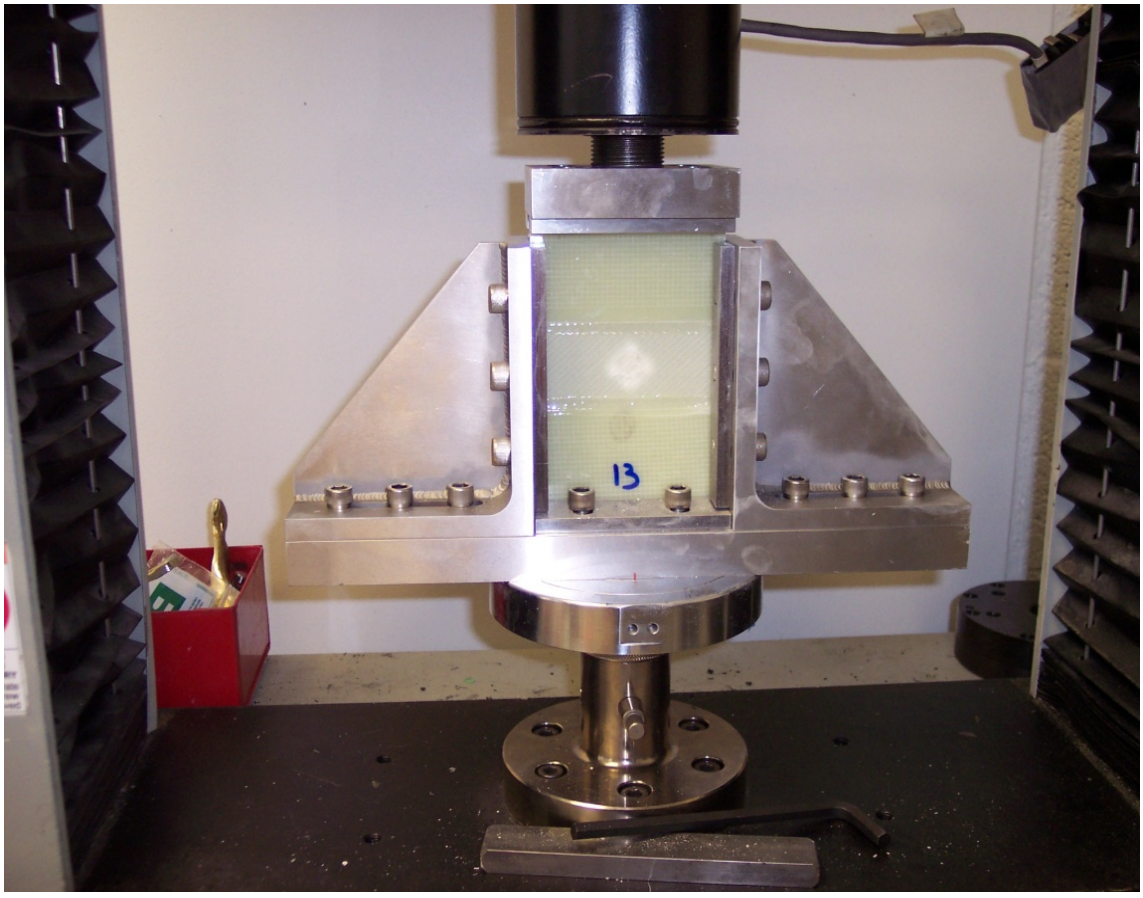

Figure 6.2. Picture of specimen inside test fixture

The compression test was displacement controlled. Test velocity of 0.030 in./sec was utilized to yield the proper failure time. This test speed was set below the suggested rate of 0.050 in./sec supplied by the ASTM standard to comply with test failure time. During the preliminary testing it was determined that failure would occur prior to a displacement of 0.100 in. Test standard D7137M requires failure to occur in 2-10 minutes after initiating the test. Failure occurred in the test specimens in approximately 3-5 minutes dependent upon the residual strength of the specimen.

Alignment of the test fixture was necessary to eliminate the influence of out of plane forces. The fixture was placed against a stop and aligned with visual indicators to ensure test consistency. Test limits of 40% load drop, 0.150 in. displacement or 12000 lb_f were used. Table 6.1 shows the acquired compression after impact. Several specimens failed prematurely. Compressive load strengths of both types of samples are shown in a bar chart in Figure 6.3. It was observed that specimens with electrospinning treatment at the interfaces experienced lower residual strengths than the non-treated specimens. Specimens without electrospinning treatment reported an average of 27% higher residual strength than those with treatment. This indicated larger damaged cross-sectional areas corresponded to lower residual strengths. Lower residual strength resulted from a smaller cross-sectional area resisting compression load due to a larger impact damage area. An example of this in the previous SEM picture (figure 5.5) showed more extensive damage at multiple interfacial layers. During compression testing, the multiple delaminated layers allowed for local micro-buckling thus, lowering residual strength of the specimen.

Table 6.1. Compression after impact data

	Without Electrospinning			With Electrospinning			
Drop Height	Compressive load	Compressive extension	Compressive stress	Compressive load	Compressive extension	Compressive stress	Increase/Decrease
(in)	(lbf)	(in)	(ksi)	(lbf)	(in)	(ksi)	% Load
5	7178	0.0710	20.3	8727	0.0648	20.3	0
5	3421	0.0835	09.7	8644	0.0615	20.5	112
5	6548	0.0708	18.8	9188	0.0718	21.6	15
11	7032	0.0701	20.1	3147	0.0625	07.4	-63
11	7990	0.0785	21.6	4472	0.0622	10.2	-53
11	7976	0.0816	21.6	5647	0.0561	12.9	-40
17	8435	0.0838	22.8	8662	0.0635	20.3	-11
17	8315	0.0858	22.6	7163	0.0514	16.6	-27
17	6982	0.0694	20.0	6708	0.0556	15.5	-22
23	6291	0.0648	18.1	7596	0.0626	18.1	0
23	6171	0.0639	17.8	7169	0.0544	17.3	-3
23	6215	0.0647	17.8	6018	0.0525	14.6	-18
29	5520	0.0613	15.8	3270	0.0516	08.0	-49
29	6529	0.0191	18.9	4320	0.0491	10.4	-45
29	6019	0.0633	17.6	3198	0.0466	07.8	-56

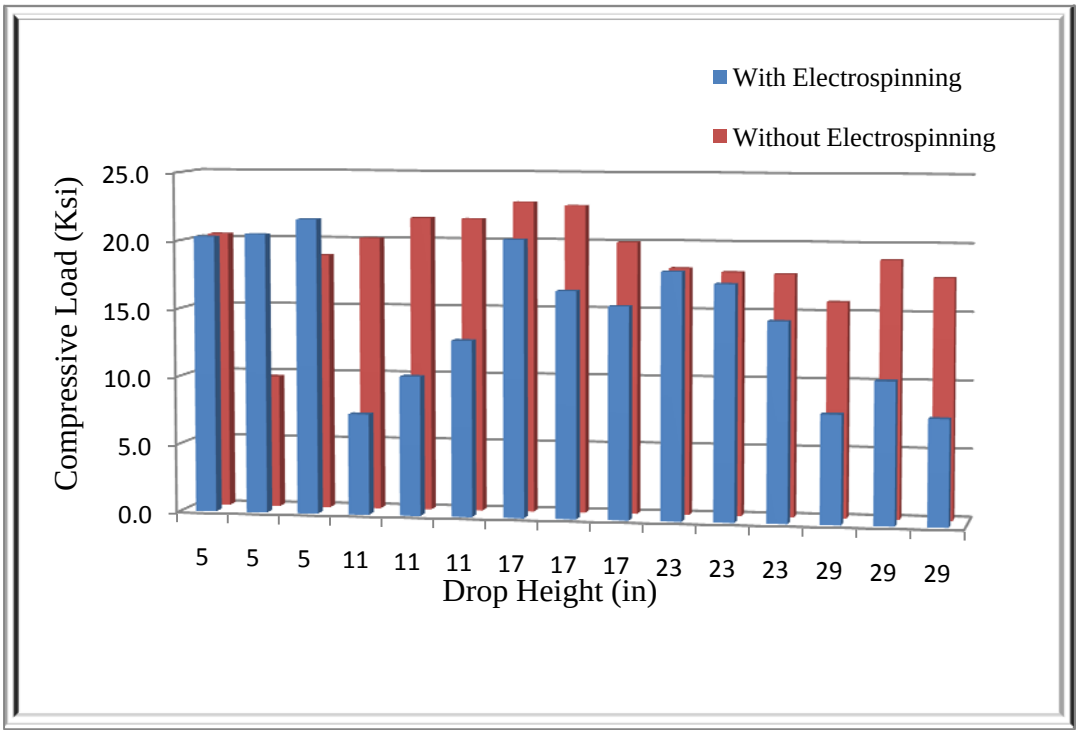

Figure 6.3. Compression after impact loading data

CHAPTER 7

CONCLUSIONS

Impact loading simulates real world conditions. Static tests sometimes do not predict damages that can occur during an impact event. Impacting a composite panel causes delamination which results in loss of strength in the laminate. The loss of strength could catastrophically affect a structure's load carrying ability. Because it absorbs energy, electrospinning glass nanofiber material can be an effective, alternative solution to situations in which protection from a projectile may be needed. Possible applications of energy absorbing composites may be implemented once the mechanical properties of composite laminates enhanced with electrospun nanofibers are obtained in greater detail. In the present work, impact specimens were produced with and without electrospun glass nanofiber enhancements at the interlaminar layers. Impact energies between 5 – 29 ft-lbs were exerted to the specimens with a drop weight tower tester. The specimens were then C-scanned for damage area quantification. Compression after impact tests were conducted to evaluate the residual strength.

It was observed from the impact tests, C-scans, and compression after impact tests that more energy was absorbed due to the sacrificial layers of electrospun glass nanofiber application. An increase of 9% of damage area was observed for specimens treated with electrospinning. A decrease of 27% residual strength was recorded for specimens that were treated with electrospinning. Both results imply that more damage was present with specimens that contained electrospun glass nanofibers at the interfacial region. SEM

images showed fractured surface with glass nanofiber breakage and fiber debonding which aided in absorbing of energy during impact crack propagation.

REFERENCES

1. Callister Jr., W.D., *Materials Science and Engineering: An Introduction*. 5th ed, ed. W. Anderson. 2000: John Wiley & Sons, Inc. 871.

2. Daniel, I.M., & O. Ishai, *Engineering Mechanics of Composite Materials.* 2nd ed. 2006. 411.

3. Guan, Z., & C. Yang, *Low-Velocity Impact and Damage Process of Composite Laminates.* Journal of Composite Materials, 2002. 36(7): p. 851-871.

4. Richardson, M.O.W., & M.J. Wisheart, *Review of low-velocity impact properties of composite materials.* Composites Part A: Applied Science and Manufacturing, 1996. 27(12): p. 1123-1131.

5. Joshi, S.P., & C.T. Sun, *Impact Induced Fracture in a Laminated Composite.* Journal of Composite Materials, 1985. 19(1): p. 51-66.

6. Shivakumar, K., W. Elber, & W. Illg, *Prediction of low-velocity impact damage in thin circular laminates.* AIAA, 1985. 23(3)(3): p. 442-449.

7. Liu, D., & L.E. Malvern, *Matrix cracking in impacted glass/epoxy plates.* Journal of Composite Materials, 1987. 21: p. 594-609.

8. Liu, D., *Impact-Induced Delamination--A View of Bending Stiffness Mismatching.* Journal of Composite Materials, 1988. 22(7): p. 674-692.

9. Sjoblom, P.O., J.T. Hartness, & T.M. Cordell, *ON LOW-VELOCITY IMPACT TESTING OF COMPOSITE MATERIALS.* Journal of Composite Materials, 1988. 22(1): p. 30-52.

10. Finn, S.R., *Composite plates impact damage : an atlas / Scott R. Finn, George S. Springer.* Lancaster, Pa. : Technomic Pub. Co., c1991, 1991.

11. Tsai, X., & J. Tang. *Impact behavior of laminated glass fiber composites by weight dropping testing method*. 1991. Covina, CA, USA: Publ by SAMPE.

12. Choi, H.Y., H.S. Wang, & F.-K. Chang, *Effect of Laminate Configuration and Impactor's Mass on the Initial Impact Damage of Graphite/Epoxy Composite Plates Due to Line-Loading Impact.* Journal of Composite Materials, 1992. 26(6): p. 804-827.

13. Wu, E., & K. Shyu, *Response of composite laminates to contact loads and relationship to low-velocity impact.* Journal of Composite Materials, 1993. 27(15): p. 1443-1464.

14. KargerKocsis, J., Q. Yuan, J. Mayer, & E. Wintermantel, *Transverse impact behavior of knitted carbon-fiber fabric-reinforced thermoplastic composite sheets.* Journal of Thermoplastic Composite Materials, 1997. 10(2): p. 163-172.

15. Abrate, S., *Impact on composite structures / Serge Abrate.* Cambridge ; New York, NY, USA : Cambridge University Press, 1998, 1998.

16. Lee, D.G., & S.S. Cheon, *Impact Characteristics of Glass Fiber Composites with Respect to Fiber Volume Fraction.* Journal of Composite Materials, 2001. 35(1): p. 27-56.

17. Kelkar, A.D., *Behavior of Thin, Moderately Thick and Thick Woven Composites Subjected to Low Velocity Impact Loads.* ASME meeting, 2002.

18. Corum, J.M., R.L. Battiste, & M.B. Ruggles-Wrenn, *Low-energy impact effects on candidate automotive structural composites.* Composites Science and Technology, 2003. 63(6): p. 755-769.

19. Zhou, R.X., H. Hu, N.L. Chen, & X.W. Feng, *An experimental and numerical study on the impact energy absorption characteristics of the multiaxial warp knitted (MWK) reinforced composites.* Journal of Composite Materials, 2005. 39(6): p. 525-542.

20. Feraboli, P., *Some recommendations for characterization of composite panels by means of drop tower impact testing.* Journal of Aircraft, 2006. 43(6): p. 1710-1718.

21. Yokoyama, T., & K. Nakai. *Evaluation of interlaminar shear strength of a unidirectional carbon/epoxy laminated composite under impact loading*. 2006.

22. Shirolikar, A., *Progressive damage analysis of impact on woven roven composites using LSDYNAÂ® / by Alok Shirolikar.* PhD Dissertation, 2008.

23. Tita, V., J. de Carvalho, & D. Vandepitte, *Failure analysis of low velocity impact on thin composite laminates: experimental and numerical approaches.* Composite Structures, 2008. 83(4): p. 413-28.

24. Yuanjian, T., & D.H. Isaac, *Combined impact and fatigue of glass fiber reinforced composites.* Composites Part B-Engineering, 2008. 39(3): p. 505-512.

25. Grassi, M., X. Zhang, & M. Meo, *Prediction of stiffness and stresses in z-fibre reinforced composite laminates.* Composites Part A: Applied Science and Manufacturing, 2002. 33(12): p. 1653-1664.

26. Mouritz, A.P., *Fracture and tensile fatigue properties of stitched fibreglass composites.* Proceedings of the Institution of Mechanical Engineers Part L-Journal of Materials-Design and Applications, 2004. 218(L2): p. 87-93.

27. Formhals, A., *US patent 1,975,504.* 1934.

28. Boland, E.D., G.E. Wnek, D.G. Simpson, K.J. Pawlowski, and G.L. Bowlin, *Tailoring tissue engineering scaffolds using electrostatic processing techniques: A study of poly(glycolic acid) electrospinning.* Journal of Macromolecular Science - Pure and Applied Chemistry, 2001. 38 A(12): p. 1231-1243.

29. Han, D., S. Goldgraben, M.D. Frame, & P.-I. Gouma. *A novel nanofiber scaffold by electrospinning and its utility in microvascular tissue engineering*. 2005. Warrendale, PA 15086, United States: Materials Research Society.

30. Khil, M.-S., S.R. Bhattarai, H.-Y. Kim, S.-Z. Kim, and K.-H. Lee, *Novel fabricated matrix via electrospinning for tissue engineering.* Journal of Biomedical Materials Research - Part B Applied Biomaterials, 2005. 72(1): p. 117-124.

31. Kidoaki, S., I.K. Kwon, & T. Matsuda, *Mesoscopic spatial designs of nano- and microfiber meshes for tissue-engineering matrix and scaffold based on newly devised multilayering and mixing electrospinning techniques.* Biomaterials, 2005. 26(1): p. 37-46.

32. Zhao, M.-L., G. Sui, X.-L. Deng, J.-G. Lu, S.-K. Ryu, and X.-P. Yang. *PLLA/HA electrospin hybrid nanofiber scaffolds: Morphology, in vitro degradation and cell culture potential*. 2006. Clausthal-Zellerfeld, D-38670, Germany: Trans Tech Publications.

33. Ashammakhil, N., A. Ndreu, A.M. Piras, L. Nikkola, T. Sindelar, H. Ylikauppila, A. Harlin, M.E. Gomes, N.M. Neves, E. Chiellini, F. Chiellini, V. Hasirci, H. Redl, and R.L. Reis, *Biodegradable nanomats produced by electrospinning: Expanding multifunctionality and potential for tissue engineering.* Journal of Nanoscience and Nanotechnology, 2007. 7(3): p. 862-882.

34. Lannutti, J., D. Reneker, T. Ma, D. Tomasko, and D. Farson, *Electrospinning for tissue engineering scaffolds.* Materials Science and Engineering C, 2007. 27(3): p. 504-509.

35. Agarwal, S., J.H. Wendorff, & A. Greiner, *Use of electrospinning technique for biomedical applications.* Polymer, 2008. 49(26): p. 5603-5621.

36. Liao, S., R. Murugan, C.K. Chan, & S. Ramakrishna, *Processing nanoengineered scaffolds through electrospinning and mineralization suitable for biomimetic bone tissue engineering.* Journal of the Mechanical Behavior of Biomedical Materials, 2008. 1(3): p. 252-260.

37. Martins, A., R.L. Reis, & N.M. Neves, *Electrospinning: Processing technique for tissue engineering scaffolding.* International Materials Reviews, 2008. 53(5): p. 257-274.

38. Ramachandran, K., & P.-I. Gouma, *Electrospinning for bone tissue engineering.* Recent Patents on Nanotechnology, 2008. 2(1): p. 1-7.

39. Sill, T.J., & H.A. von Recum, *Electrospinning: Applications in drug delivery and tissue engineering.* Biomaterials, 2008. 29(13): p. 1989-2006.

40. Sayers, K.H., & B. Harris, *Interlaminar Shear Strength of a Carbon Fibre Reinforced Composite Material Under Impact Conditions.* Journal of Composite Materials, 1973. 7(1): p. 129-133.

41. Wu, H.-Y.T., & G.S. Springer, *Impact Induced Stresses, Strains, and Delaminations in Composite Plates.* Journal of Composite Materials, 1988. 22(6): p. 533-560.

42. Zhang, X., G.A.O. Davies, & D. Hitchings, *Impact damage with compressive preload and post-impact compression of carbon composite plates.* International Journal of Impact Engineering, 1999. 22(5): p. 485-509.

43. http://www.besportier.com/archives/dunlop-aerogel-300-tennis-racq.html.

44. Shyr, T.-W., & Y.-H. Pan, *Impact resistance and damage characteristics of composite laminates.* Composite Structures, 2003. 62(2): p. 193-203.

45. Bledzki, A.K., J. Gassan, & A. Kessler, *Loss energy of composite materials. II. Impact loading.* Journal of Testing and Evaluation, 1999. 27(1): p. 36-41.

46. Aktas, M., R. Karakuzu, & Y. Arman, *Compression-after impact behavior of laminated composite plates subjected to low velocity impact in high temperatures.* Composite Structures, 2009. 89(1): p. 77-82.

47. Liu, D., *Delamination Resistance in Stitched and Unstitched Composite Plates Subjected to Impact Loading.* Journal of Reinforced Plastics and Composites, 1990. 9(1): p. 59-69.

48. Jih, C.J., & C.T. Sun, *Prediction of Delamination in Composite Laminates Subjected to Low Velocity Impact.* Journal of Composite Materials, 1993. 27(7): p. 684-701.

49. Liu, S., Z. Kutlu, & F.-K. Chang, *Matrix Cracking and Delamination in Laminated Composite Beams Subjected to a Transverse Concentrated Line Load.* Journal of Composite Materials, 1993. 27(5): p. 436-470.

50. Hirai, Y., H. Hamada, & K. Jang-Kyo, *Impact response of woven glass-fabric composites. - I. Effect of fibre surface treatment.* Composites Science and Technology, 1998. 58(1): p. 91-104.

51. Hull, D., *An Introduction to Composite Materials.* 1981.

52. Icten, B.M., *Repeated impact behavior of glass/epoxy laminates.* Polymer Composites, 2009. 30(11): p. 1562-1569.

53. Elawadly, K.M., *On the Interlaminar Shear Stress Response for E-Glass/Epoxy Composite.* Journal of Composite Materials, 2003. 37(23): p. 2149-2158.

54. Mouritz, A.P., *Ballistic impact and explosive blast resistance of stitched composites.* Composites Part B-Engineering, 2001. 32(5): p. 429-437.

55. Mouritz, A.P., *Review of z-pinned composite laminates.* Composites Part a-Applied Science and Manufacturing, 2007. 38(12): p. 2383-2397.

56. Freitas G, Magee C, Dardzinski P, & Fusco T, *Fibre insertion process for improved damage tolerance in aircraft laminates.* Journal of Advanced Materials, 1994. 25: p. 36-43.

57. Barrett, D.J., *The mechanics of z-fiber reinforcement.* Composite Structures, 1996. 36(1-2): p. 23-32.

58. Rugg, K.L., B.N. Cox, & R. Massabò, *Mixed mode delamination of polymer composite laminates reinforced through the thickness by z-fibers.* Composites Part A: Applied Science and Manufacturing, 2002. 33(2): p. 177-190.

59. Birman V, & Byrd LW, *Effect of z-Pins on Fracture in Composite Cocured Double Cantilever Beams.* Journal of Aerospace Engineering, 2005. 18(1): p. 51-59.

60. Byrd, L.W., & V. Birman, *The estimate of the effect of z-pins on the strain release rate, fracture and fatigue in a composite co-cured z-pinned double cantilever beam.* Composite Structures, 2005. 68(1): p. 53-63.

61. Dickinson, L.C., G.L. Farley, & M.K. Hinders, *Prediction of Effective Three-Dimensional Elastic Constants of Translaminar Reinforced Composites.* Journal of Composite Materials, 1999. 33(11): p. 1002-1029.

62. Chang, P., A.P. Mouritz, & B.N. Cox, *Flexural properties of z-pinned laminates.* Composites Part A: Applied Science and Manufacturing, 2007. 38(2): p. 244-251.

63. Aymerich, F., R. Onnis, & P. Priolo, *Analysis of the fracture behaviour of a stitched single-lap joint.* Composites Part a-Applied Science and Manufacturing, 2005. 36(5): p. 603-614.

64. Rydin, R.W., H.Y. Ma, & E.T. Thostenson, *An assessment of the impact response of knit/knit stitch fabric reinforced epoxy composites.* Science and Engineering of Composite Materials, 1998. 7(3): p. 269-277.

65. Kang, T.J., & S.H. Lee, *EFFECT OF STITCHING ON THE MECHANICAL AND IMPACT PROPERTIES OF WOVEN LAMINATE COMPOSITE.* Journal of Composite Materials, 1994. 28(16): p. 1574-1587.

66. Mouritz, A.P., J. Gallagher, & A.A. Goodwin, *Flexural strength and interlaminar shear strength of stitched GRP laminates following repeated impacts.* Composites Science and Technology, 1997. 57(5): p. 509-522.

67. Jain, L.K., & Y.W. Mai, *Determination of mode II delamination toughness of stitched laminated composites.* Composites Science and Technology, 1995. 55(3): p. 241-253.

68. Sankar, B.V., & H.S. Zhu, *The effect of stitching on the low-velocity impact response of delaminated composite beams.* Composites Science and Technology, 2000. 60(14): p. 2681-2691.

69. Hosur, M.V., M. Adya, J. Alexander, S. Jeelani, U. Vaidya, and A. Mayer, *Studies on impact damage resistance of affordable stitched woven carbon/epoxy composite laminates.* Journal of Reinforced Plastics and Composites, 2003. 22(10): p. 927-952.

70. Wu, E.B., & J. Wang, *Behavior of stitched laminates under in-plane tensile and transverse impact loading.* Journal of Composite Materials, 1995. 29(17): p. 2254-2279.

71. Dzenis YA, & W. YK, *Delamination resistant composites prepared by small diameter fiber reinforcement at ply interfaces.* US Patent No: 6265333, 2001.

72. Krishnan, V., *Performance evaluation and modeling of woven roving glass, stitch bonded glass, and stitch bonded carbon composites subjected to low velocity impact loads / by Vijay Krishnan.* 2004, 2004.

73. Liu, L., Z.-M. Huang, G.-Y. Xu, Y.-M. Liang, and G.-H. Dong, *Mode II interlaminar delamination of composite laminates incorporating with polymer ultrathin fibers.* Polymer Composites, 2008. 29(3): p. 285-292.

74. Bolick, R., *A comparative study of unstitched, stitched, and Z-pinned plain woven composites under fatigue loading,*, in *PhD dissertation*. 2005.

75. Doshi, J., & D.H. Reneker, *Electrospinning process and applications of electrospun fibers.* Journal of Electrostatics, 1995. 35(2-3): p. 151-160.

76. Rayleigh, L., *On the equilibrium of liquid conducting masses charged with electricity.* Philosophical Magazine, 1882. 14: p. 184-186.

77. Formhals, A., *Production of Artificial Fibers.* US patent 2,077,373, 1936.

78. Formhals, A., *Artificial fiber construction.* US patent 2,109,333, 1938.

79. Formhals, A., *Method and Apparatus for the Production of Fibers.* US patent 2,116,942, 1938.

80. Formhals, A., *Method and Apparatus for the production of fibers.* US patent 2,123,992, 1938.

81. Formhals, A., US patent 2,160,632, 1939. patentstorm.com.

82. Formhals, A., *Method and Apparatus for the production of artificial fibers.* US patent 2,158,416, 1939.

83. Formhals, A., *Method and apparatus for spinning.* US patent 2,160,962, 1939.

84. Formhals, A., *Method of producing artificial fibers.* US patent 2,158,415, 1939.

85. Formhals, A., US patent 2,187,306, 1940.

86. Formhals, A., *Production of artificial fibers from fiber forming liquids.* US patent 2,323,025, 1943.

87. Formhals, A., *Method and Apparatus for Spinning.* US patent 2,349,950, 1944.

88. Dan Li, & Y. Xia, *Electrospinning of Nanofibers: Reinventing the Wheel.* Advanced Materials, 2004. 16(14): p. 1151.

89. Vonnegut, B., & R.L. Neubauer, *Production of monodisperse liquid particles by electrical atomization.* Journal of Colloid Science, 1952. 7: p. 616.

90. Taylor, G.I., *Disintegration of water drops in an electric field.* Proceedings of Royal Society of London, Ser A, 1964. 280: p. 383-397.

91. Simons, H.L., *Process and apparatus for producing patterned non-woven fabrics.* US patent 3,280,229, 1966.

92. Baumgarten, P.K., *Electrospinning process and applications of electrospun fibers.* Journal of Colloid and Interface Science, 1971. 36: p. 71-79.

93. Boland, E., G. Wnek, D. Simpson, Palowski KJ, and G. Bowlin, *Tailoring tissue engineering scaffols using electrostatic processing techniques: a study of poly (glycolic acid) electrospinning.* Journal of Macromolecule Science Pu Appl Chem, 2001. A38(12): p. 1231-43.

94. Huang, Z.-M., Y.Z. Zhang, M. Kotaki, & S. Ramakrishna, *A review on polymer nanofibers by electrospinning and their applications in nanocomposites.* Composites Science and Technology, 2003. 63(15): p. 2223-2253.

95. Bornat, A., *Production of Electrostatically Spun Products.* US patent 4,689,186, 1987.

96. Fong, H., & D.H. Reneker, *Elastomeric nanofibers of styrene–butadiene–styrene triblock copolymer*. 1999, John Wiley & Sons, Inc. p. 3488-3493.

97. Theron A, Zussman E, & A.L. Yarin, *Electrostatic field-assisted alignment of electrospun nanofibres.* Nanotechnology, 2001. 12: p. 384-90.

98. Reneker, D.H., A.L. Yarin, H. Fong, & S. Koombhongse, *Bending instability of electrically charged liquid jets of polymer solutions in electrospinning*, in *Journal of Applied Physics*. 2000, American Institute of Physics. p. 4531.

99. Craighead, G., *A scanning tip electrospinning for deposition of oriented nanofibers.* Nanotechnology, 2003. 14: p. 1124-1129.

100. Huang, Z.M., Y.Z. Zhang, S. Ramakrishna, & C.T. Lim, *Electrospinning and mechanical characterization of gelatin nanofibers.* Polymer, 2004. 45(15): p. 5361-5368.

101. Deitzel, J.M., J. Kleinmeyer, D. Harris, & N.C. Beck Tan, *The effect of processing variables on the morphology of electrospun nanofibers and textiles.* Polymer, 2001. 42(1): p. 261-272.

102. Fong, H., I. Chun, & D.H. Reneker, *Beaded nanofibers formed during electrospinning.* Polymer, 1999. 40(16): p. 4585-4592.

103. S., C., *Review: carbon fibers for composites.* Jounrla of Material Science, 2000. 35: p. 1303-1313.

104. Kelkar, A., R. Mohan, R. Bolick, & S. Shendokar, *Effect of Electrospun Fibers on the Interlaminar Properties of Woven Composites.* Advanced Materials Research, 2008. 47-50: p. 1031-1034.

105. Thompson, C.J., G.G. Chase, A.L. Yarin, & D.H. Reneker, *Effects of parameters on nanofiber diameter determined from electrospinning model.* Polymer, 2007. 48(23): p. 6913-6922.

106. Ajit D. Kelkar, Ram Mohan, Ronnie Bolick, & S. Shendokar, *Effect of Electrospun Fibers on the Interlaminar Properties of Woven Composites.* Advanced Materials Research 2009.

107. Kong, C., T. Lee, S. Lee, & H. Kim, *Nano-web formation by the electrospinning at various electric fields.* Journal of Materials Science, 2007. 42(19): p. 8106-8112.

108. Wong, E.W., & P.E. Sheehan, *Nanobeam mechanics: Elasticity, strength, and toughness of nanorods and nonotubes.* Science, 1997. 277(5334): p. 1971.

109. Suthat A, & C. G, *Chemical Engineer.* 2001: p. 26-8.

110. Smith, D., D. Reneker, G. Schreuder, C. Mello, M. Sennett, and P. gibson, *PCT/US00.* 2001: p. 27776.

111. King, R.S. *Boeing 787*. 2010; http://www.airliners.net/photo/Boeing/Boeing-787-8-Dreamliner/1771901/L/&sid=60821893fd00ad4184c983e10ddb5b67.

112. Pipes, R.B., & N.J. Pagano, *Interlaminar Stresses in Composite Laminates Under Uniform Axial Extension.* Journal of Composite Materials, 1970. 4: p. 538-548.

113. Daniel, I.M., R.E. Rowland, & J.B. Whiteside, *Effects of Material and Stacking Sequence on Behavior of Composite Plates with Holes.* Experimental Mechanics, 1974. 14: p. 1-9.

114. Shivakumar, K., *MEEN 813 Chapter 9 Class Presentation*. 2010. p. 10.

115. Xia, Y., P. Yang, Y. Sun, Y. Wu, B. Mayers, B. Gates, Y. Yin, F. Kim, and H. Yan, *One-Dimensional Nanostructures: Synthesis, Characterization, and Applications*. 2003, WILEY-VCH Verlag. p. 353-389.

116. Sakka, S., & K. Kamiya, *The Sol-Gel Transition in the Hydrolysis of Metal Alkoxides in the Relation to the Formation of Glass Fibers and Films.* Journal of Non-Crystalline Solids, 1982. 48: p. 31-46.

117. Boyd, T., Journal of Polym. Sci., 1951. 7: p. 591.

118. Bradley, D.C., F.G.A. Stone, & W.A.G. Gaham, Inorganic polymers, 1962: p. 410.

119. Taylor, G.I., *Disintegration of Water Drops in an Electric Field.* Proceedings of the Royal Society of Lond. Series A, Mathematical and Physical Sciences, 1964. 280(1382): p. 383-397.

120. Shendokar, S., *Manufacturing and Characterization of Advance Delamination Resistant Composites Interleaved with Electrospun Nanofibers*, in *PhD dissertation*. 2010, North Carolina Agricultural & Technical University: Greensboro. p. 86.

121. Shendokar, S., A. Kelkar, R. Mohan, R. Bolick, and G. Chandekar, *Effect of Sintering Temperature on Mechanical Properties of Electrospun Silica Nanofibers.* Proceedings of IMECE2008 ASME International Engineering Congress and Exposition, 2008.

122. Bolick, R.L., & A. Kelkar, *Heated vacuum assisted resin transfer molding process for manufacturing composite materials.* US Patent, 2009. 0189320A1.

APPENDIX A

PREPREG PROPERTIES

Advanced Composites Group
umeco composites

ACG VTM®260 SERIES
VARIABLE TEMPERATURE MOULDING
PREPREG SYSTEM

Product Description

ACG VTM®260 Series resin systems are toughened, flexible cure temperature epoxy resin matrices specifically developed for vacuum bag processing and the manufacture of large structures.

VTM260 Series resin systems offer excellent handling and processing characteristics across a range of reinforcements in both standard prepreg and ZPREG® selective impregnation formats.

All VTM260 Series resin systems and their associated, complementary adhesives, surfacing films and syntactic plies can be co-cured.

VTM260 Series resin systems can be used for both component and tooling applications.

Features

- Outstanding vacuum-only processing capability on a wide range of reinforcement formats.
- Flexible curing capability in a single prepreg system; low temperature, i.e. 65 to 80°C (150 to 180°F) and medium temperature, i.e. 80 to 120°C (180 to 250°F).
- Up to 30 days out life at 21°C (70°F).
- 12 months freezer storage life at –18°C (0°F).
- Service temperature up to 100°C (212°F).
- VTM263 high viscosity, low flow variant - suitable for selective impregnation of fabrics or full impregnation of lightweight fabric reinforcements.
- VTM264 intermediate viscosity and tack - suitable for full impregnation of light and medium weight unidirectional and fabric reinforcements. Also available as a flame retarded variant VTM264FRB
- VTM266 low viscosity - suitable for the full impregnation of ultra-heavyweight fabric reinforcements up to 2400g/m².
- VTM267 - reduced temperature sensitivity and controlled tack for sided impregnation and film infusion. Flame retarded variant VTM267FRB also available.
- Available in ZPREG® selective impregnation formats.
- Complementary range of VTM260 Series adhesives, surfacing films and syntactic plies.

- All VTM260 Series resins are fully compatible and can be co-cured.

Resin Selector Guide

Resin	Tack @15°C (60°F)	Tack @21°C (70°F)	Glass UD	Carbon UD	Glass Woven	Carbon Woven
VTM263	Low	Low/Medium	N/A	N/A	<300gsm	<300gsm
VTM264	Low	Medium	<400gsm	<600gsm	<900gsm	<900gsm
VTM266	Medium	High	<600gsm	<600gsm	>900gsm	>900gsm
VTM267	Very Low	Low	Differential coating of heavy reinforcements			

* The practical work life at 21°C (70°F) will depend on a number of factors, including fibre type, reinforcement weight, degree of impregnation and cure temperature. The work life may be reduced for heavy or partially impregnated reinforcements, potentially leading to incomplete wet out.

Instructions for Use

The prepreg should be removed from the freezer, thawed and allowed to reach room temperature before removal from the polythene protective bag.

Prepreg should be cut to shape and laid up in accordance with design instructions. Care must be taken to ensure that the prepreg conforms exactly to the tool shape, especially around internal corners. The lay up should be vacuum debulked at regular intervals using a P3 (pin pricked) Halar release film on the prepreg surface and a lightweight breather. Depending on prepreg format, vacuum of 980 mbar (29in Hg) should be applied for up to 30 minutes.

Recommended Bagging arrangement:

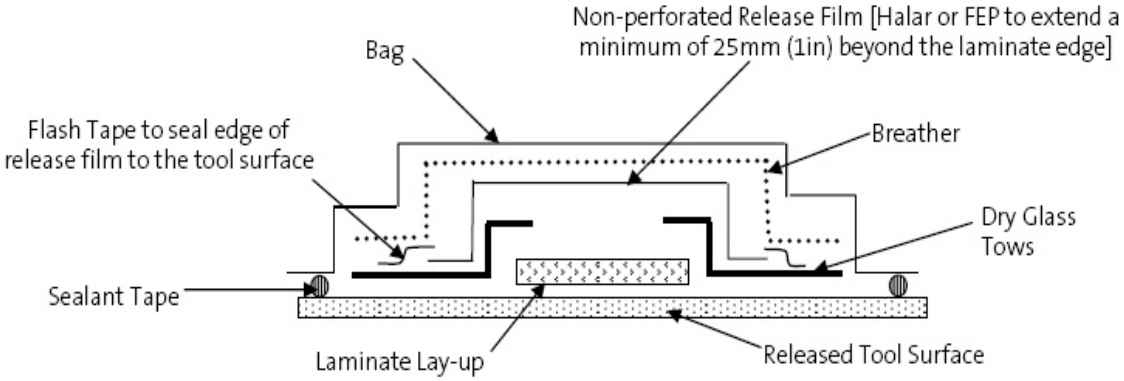

Glass Tows Detail

Placing dry glass tows at 0.5m (20in) intervals around the edge of the laminate will provide air paths under the release film and into the breather (depicted above).

VTM260 Series Recommended Cure Times and Tg Development

Cure Temperature	Recommended Cure Time	Developed Tg (DMA Onset)
65°C (150°F)	16 hours	80°C (176°F)
80°C (180°F)	5 hours	95°C (203°F)
100°C (210°F)	2 hour	115°C (239°F)
120°C (250°F)	1 hour	120°C (248°F)

Note: The minimum cure temperature for the VTM260 Series of prepregs is 65°C (150°F).

Post-Cure

Laminates may be post-cured unsupported unless the size, shape and laminate thickness would allow excessive distortion under self-weight, in which case some minimal support is desirable.

In applications demanding maximum temperature or environmental resistance it is essential that the component is post-cured to fully develop the glass transition temperature.

Heat the component from room temperature (RT) to 120 ±2°C (250 ±4.0°F) at 20°C (40 °F)/hour.

Note:
Parts may be loaded into a pre-heated oven set at the original cure temperature.

Dwell at 120 ±2°C (250 ±4.0°F) for 1 hour (minimum), as measured by the lagging thermocouple attached to the laminate.

Cool to room temperature.

Technical Data

Matrix Resin Properties:

Cured Resin Property	VTM260 Series
Cured resin density g/cm^3	1.19

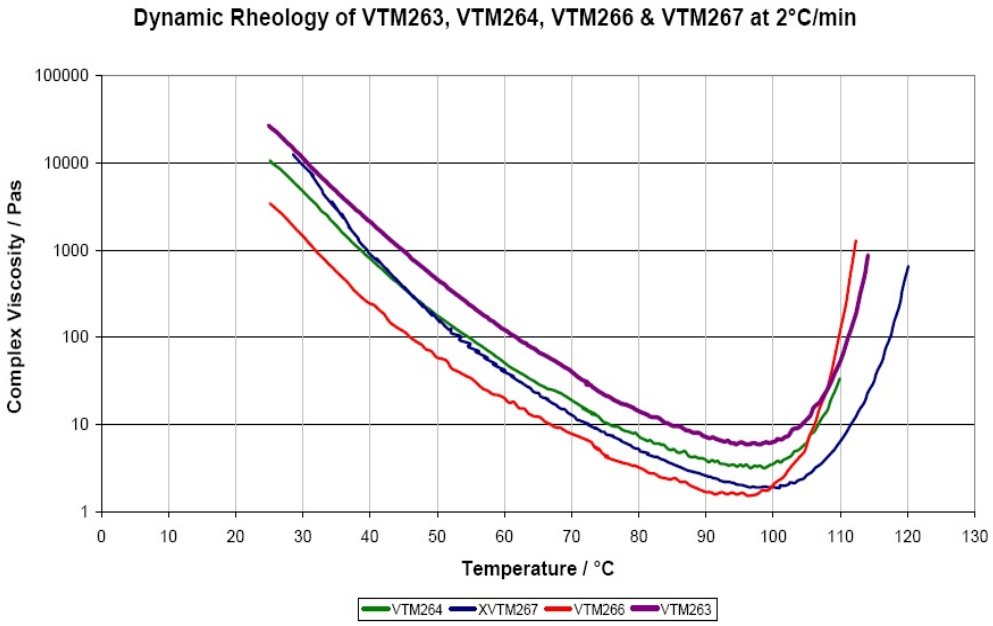

APPENDIX B

DROP TEST DATA

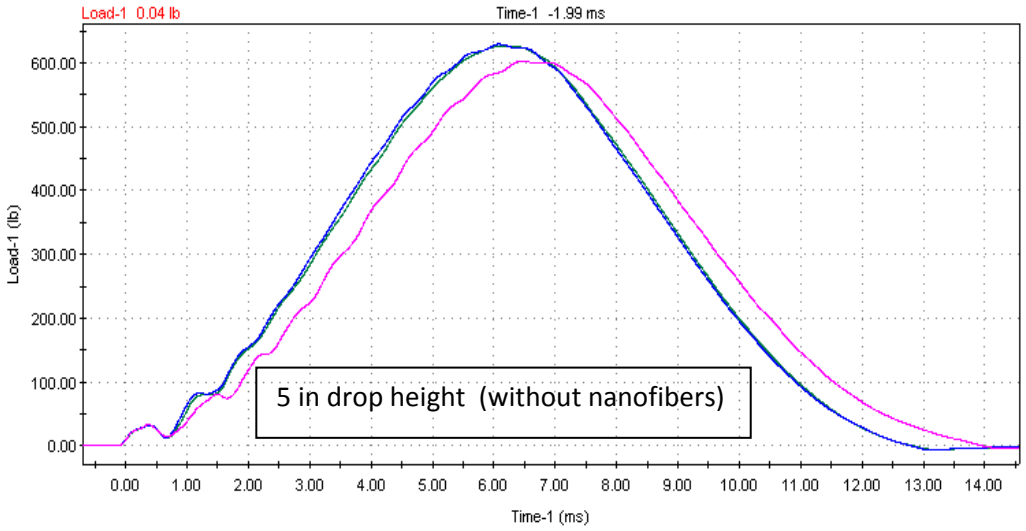

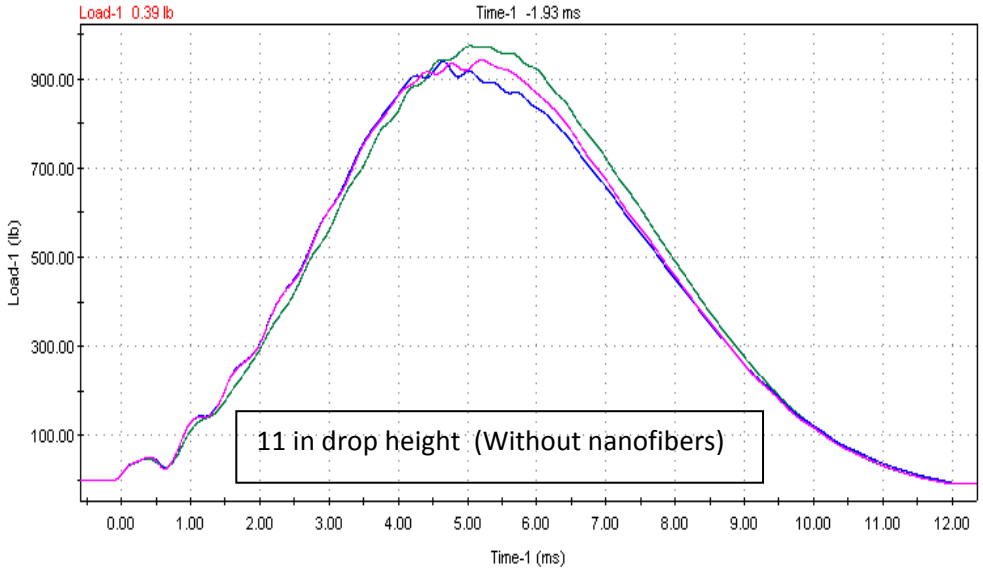

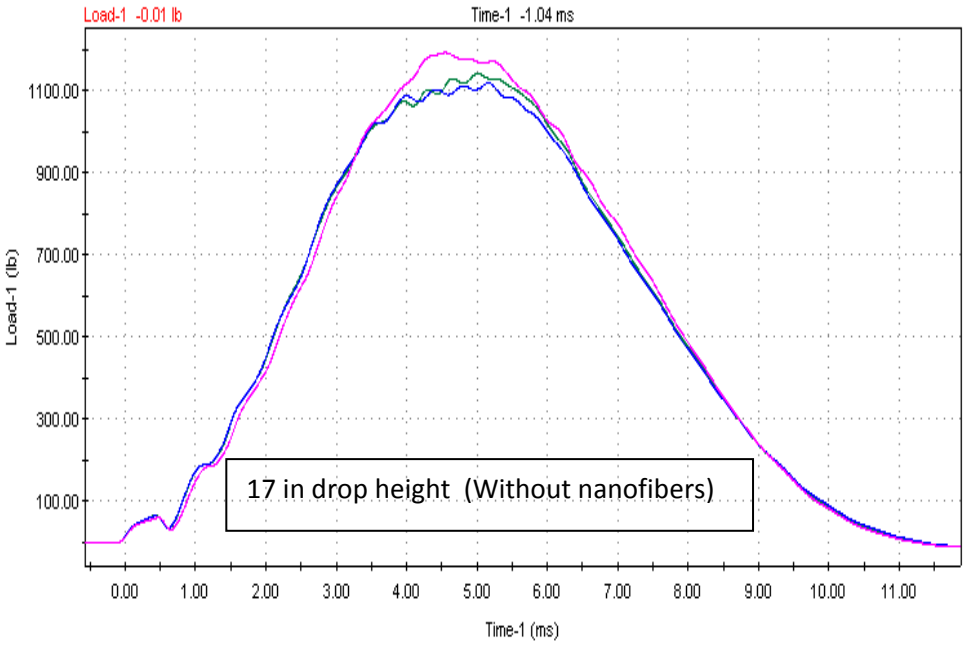
Load-1 -0.01 lb
Time-1 -1.04 ms
1100.00
900.00
700.00
500.00
300.00
100.00
Load-1 (lb)
17 in drop height (Without nanofibers)
0.00
1.00
2.00
3.00
4.00
5.00
6.00
7.00
8.00
9.00
10.00
11.00
Time-1 (ms)

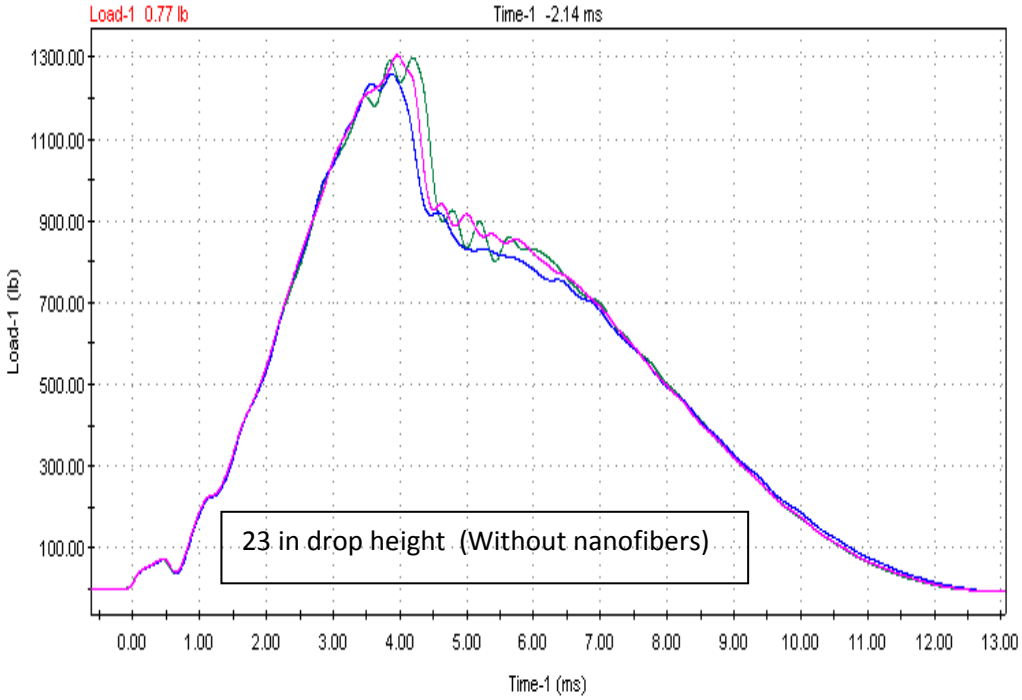
Load-1 0.77 lb
Time-1 -2.14 ms
1300.00
1100.00
900.00
700.00
500.00
300.00
100.00
Load-1 (lb)
23 in drop height (Without nanofibers)
0.00
1.00
2.00
3.00
4.00
5.00
6.00
7.00
8.00
9.00
10.00
11.00
12.00
13.00
Time-1 (ms)

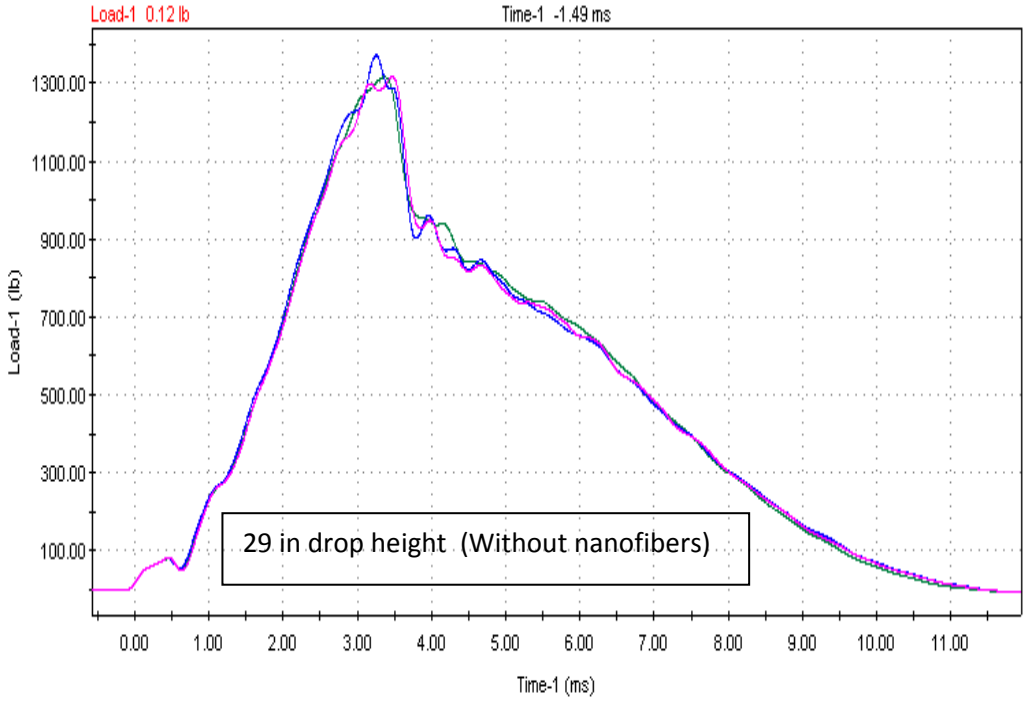
Load-1 0.12 lb
Time-1 -1.49 ms
1300.00
1100.00
900.00
700.00
500.00
300.00
100.00
Load-1 (lb)
29 in drop height (Without nanofibers)
0.00
1.00
2.00
3.00
4.00
5.00
6.00
7.00
8.00
9.00
10.00
11.00
Time-1 (ms)

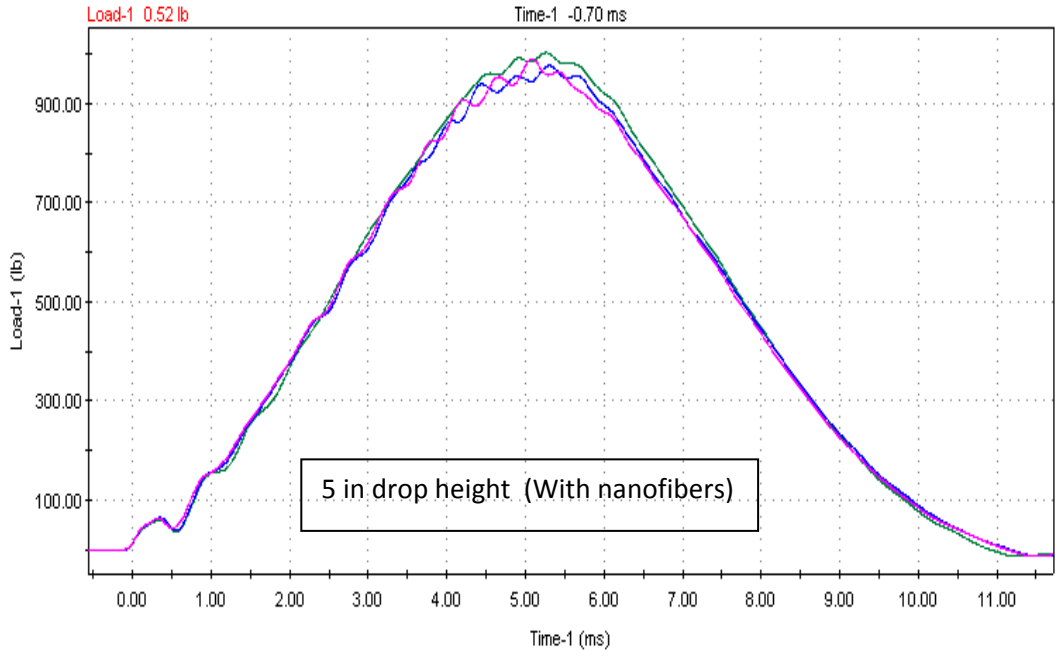
Load-1 0.52 lb
Time-1 -0.70 ms
900.00
700.00
500.00
300.00
100.00
Load-1 (lb)
5 in drop height (With nanofibers)
0.00
1.00
2.00
3.00
4.00
5.00
6.00
7.00
8.00
9.00
10.00
11.00
Time-1 (ms)

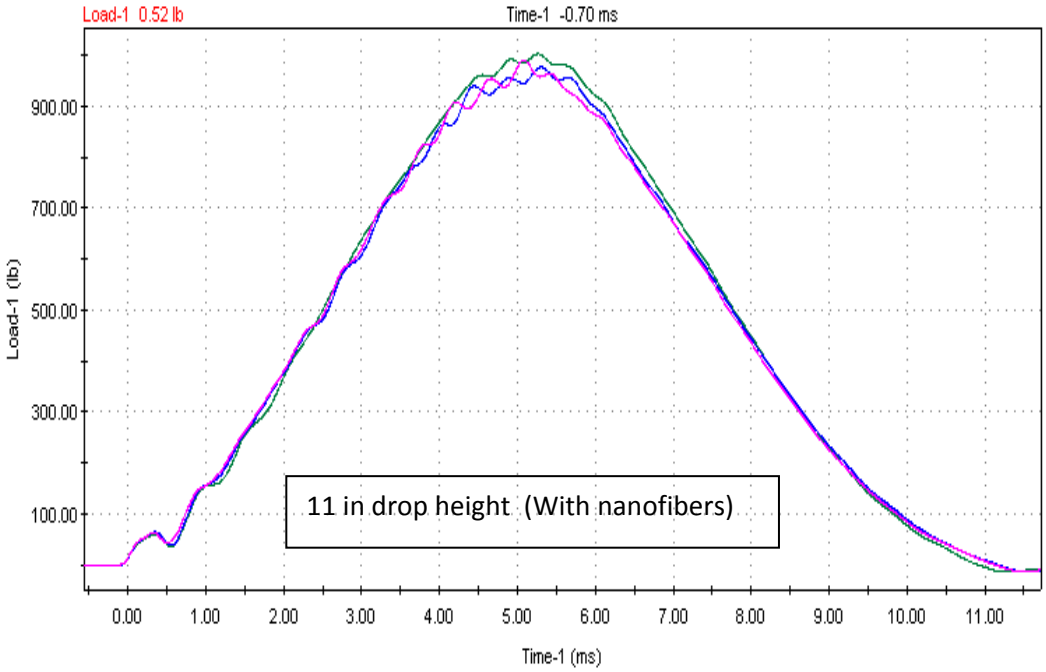
Load-1 0.52 lb
Time-1 -0.70 ms
900.00
700.00
500.00
300.00
100.00
Load-1 (lb)
11 in drop height (With nanofibers)
0.00
1.00
2.00
3.00
4.00
5.00
6.00
7.00
8.00
9.00
10.00
11.00
Time-1 (ms)

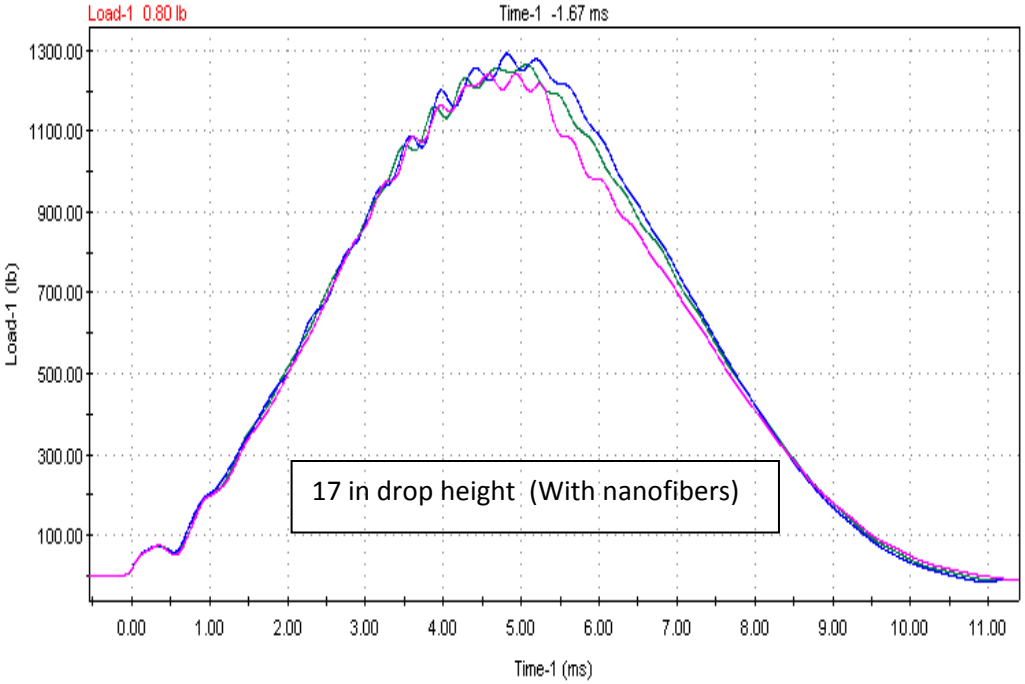
Load-1 0.80 lb
Time-1 -1.67 ms
1300.00
1100.00
900.00
700.00
500.00
300.00
100.00
Load-1 (lb)
17 in drop height (With nanofibers)
0.00
1.00
2.00
3.00
4.00
5.00
6.00
7.00
8.00
9.00
10.00
11.00
Time-1 (ms)

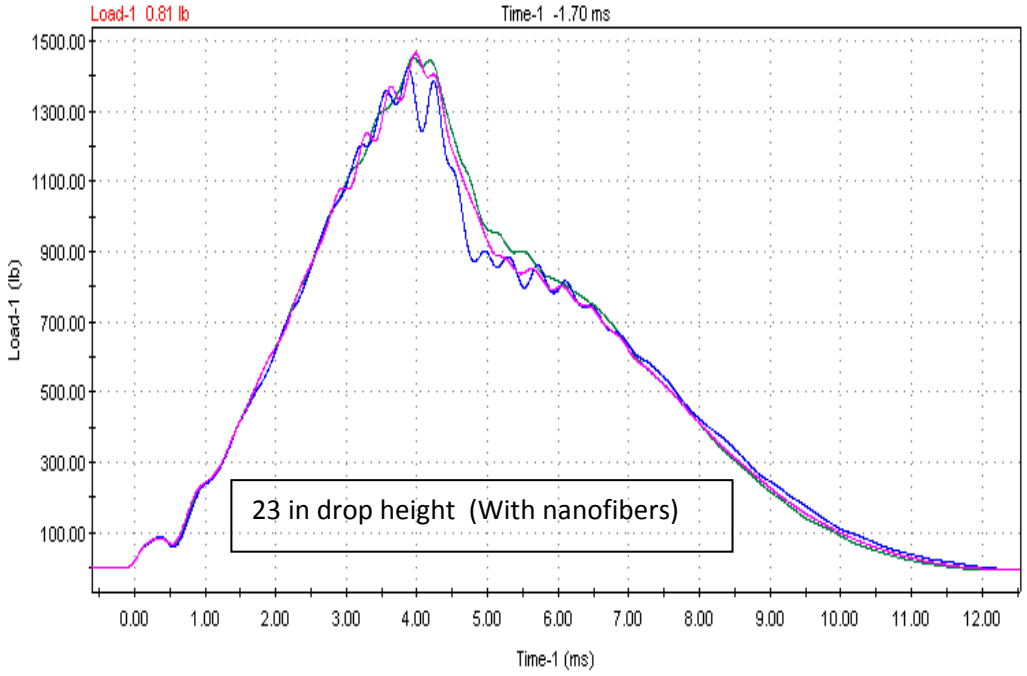
Load-1 0.81 lb
Time-1 -1.70 ms
1500.00
1300.00
1100.00
900.00
700.00
500.00
300.00
100.00
Load-1 (lb)
23 in drop height (With nanofibers)
0.00
1.00
2.00
3.00
4.00
5.00
6.00
7.00
8.00
9.00
10.00
11.00
12.00
Time-1 (ms)

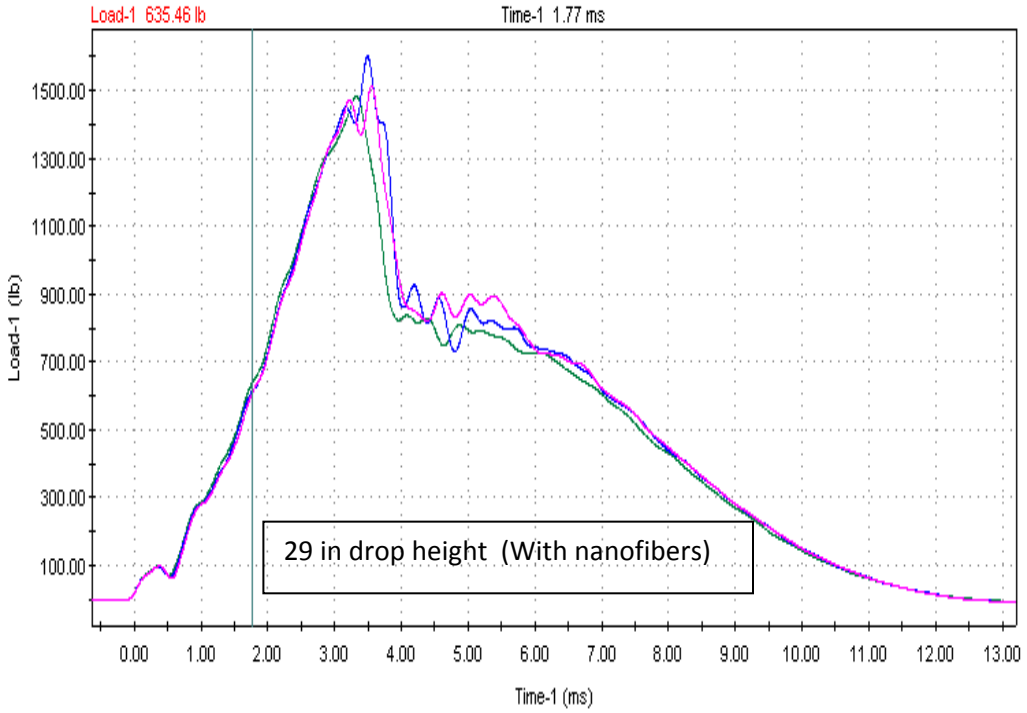
Load-1 635.46 lb
Time-1 1.77 ms
1500.00
1300.00
1100.00
900.00
700.00
500.00
300.00
100.00
Load-1 (lb)
29 in drop height (With nanofibers)
0.00
1.00
2.00
3.00
4.00
5.00
6.00
7.00
8.00
9.00
10.00
11.00
12.00
13.00
Time-1 (ms)